

**EFFECT OF PRESSURE AND ROAD CONDITION
ON POWER PRODUCTION BY A PRE-STRESSED
PIEZOELECTRIC TIRE**

SOLOMON WEKESA WAKOLO

MASTER OF SCIENCE

(Mechanical Engineering)

**JOMO KENYATTA UNIVERSITY OF
AGRICULTURE AND TECHNOLOGY**

2019

**Effect of Pressure and Road Condition on Power Production By a
Pre-stressed Piezoelectric Tire**

SOLOMON WEKESA WAKOLO

**A thesis submitted in partial fulfillment for the degree of Master of
Science in Mechanical Engineering in the Jomo Kenyatta
University of Agriculture and Technology**

2019

DECLARATION

This thesis is my original work and has not been presented for a degree in any other university.

Signature..... Date.....

Solomon Wekesa Wakolo

This thesis has been submitted for examination with our approval as the University

Supervisors:

Signature..... Date.....

Eng. Prof. John Kihiu, PhD

JKUAT, Kenya

Signature..... Date.....

Eng. Dr. Kenneth Njoroge, PhD

JKUAT, Kenya

Signature..... Date.....

Dr. Peter Kihato, PhD

JKUAT, Kenya

DEDICATION

This work is dedicated to my parent Mr. Penuel Wakolo and my wife Dorcas Wekesa for being there for me throughout the research period.

ACKNOWLEDGEMENTS

My greatest gratitude goes to the Almighty God for His divine protection and guidance throughout my study. I'm also grateful to my supervisors; Eng. Prof. John M. Kihiu, Eng. Dr. Kenneth Njoroge and Dr. Peter Kihato for their supervision and assistance throughout my study period. I also thank Dr. Onesmus Muvengi for his selfless intervention to ensure the resources I needed were availed. I thank JKUAT for supporting me financially during my study. My final thanks goes to all members of JKUAT staff that I worked with at different stages of the research and all my well-wishers.

TABLE OF CONTENTS

DECLARATION	ii
DEDICATION	iii
ACKNOWLEDGEMENTS	iv
TABLE OF CONTENTS	v
LIST OF TABLES	x
LIST OF FIGURES	xi
LIST OF APPENDICES	xv
LIST OF ABBREVIATIONS	xvi
LIST OF SYMBOLS	xvii
ABSTRACT	xix
CHAPTER ONE	1
1.0 INTRODUCTION	1
1.1 Background	1
1.1.1 Power Consumption by Different Cars	2
1.1.2 Research on Green Energy for Cars	4
1.2 Problem Statement	5

1.3	Objectives	6
1.3.1	General Objective	6
1.3.2	Specific Objectives	6
1.4	Justification	6
1.5	Organization of the Thesis	8
CHAPTER TWO		9
2.0 LITERATURE REVIEW		9
2.1	Overview	9
2.1.1	Piezoelectric Materials and Working Principle	10
2.1.2	Types of Piezoelectric Materials and Selection	12
2.1.3	Energy Harvesting Piezoelectric Circuits	17
2.1.4	Common Configurations of Piezoelectric Energy Harvesters	20
2.1.4.1	Direct and Indirect Method	20
2.1.4.2	Cymbal Transducers	21
2.1.4.3	Circular Diaphragms	23
2.1.5	Methods for Improving Efficiency and Power Generation	24
2.1.6	Relevant Equations and Calculations	25
2.1.6.1	Mechanical Equations for Vehicle Vibrations	25
2.1.6.2	Electromechanical Equations	28
2.1.7	Electric Vehicles (EV)	29
2.1.8	Solar Powered Vehicles	33
2.1.9	Vibration and Stress in Car Tires	34

2.1.10	Previous Works on Piezoelectricity Generation from Vehicles	38
2.2	Use of Simscape	43
2.3	Use of COMSOL Multi-physics	44
2.4	Summary of Gaps	46
CHAPTER THREE		48
3.0	METHODOLOGY	48
3.1	Introduction	48
3.2	Modeling of the Vehicle Using Simscape	49
3.3	Modeling of Piezoelectric Element in COMSOL	51
3.4	Development of the Experimental Model and Testing	54
3.4.1	Discs Used	54
3.4.2	Wiring of The Discs	55
3.4.3	Assembly of the Patch-tire Units	56
3.4.4	Terminals Through the Rim	58
3.4.5	Power Delivery into the Inner Vehicle Compartment	61
3.4.6	Stationary Tests	62
3.4.7	Road Tests	64
CHAPTER FOUR		66
4.0	RESULTS AND DISCUSSION	66
4.1	Introduction	66

4.2	Stationary tests for 0.3 mm Thick Disc	73
4.2.1	Drop Test of the Tire with an Inner Tube and Elements Be- tween Inner Tube and Tire Carcass	73
4.2.1.1	Power generation by elements at the 0° position	74
4.2.1.2	Power generation by elements at points away from 0° position	77
4.2.1.3	Power generation by elements at 10° position	78
4.2.1.4	Power generation by elements at 20°-180° position	79
4.2.1.5	Total produced power	81
4.2.2	Variation of Power Generation with Changing Tire Pressure for 0.3 mm Discs	86
4.2.3	Drop Test of the Tubeless Tire with Piezoelectric Elements	89
4.3	Stationary Tests for 2 mm Thick Disc	90
4.4	Power Generation on a Rough Road	93
4.5	Power Generation on a Tarmacked Road	97
4.6	Variation of Power Generated with Vehicle Vibrations	99
4.7	Comparison with Previous Researches on Cars	101
CHAPTER FIVE		102
5.0 CONCLUSIONS AND RECOMMENDATIONS		102
5.1	Conclusions	102
5.2	Recommendations	103

REFERENCES	104
References	104
APPENDICES	111

LIST OF TABLES

Table 1.1:	2018 State of fuel consumption rates in different car models .	3
Table 1.2:	Power output for various energy storage and harvesting methods	7
Table 2.1:	Properties of different piezoelectric materials	15
Table 2.2:	USABC goals for advanced batteries for EVs 2009	32
Table 3.1:	Parameters used in Simscape model	51
Table 4.1:	Impact force developed for the 16.25 kg tire at 30 psi pressure	73
Table 4.2:	Drop test for tire with inner tube with patch at 0° position . .	74
Table 4.3:	Drop test for 2 mm thick elements	90

LIST OF FIGURES

Figure 2.1:	Cartesian plane showing directions 1,2 and 3	16
Figure 2.2:	Circuit diagram showing connection to rectifier	19
Figure 2.3:	Direct and indirect power harvesting methods	20
Figure 2.4:	Piezoelectric ‘cymbal’ transducer	21
Figure 2.5:	The Moonie harvester	22
Figure 2.6:	Quarter car mass damper system	26
Figure 2.7:	Tuned mass damper spring system	27
Figure 2.8:	The general layout of an electric car	31
Figure 2.9:	Main vibrations experienced in a tire	35
Figure 2.10:	Time profile of car wheel holder vibrations	36
Figure 2.11:	Change in wheel deformation with changing tire pressure	37
Figure 2.12:	Variation of tire stiffness and grip with reducing tire pressure	37
Figure 2.13:	Piezoelectric shock absorber	42
Figure 2.14:	Information fed into COMSOL software	46
Figure 3.1:	Physical model of the car	49
Figure 3.2:	Model of car with piezoelectric tire in Simscape	50
Figure 3.3:	Piezoelectric disc model	52
Figure 3.4:	Meshed piezoelectric disc	53
Figure 3.5:	Dimensions of selected discs	54
Figure 3.6:	Wiring of the piezoelectric elements	55

Figure 3.7:	Assembly of the piezoelectric elements	56
Figure 3.8:	Power harvesting circuit diagram	57
Figure 3.9:	Gluing of the patch	58
Figure 3.10:	Introduced electric terminal-nozzles for power harvesting . . .	59
Figure 3.11:	Connection of cables in the nozzles	60
Figure 3.12:	Section drawing of the nozzle as modified in the current research	60
Figure 3.13:	Slip ring mounted on the tire	61
Figure 3.14:	Power harvesting probe	62
Figure 3.15:	Initial angular position of the patch in the tire	62
Figure 3.16:	Deflection measuring probe	63
Figure 3.17:	Equipment used during the experimental tests	65
Figure 4.1:	Screen shot of simulation showing force variation at the point of contact	66
Figure 4.2:	Stress distribution in the piezo electric disc after loading . . .	68
Figure 4.3:	Electromotive force distribution plot	70
Figure 4.4:	Variation of Voltage generated with element thickness for dif- ferent forces	71
Figure 4.5:	Variation of voltage generated per unit volume with element thickness for different forces	72
Figure 4.6:	Variation of power output with impact force for patch posi- tioned at $\psi = 0^\circ$	75

Figure 4.7:	Power production at various angular positions from contact point	77
Figure 4.8:	Variation of power output with changing impact force for patch positioned at $\psi = 10^\circ$	78
Figure 4.9:	Variation of Power output with angular position for patch positioned at 20° - 180°	80
Figure 4.10:	Effect of increasing pressure on a piezoelectric tires with inner tube	86
Figure 4.11:	Effect of increasing impact force on a piezoelectric tires with inner tube	88
Figure 4.12:	Power production in a pressurized tubeless tire with changing drop height	89
Figure 4.13:	Effect of increasing impact force on a 2 mm thick piezoelectric element pre-stressed between the inner tube and tire carcass	91
Figure 4.14:	Effect of tire pressure on a 2 mm thick piezoelectric element pre-stressed between the inner tube and tire carcass	92
Figure 4.15:	Condition of the rough road used in the research	93
Figure 4.16:	Variation of power generated with changing Vehicle speed for different rough road inclinations	94
Figure 4.17:	Variation of power generated with changing speed for tubeless tire	96
Figure 4.18:	A photograph of the tarmac road used in the research	97

Figure 4.19: Variation of power generated with speed for different tarmac
road inclinations 98

Figure 4.20: Variation in power output with changing vibrations 100

LIST OF APPENDICES

Appendix I	Tyre without piezo elements	111
Appendix II	Tire with piezo elements	112
Appendix III	Harvesting probe assembly	113
Appendix IV	Harvesting probe exploded diagram	114
Appendix V	Harvesting probe individual components	115
Appendix VI	Simscape symbols	116

LIST OF ABBREVIATIONS

AC	Alternating Current
AWD	All Wheel Drive
CAD	Computer Aided Design
DC	Direct Current
DOD	Depth of Discharge
EMF	Electromotive Force
EV	Electric Vehicle
FEA	Finite Element Analysis
HEV	Hybrid Electric Vehicle
ICE	Internal Combustion Engine
LDV	Laser Doppler Vibrometer
SSH	Synchronized Switch Harvesting Inductor
PHEV	Plug-in Hybrid Electric Vehicle
PVDF	Polyvinylidene Fluoride
PZT	Lead Zirconate Titanate
SOC	State of Charge
TPMS	Tire Pressure Monitoring Sensor
USABC	United States Advanced Battery Consortium
VDRG	Velocity Damped Resonant Generators
VSS	Vehicle Speed Sensor

LIST OF SYMBOLS

c	Viscous damping coefficient (Ns/m)
d	Electric charge constant (V/m)
d_{33}	Induced polarization in direction 3 per unit stress applied in direction 3 (pC/N)
D	Vector of electric displacement (C/m ²)
E	Vector of applied electric field (V/m)
F_{load}	Load applied on a piezoelectric disc (N)
g	Matrix of piezoelectric constants (m ² /N)
g_{33}	Induced electric field in direction 3 per unit stress applied in direction 3 (Vm/N)
k	Spring constant (N/m)
k_t	Factor for electric field in direction 3 and vibrations in direction 3
k_p	Factor for electric field in direction 3 and radial vibrations in direction 1
m	Mass (Kg)
p	The load on the main system (N)
p_{Tot}	The power produced by a single disc in a full cycle (W)
q	Force at the tire-road interface (N)
Q_m	Mechanical quality factor
S	matrix of compliance coefficients (m ² /N)
t	Time (s)
T_c	Curie point temperature (°C)
u	Displacement (m)
β	Impermitivity component (m/F)

σ	Stress (N/m ²)
ε	Strain (m/m)
$\varepsilon_3^\times / \varepsilon_0$	Relative permittivity
ψ	Angular position of a disc (Degrees)

ABSTRACT

The need to develop alternative energy sources for road transport has been growing daily due to depleting fossil fuels as well as the need to control toxic vehicular emissions. One of the most viable solutions developed in response to these concerns has been the electric car. The current electric cars however suffer from reduced range (in comparison to an Internal Combustion Engine (ICE) vehicle of the same price). Therefore there is need to research on additional green energy sources to supplement the energy stored in the batteries of electric cars.

This research sought to develop an additional energy source for electric cars by exploiting the fact that any vibrations and strains like the ones experienced in a car's tire can be converted into electrical energy using pre-stressed piezoelectric elements. This was done by first simulating the vehicle tire behavior using Simscape software to model the kind of forces that would be expected at the contact patch of the tire when in use. This information was then used with COMSOL multiphysics software to establish the most suitable piezoelectric element size (in terms of thickness) to use with such tires. Equipped with this data, a trial tire with embedded piezoelectric elements was developed and tested in the lab before fixing it on a Nissan Wingroad DBA Y12 car for the testing. The power output under all the above different road conditions was analyzed in order to understand the specific behavior of pre-stressed piezoelectric tires in automobiles

It was found out that each 25 mm diameter piezoelectric disc gives out a maximum of

0.5 mW of power.

Using the Nissan Wingroad as the experimentation car with the maximum $192 \times 2.65 = 508$ piezoelectric elements per wheel, it is possible to generate 1.1 Watts from the four tires at any given instance. The results from this research therefore can be used as a guideline in designing of future piezoelectric tires.

CHAPTER ONE

1.0 INTRODUCTION

1.1 Background

A well functioning and efficient transport sector remains a requirement for economic and social development, bringing people together and enabling trade and exchange of goods and services (Ahman et al.2009, Ahman et al.2009). Currently, cleaner and more sustainable forms of energy are needed in the transport sector in order to keep operational costs low and ensure a healthier environment for future generations (Dhingra et al.2012, Dhingra et al.2012). Globally, the primary energy resources consist of the traditionally used fossil fuels (such as coal, diesel, gasoline, and natural gas) which have notably been supplemented by nuclear energy (Bauer2015, Bauer2015). In terms of percentage contribution, fossil fuels contribute 83% of the energy used either directly or indirectly (Fakhri et al.3015, Fakhri et al.3015).

According to world energy outlook report, one person in eight people has no access to electricity. This is despite the fact that in 2017 global energy-related carbon (II)oxide (CO_2) emissions rose by 1.6%, with early data from across the globe suggesting continued growth in 2018 (Outlook2013, Outlook2013). The conclusion from this observation among others was that earth as a planet is very far from a trajectory consistent with its energy and hence climatic goals (Outlook2013, Outlook2013). Going into the future it is predicted that with the current rate of consumption, the available coal will last for 200 years, the oil will last for 100 years while the gas will last 150 years (Fakhri et al.3015, Fakhri et al.3015). The demand for cleaner cars in particular is being fueled

by the fact that transport sector accounts for about 27% of global energy usage and is the highest green house gas emitter at 29%.

1.1.1 Power Consumption by Different Cars

The present day car manufacturer's have to continuously work on the fuel efficiency of their engines at design stage. This is because consumers are increasingly basing their selection of cars on performance and running costs (Chiara et al.2016, Chiara et al.2016). Part of the above mentioned running cost is fuel consumption. A vehicle's fuel/energy expenditure on a flat road consists of three components: the energy required for overcoming the resistance of the air, the energy required for overcoming the resistance of the road, and the energy required for overcoming the resistance of the inertial acceleration (Ben-Chaim et al.2013, Ben-Chaim et al.2013). According to Momani and Omar (Al-Momani and Omar2007, Al-Momani and Omar2007), the main design aspects affecting expenditure on energy are: aerodynamic drag, type of transmission, gross weight, engine type/size and fuel type. Table 1.1 shows typical fuel consumption rates (regular gasoline) of different vehicles extracted from the 2018 Canada fuel consumption guide (EnerGuide2018, EnerGuide2018).

Where in the Table 1.1: AWD is an all-wheel drive vehicle, 2wd is a two-wheel drive vehicle, AV is a continuously variable gearbox, AV7 is a continuously variable gearbox with 7 speed manual shift option, M6 is a manual gearbox with six speeds, and M5 is a manual gearbox with five speeds

The sampling of the cars in the table was based on the popularity of the vehicles in Kenya. From Table 1.1, a hybrid vehicle consumes less than the pure gasoline vari-

Table 1.1: 2018 State of fuel consumption rates in different car models (EnerGuide2018, EnerGuide2018)

Make Model	Engine Size	Cylinders	Transmission	Consumption L/100Km			CO ₂ Emmissions (g/Km)
				City	Highway	Combined	
TOYOTA							
Toyota Corolla	1.8	4	AV	8.3	6.5	7.5	174
Toyota Corolla	1.8	4	AV7	8.3	6.7	7.5	178
Toyota Corolla	1.8	4	M6	8.4	6.6	7.6	178
Prius	1.8	4	AV	4.3	4.6	4.5	105
Prius c	1.5	4	AV	4.9	5.5	5.1	120
RAV4 AWD Hybrid	2.5	4	AV	6.9	7.8	7.3	171
RAV4 AWD	2.5	4	AV	10.5	8.3	9.5	222
HONDA							
Accord	1.5	4	AV	7.9	6.3	7.2	168
Accord	2.0	4	M6	10.7	7.3	9.2	214
Fit	1.5	4	AV	7.0	5.9	6.5	151
Fit	1.5	4	M6	8.1	6.6	7.4	174
NISSAN							
Dualis 2WD	2.0	4	AV	8.8	7.3	8.1	191
Dualis 2WD	2.0	4	M6	10.0	8.1	9.8	216
Dualis AWD	2.0	4	AV	9.0	7.5	8.4	196
SUBARU							
Impreza AWD	2.0	4	AV	8.4	6.5	7.5	176
Impreza AWD	2.0	4	M5	10.1	7.7	9.0	211

ant of the same model under similar driving conditions. Similarly a two wheel drive vehicle always consumes less fuel than the all wheel drive variant of the same model because of reduced friction in the transmission as well as weight. It can also be observed that the continuously variable transmission installed in cars returns better fuel mileage than a manual drive. The hybrid version further gives very low CO₂ emissions compared to the regular gasoline car. This table therefore demonstrates the need for further development of clean energy sources for vehicles so as to reduce fuel consumption (and hence the running cost) as well as lower the CO₂ emissions.

1.1.2 Research on Green Energy for Cars

A good percentage of research in the energy field is to develop sources of energy for the future in order to address some of the challenges mentioned earlier. Solar energy is very attractive in this regard, and the technology can be considered to have matured over the years. One of the major challenges in the implementation of solar technology on “energy-on-demand” platforms has however been the requirement of bulky solar panels. This would be more relevant for stationary equipment factoring in the variation in the intensity of sunlight (Priya2007, Priya2007). The other noble ways that have been developed to accomplish this desire for clean energy in automobiles include regenerative braking and using battery powered vehicles. Regenerative braking is whereby the vehicle’s electric motor is switched to reverse mode (starts working like an alternator) once the driver steps slightly on the brakes. This slows down the car’s wheels but at the same time generates electricity which is fed into the vehicle’s batteries. Bakker (Bakker2010, Bakker2010) however noted that successful introduction of the battery powered electric vehicles for individual consumers will be slowed down by their short range, lack of enough charging facilities and the high retail price of the vehicle. Currently the longest range is averagely 507 Km for the 2019 model S Tesla with most cars limited to 150Km (EPRI2019, EPRI2019), where range refers to the distance traveled between recharge of the car. One survey of American consumers found out that 75% of respondents considered the range to be the major disadvantage of Electric Vehicles (EVs) (Trigg et al.2013, Trigg et al.2013). The same demand for clean energy could however also be addressed through introduction of several energy

harvesting techniques in the cars which would reduce the size of battery required while increasing the range.

Energy harvesting is a process that captures small amounts of energy that would otherwise be lost as heat, light, sound, vibration or movement (Dhingra et al.2012, Dhingra et al.2012). One of the approaches that can be adopted to achieve energy harvesting is use of piezoelectric materials

1.2 Problem Statement

Mass commercialization of EVs that can be afforded by middle and low income earners is mainly limited by short range of travel before requiring a recharge, in the case of solar vehicles there is limited power due to a restriction in the available surface area for solar energy harvesting. Over the years a number of solar cars have been designed for public use, but their performance is still unsatisfactory due to their low power generation and consequently speed limitations. Rechargeable electric cars can be developed with larger capacity lithium batteries, but the battery alone ends up being more expensive than a whole new petrol vehicle (Lebeau et al.2013, Lebeau et al.2013). Although the battery cost is also dropping with time, inadequate mains power supply in most developing countries, and long charging hours compared to refueling a gasoline car still makes the vehicles impractical. There is therefore need to research on other on-demand green energy sources that can work with the above options and make these cars more desirable. This will not only reduce the storage capacity required by battery powered vehicles but also reduce the strain on the mains electricity in developing economies.

1.3 Objectives

1.3.1 General Objective

The main objective of this study was to establish the viability of using pre-stressed piezoelectric tires as a supplementary source of power in electric cars.

1.3.2 Specific Objectives

The specific objectives are

1. Establish the best size of piezoelectric elements to use by simulation means
2. Design and assemble a pre-stressed piezoelectric tire
3. Characterize the energy output of the piezoelectric tire under different operating conditions
4. Develop a mathematical model to predict the output of the harvester

1.4 Justification

Availability of an extra source of power on board means it will be possible to use a slightly smaller and affordable battery in electric cars without compromising on operational efficiency. The major reason to pursue piezoelectric materials for extra energy harvesting in vehicles is that they yield more power per unit mass than other sources of electric energy including the currently preferred rechargeable lithium battery. This is illustrated in Table 1.2.

Table 1.2 also shows that the output from piezoelectric modules does not change sig-

Table 1.2: Volume normalized power output for various energy storage and harvesting methods [6]

	Technique	Power Density (1Yr)[$\mu\text{w}/\text{cm}^3$]	Power Density (10Yr)[$\mu\text{w}/\text{cm}^3$]
Constant Output	Solar (Outdoor)	150-15,000	150-15,000
	Solar (indoor)	6	6
	Vibration (Piezoelectric)	250	250
	Vibration (Electrostatic)	50	50
	Acoustic Noise (75dB)	0.003	0.003
	Acoustic Noise (100dB)	0.96	0.96
	Thermal Gradient	15 (10°C)	15 (10°C)
Fixed Content	Non rechargeable lithium battery	45	3.5
	Rechargeable lithium battery	7	0
	Micro heat engine (hydrocarbon)	333	33
	Methanol Fuel Cell	280	28

nificantly ten years down the line. Power output from lithium batteries on the other hand is shown to go as low as zero in a similar duration. This suggests that with good design, the piezoelectric module is likely to give long service life and hence less maintenance cost.

Chen et al. (Chen et al.2012, Chen et al.2012), has shown that one way to improve the power generated from piezoelectric elements as well as lower the resonance frequency of the harvester, is to introduce a pre-stress in the supporting device. Past works (Minazara et al.2008, Minazara et al.2008; Khameneifar and Arzanpour2008, Khameneifar and Arzanpour2008; Manla et al.2009, Manla et al.2009; Sadeqi et al.2015, Sadeqi et al.2015; Keck2007, Keck2007; Makki and Popiliev2011, Makki and Popiliev2011) reviewed in this research before and after Chen's work on piezoelectric power generation from a car tire however all seem to have overlooked this crucial observation which might have led to the low power output levels reported.

There was therefore a need to look at power generation from pre-stressed piezoelectric tires in an effort to contribute to development of better electric vehicles for the society.

1.5 Organization of the Thesis

This thesis is composed of five themed chapters, including this introductory chapter. Chapter 2 is a review of research that has been carried out in the quest to develop piezoelectric tires. Chapter 3 outlines the procedure used to obtain the data for the research. In chapter 4, the outcomes from simulation as well as experimentation are presented and discussed. The final chapter includes the conclusions deduced from the research, and the recommendations given for further research to be carried out in order to develop the best possible piezoelectric wheel.

CHAPTER TWO

2.0 LITERATURE REVIEW

2.1 Overview

One condition that favors the idea of energy harvesting in vehicles is that anything that moves, rotates or is susceptible to fluid flow always vibrates (Anton and Sodano2007, Anton and Sodano2007). When this vibrations is undesired and hence unused, it becomes a potential source of energy (Pieter2013, Pieter2013). There are various methods to convert mechanical energy from vibrating or moving objects into electrical energy including electromagnetic induction, electrostatic induction, and the piezoelectric effect (Li et al.2014b, Li et al.2014b; Shah et al.2015, Shah et al.2015). While each of the aforementioned techniques can provide a useful amount of energy, piezoelectric materials have received the most attention due to their ability to directly convert applied strain energy into usable electric energy, and the ease at which they can be integrated into a system (Anton and Sodano2007, Anton and Sodano2007).

A piezoelectric material is one that produces an electric charge when a mechanical strain is applied (Dhingra et al.2012, Dhingra et al.2012). Conversely, a mechanical deformation is produced when an electric field is applied. This effect is formed in crystals that have no centre of symmetry (Dhingra et al.2012, Dhingra et al.2012). These materials respond to stress and strains, which makes them ideal in an application such as harvesting energy from automobile tire stresses and vibrations. Considering the nature of vibrations in most mobile devices, vibration power harvesting represents a huge potential for commercial applications (Motter et al.2006, Motter et al.2006).

In the harvesting process, it is usually important to keep in mind the fact that a piezo-electric material exhibits electric behavior and acts as a dipole only below a certain temperature called the Curie temperature (Ledoux and J2011, Ledoux and J2011). Above the Curie point, the crystalline structure will have a simple cubic symmetry and so no dipole moment. On the other hand, below the Curie point, the crystal will have a tetragonal or rhombohedral symmetry, hence a dipole moment. This means that a piezo-electric element will perform differently under different operation conditions (such as temperature and pressure). This necessitates carrying out of tests to ascertain the actual harvester performance.

2.1.1 Piezoelectric Materials and Working Principle

Piezoelectricity from the Greek word "piezo" means pressure electricity (Ebrahimi and Ogawa2013, Ebrahimi and Ogawa2013). Applications of piezoelectric materials have expanded into many fields since the discovery of the effect by the Curie brothers (Pierre Curie and Jacques Curie) in 1880-1881 (Nuffer and Bein2006, Nuffer and Bein2006). The brothers found out that when a mechanical stress was applied on some specified crystals, electricity was produced and the voltage of these electrical charges was proportional to the stress (Ledoux and J2011, Ledoux and J2011). Soon after it was revealed that piezoelectric materials could be used for energy harvesting using vibration, repetitive impacts and bending of structures (Kunchala and Sreekanth2014, Kunchala and Sreekanth2014). These effects were originally limited to naturally occurring materials. This however changed during the second world war when man-made polycrystalline ceramic materials were produced that also showed piezoelectric

properties (Ebrahimi and Ogawa2013, Ebrahimi and Ogawa2013). More research on piezoelectric materials revealed that they produce a voltage. This is because, when a mechanical stress is applied, the crystalline structure is disturbed and the direction of the polarization of the electric dipoles is changed. As a consequence, the bigger the mechanical stress, the bigger the change in polarization and the more voltage produced (Ledoux and J2011, Ledoux and J2011).

The property of piezoelectric ceramics to withstand harsh environmental conditions (especially chemical) made it a candidate material for application in most industries (Jürgen and Thilo2006, Jürgen and Thilo2006). The energy transforming characteristics of the material further enabled the material to function as sensors, actuators or transducers (Duan et al.2010, Duan et al.2010).

Early applications of piezoelectric materials in the industry include the quartz electrometer invented in 1880 (Uchino2017a, Uchino2017a), Quartz oscillators invented in 1921 (Walter1920, Walter1920), piezoelectric ultrasonic transducer invented in 1965 (Colbert1965, Colbert1965), distance sensors in cars invented in 1974 (Fathauer1974, Fathauer1974), knock sensors in cars invented in 1978 (Baier and Schulz1978, Baier and Schulz1978), and piezoelectric energy harvesting devices among others.

In 2005 the first battery-less tire pressure monitoring system that purely depended on piezoelectric property was released (Li et al.2014b, Li et al.2014b).

In the current research, the effect of differences in operating conditions on energy harvesting using pre-stressed piezoelectric modules in an automobile tire was studied. As

a result, precise guidelines on the precautions that ought to be taken when applying piezoelectric power generation in tires according to the proposed model were developed as well as a formula to predict the power produced from such a tire. To pre-stress means to introduce internal stresses into a structure in order to counteract the stresses that will result from an applied load or improve response to the external loads.

2.1.2 Types of Piezoelectric Materials and Selection

Piezoelectric materials are generally divided into four categories based on their structural characteristics:

1. Ceramics; These are the most commonly used piezoelectric materials because they are readily available. They include Barium Titanate ($BaTiO_3$), Lead Titanate ($PbTiO_3$) and lead zirconate titanate (PZT).
2. Single crystals; These are usually expensive to fabricate and therefore only used where there is no other alternative. They include quartz, lithium niobate ($LiNbO_3$) and lithium tantalite ($LiTaO_3$).
3. Polymers; These consist of multiple constituent parts: mers. They include Polypropylene, polystyrene, poly(methyl methacrylate), vinyl acetate, polyvinylidene fluoride ($PVDF$ or PVF_2) and PVDF copolymers .
4. Composites which have the advantage of a high coupling factor, low acoustic impedance, mechanical flexibility, a broad bandwidth in combination with low mechanical quality factor, e.g., 1-3 PZT-Polymer composite (Konka and Kun2010, Konka and Kun2010). They are especially useful for underwater sonar

and medical diagnostic ultrasonic transducers

Piezoelectric devices, similarly fall into four general categories, depending on what type of physical effect is used: generators, sensors and transducers (Nuffer and Bein2006, Nuffer and Bein2006). In this research the main interest was on generators because they have the highest power outputs.

Polyvinylidene difluoride (PVDF) is the most commonly used piezoelectric polymer. It is a semi-crystalline polymer with a repeating unit of $CH_2 - CF_2$. PVDF contains about 50% crystals which are embedded in an amorphous matrix. These piezoelectric polymers are flexible and easy to deform, which makes them resilient to mechanical shock and with densities less than 1/4 of that of PZT ceramics (PZT density is 7600 Kg/m^3). This low density makes them very desirable in mobile generation applications such as in automobiles which is the target of this research. They also have the ability to sustain much higher strain due to their intrinsic flexibility, making them better suited for applications where the device would be subjected to large amounts of bending or conforming to a curved mounting surface (Li et al.2014b, Li et al.2014b). Ferroelectric single crystals, ceramics and composites however, have much better piezoelectric properties than polymers.

Irrespective of the application, the nature of any given piezoelectric material is closely linked to the quantity of electric dipoles within the material. It follows that, to produce piezoelectric effect in the man-made materials, the poly-crystal must undergo a poling process. In this poling process the piezoelectric ceramic element is subjected to a strong DC electric field, usually at temperature slightly below the Curie temperature

(Konka and Kun2010, Konka and Kun2010). The heat allows the molecules to move more freely and the electric field forces all of the dipoles in the crystal to line up and face in nearly the same direction (Ledoux and J2011, Ledoux and J2011). The resultant alignment of the domains in the piezoelectric ceramic element allows it to become electrically polarized when exposed to a strain and thus produce an electrical charge. It is however important to point out that not every piezoelectric material can be poled and so not all can be applied with the same degree of success. Quartz, for example, is not spontaneously polarized but gets polarized upon application of stress, while ferro-electrics such as PZT are spontaneously polarized in addition to displaying change of polarization upon application of stress. Similarly different piezoelectric materials possess Weiss domains (regions of local alignment) with diverse flexibility leading to different success rates when polling (Raj et al.2015, Raj et al.2015).

A piezoelectric crystal bends in different ways at different frequencies. This bending is called the vibration mode. To realize small, cost effective, and high performance products, several modes have been developed to operate over several frequency ranges (Motter et al.2006, Motter et al.2006; Kong et al.2014, Kong et al.2014; Behera et al.2015a, Behera et al.2015a). These modes allow development of products working in frequencies ranging from few kilo hertz to several mega hertz (Dakua and Afzulpurkar2013, Dakua and Afzulpurkar2013). Most piezoelectric ceramics and single crystals used to date for energy harvesting are a subgroup of piezo-electrics called “ferroelectrics” (Li et al.2014b, Li et al.2014b). The most common examples are lead zirconate titanate (PZT) and solid solution of lead magnesium niobate and lead ti-

tanate (PMN-PT). These materials possess spontaneous dipoles below the Curie temperature, which makes them have excellent piezoelectric properties (Li et al.2014b, Li et al.2014b). Piezoelectric ceramics are commonly used for energy harvesting applications because of their good piezoelectric properties, low cost, and ease of incorporation into energy harvesting devices (Li et al.2014b, Li et al.2014b). Of all the piezoelectric ceramics available today, PZT has one of the best piezoelectric properties as shown in Table 2.1, Where d_{33} is induced polarization in direction 3 per unit stress applied in direction 3, g_{33} is the induced electric field in direction 3 per unit stress applied in direction 3, k_t is the factor for electric field in direction 3 and vibrations in direction 3, k_p is the factor for electric field in direction 3 and radial vibrations in direction 1 and direction 2, ϵ_3^x/ϵ_0 is the relative permittivity, Q_M is the mechanical quality factor and T_c is the curie point temperature. The cartesian coordinate system referred to is as captured in Figure 2.1.

Table 2.1: Properties of different piezoelectric materials (Uchino2017b, Uchino2017b)

Parameter	Quartz	BaTiO ₃	PZT 4	PZT 5A	PZT 5J	PZT 5H	PVDF TrFE	Pb,Sm TiO ₃
d_{33} (Pc/N)	2.3	190	289	390	500	593	33	65
g_{33} (10 ⁻³ Vm/N)	57.3	12.6	26.1	24	23	19.7	380	42
k_t	0.09	0.38	0.51	0.4	0.45	0.5	0.3	0.5
k_p		0.33	0.58	0.5	0.54	0.65		0.03
ϵ_3^x/ϵ_0	5	1700	1300	1400	1700	3400	6	175
Q_M	>10 ⁵		500	160	120	65	3-10	900
T_c (°C)		120	328	350	320	193		355

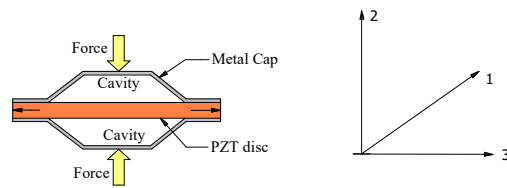


Figure 2.1: Cartesian plane showing directions 1,2 and 3

PZT is also very economical and practical for power harvesting unlike quartz which has good piezoelectric properties but very expensive. This is because its easy to fabricate any shapes/size of PZT (Li et al.2014b, Li et al.2014b). PZT5A in particular has the best thermal stability with a curie temperature of $350^{\circ}C$ which made it the material of choice in this research.

The efficiency and power density of a piezoelectric vibration energy harvesting device is frequency dependent because the piezoelectric element generates maximum power at its resonance frequency (Li et al.2014b, Li et al.2014b). Therefore, the fundamental frequency of the host determines the size of the piezoelectric element in a piezoelectric energy harvesting unit. This is because size is the only factor which affects the fundamental frequency of a ceramic which can be manipulated by the researcher after the material sets. The potential output power of these systems is inversely proportional to ω the frequency of the fundamental vibration mode (Li et al.2014b, Li et al.2014b). Piezoelectric ceramics being metal oxides, have much higher fundamental frequencies compared to composites and polymers of the same size, geometry and with the same vibration mode (Kong et al.2014, Kong et al.2014). The lower the frequency of the vibration host, the more complex it becomes to design the energy harvesting unit. The main reason for this being, the dimensional and weight constraints limit the use of ceramics to achieve the desired fundamental frequency. For such situations, piezoelectric

composites and polymers are likely to be the best candidates. Frequency tuning techniques are also utilized where the application doesn't involve large direct mechanical impact on the piezoelectric elements which usually generate sufficient power without any further alteration. Wheel rotation results in both direct impacts and vibration. This means that in the current research frequency tuning was not necessary.

2.1.3 Energy Harvesting Piezoelectric Circuits

A piezoelectric harvester is usually represented in an electric circuit as a current source in parallel with a capacitor and resistor (illustrated in figure 2.2). The power output is proportional to the input vibration amplitude (Dhingra et al.2012, Dhingra et al.2012). This output (voltage and current) which is usually sinusoidal then needs to be conditioned and converted to a form usable by the load circuits. The power conditioning and converting circuits should be able to extract most of the power generated by the piezoelectric energy harvester (Dongwon and Gabriel2009, Dongwon and Gabriel2009).

To convert the output AC voltage to DC voltage (since most electronics can only use DC power), some form of rectification is used (Townley2010, Townley2010). There are three primary harvesting circuits that can be employed for this: passive, active and semi-active (Ledoux and J2011, Ledoux and J2011). Passive circuits do not manipulate the voltage of the patch in any way; active circuits on the other hand manipulate the voltage in order to increase power output of the component. Each of these structural controls has advantages as well as shortcomings depending on the coupling of the harvester under consideration. In most applications a passive circuit may suffice. This is because the active variants may suppress the motion so much that less power is

harvested for low voltage harvesters (Pieter2013, Pieter2013).

Lallart and Guyomar (Lallart and Guyomar2008, Lallart and Guyomar2008) developed Synchronized Switch Harvesting on Inductor (SSHI) taking the efficiency up to 160 % above the standard rectifier. This particular class of rectifiers however only performs where the signal is sinusoidal with a constant frequency. Such conditions are practically impossible to achieve in a vehicle tire. Kwon and Rincón-Mora (Dongwon and Gabriel2009, Dongwon and Gabriel2009) on a similar quest proposed a rectifier-free piezoelectric harvester circuit. Their circuit used an inverting boost converter and provided two energy-flow paths to the output; one for positive piezoelectric voltage and another one for the negative voltage. This circuit allowed the harvester to process voltages that a rectifier would otherwise be unable to process. This particular concept was however not considered in this research since currently the diode rectifier is more reliable under the kind of operating condition the pressurized tire provides.

Eventually after rectification, the DC voltage generated is used to charge a capacitor or battery. This accumulation of power before use allows the targeted device to draw more power over a short period than the harvester might be able to provide (Leinonen et al.2011, Leinonen et al.2011). In this research, power storage was replaced with meters in the passive circuit for real time measurement of the changes in the output. The passive circuit was selected because it has been shown to work satisfactorily in piezoelectric shoes (Palosaari2017, Palosaari2017). An active circuit would however be necessary when the system is working in combination with another energy source for purposes of achieving effective energy flow management.

To determine the power production, a load resistor R_L is usually connected at the output of this rectified energy as shown in Figure 2.2. The resistor R_L is chosen such that it does not significantly affect the output voltage ripple, thereby causing the capacitive load time to be significantly longer than the period of the signal voltage at the terminals of the PZT transducer (Motter et al.2012, Motter et al.2012).

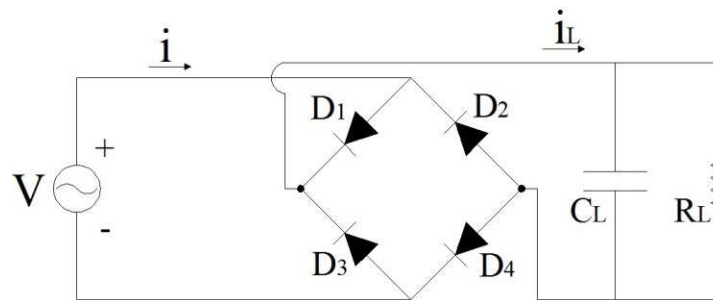


Figure 2.2: Circuit diagram showing connection to rectifier [40].

With the above arrangement it follows that the energy stored in the capacitor is given by

$$E_c = \frac{1}{2}C_L V_L^2 \quad (2.1)$$

Its however important to note that the greater the capacitance C_L , the more time is consumed to power the load in the form of electric field. It is therefore not always beneficial to increase the capacitance in the expression. In this research the capacitance was completely left out in order to accurately evaluate the instantaneous changes in power output.

2.1.4 Common Configurations of Piezoelectric Energy Harvesters

Piezoelectric harvesters can be mounted in various ways depending on the type of harvester material and the properties of the source of disturbance. The following are common configurations available.

2.1.4.1 Direct and Indirect Method

The two basic methods for tapping vibrations using piezoelectric element are

1. The direct method where the vibrations from the source are fed directly to the material. This method is the most efficient when the ambient conditions (vibration frequency) are as shown in Figure 2.3.
2. The indirect method which is accomplished by attaching a tuned harvester beam to the host as shown in Figure 2.3. The piezo material is attached as an additional layer at the base of the beam and is stressed as the beam flexes.

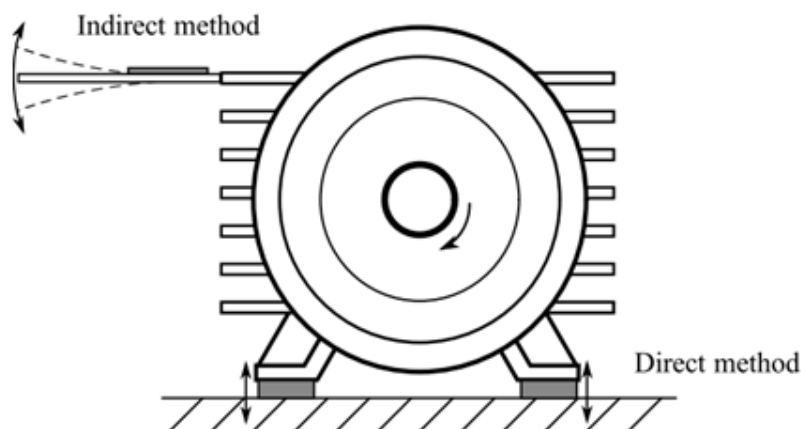


Figure 2.3: Direct and indirect power harvesting methods [7]

It is however a known fact that the harvester beam can generate high stresses in the piezo material using a modest external force or displacement (Pieter2013, Pieter2013). This makes the latter method more efficient for the vast majority of stationary appli-

cations. This point was however not used in this research due to the impracticality of attaching beams on a tire. The direct method was therefore adopted.

2.1.4.2 Cymbal Transducers

Cymbal transducers were developed for applications that have high impact forces. It typically consists of a piezo-electric ceramic disc and a steel end cap on each side as shown in Figure 2.4. Steel is typically used because it provides higher yield strength than brass and aluminum, thus leading to higher force loading capability of the transducer.

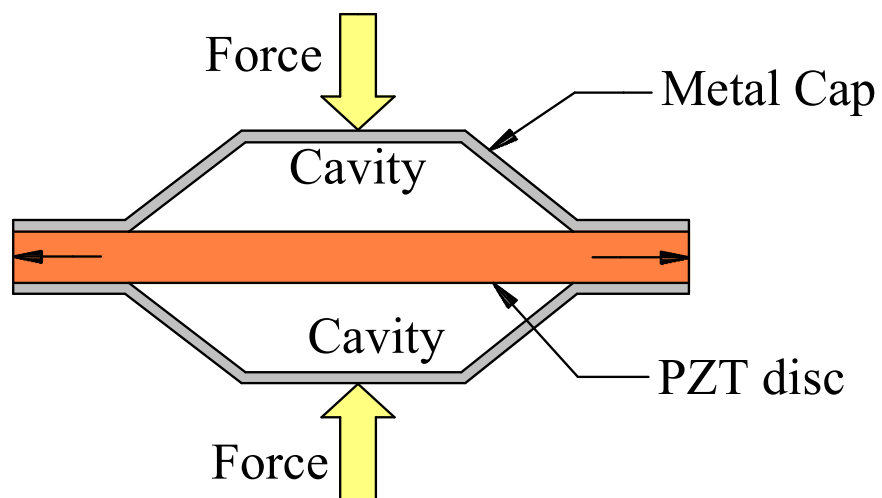


Figure 2.4: Piezoelectric ‘cymbal’ transducer

Since this configuration performs better than all the others available because of the pre-stress in its design, it greatly influenced the design of the harvester in this research. The effective piezo-electric charge constant of a cymbal transducer is expressed as

shown in equation 2.2:

$$d^{eff} = d_{33} + A|d_{31}| \quad (2.2)$$

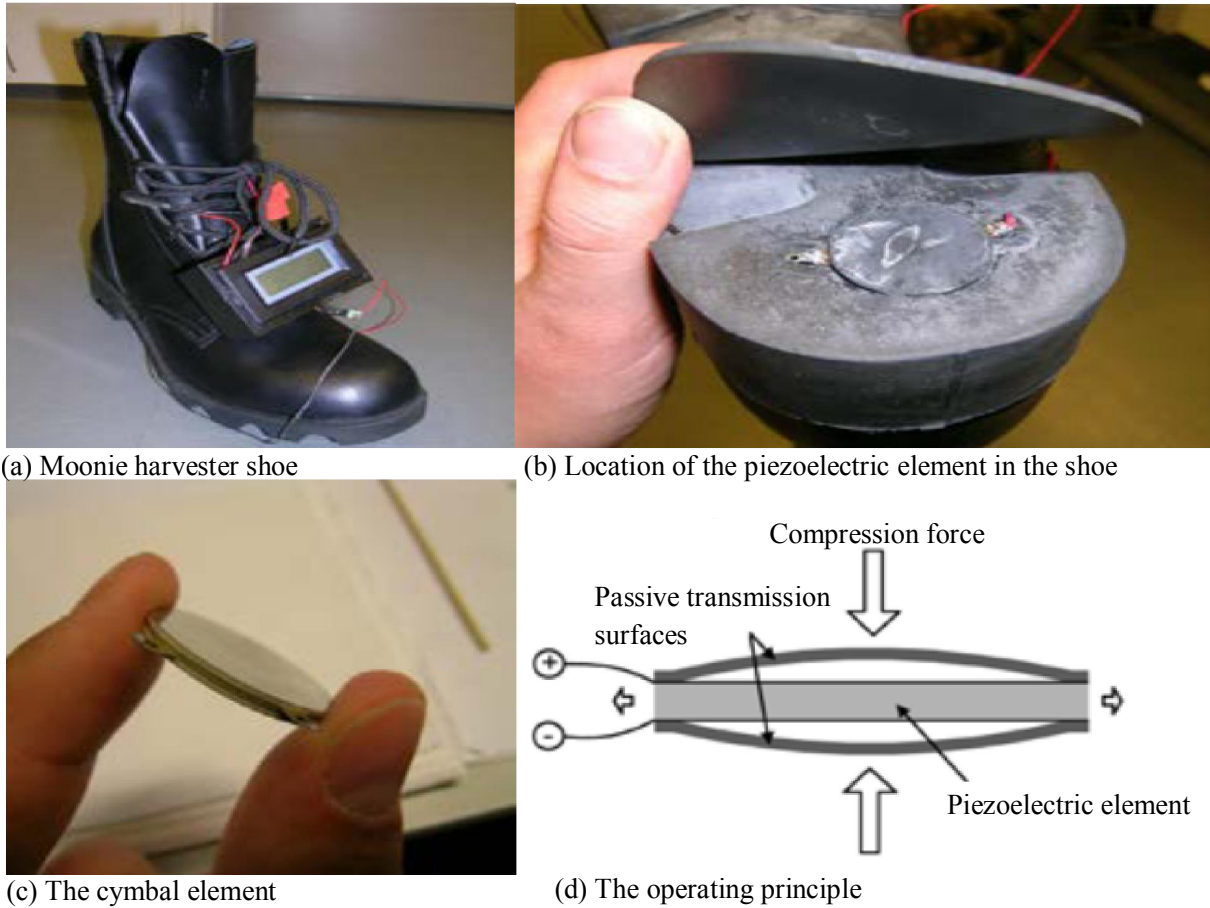


Figure 2.5: The Moonie harvester assembly [2]

where the Piezoelectric Constant d_{ij} is the ratio of the strain in j -axis to the electric field applied along the i -axis, when all external stresses are held constant. For example d_{31} is the ratio of strain along axis 1 to the electric field applied along axis 3 (directions are as captured in Figure 2.1). A is the amplification factor, and d^{eff} is the effective piezoelectric charge constant. In applications with high impact forces, cymbal transducers provide a higher energy output than cantilever energy harvesters because the cymbal structure withstands a higher impact (Li et al.2014b, Li et al.2014b). Figure 2.5 shows

application of the cymbal configuration in a shoe. The energy output of one step in this moonie harvester was recorded as $81 \mu\text{J}$ which translates to $162 \mu\text{W}$ for two shoes when walking 2 steps per second (Leinonen et al.2011, Leinonen et al.2011).

2.1.4.3 Circular Diaphragms

To construct a piezoelectric circular diaphragm transducer, a thin circular piezoelectric ceramic disc is first bonded to a metal shim and then the whole structure is clamped on the edge. On the contrary, piezoelectric cantilevers are only clamped at one end of the cantilever beam. In some cases, a proof mass is attached at the center of the diaphragm to provide pre-stress to the piezoelectric ceramic which improves the low-frequency performance of the energy harvester and increase the power output (Li et al.2014b, Li et al.2014b). Another method of introducing pre-stress within the piezoelectric ceramic occurs during the fabrication stage of the piezoelectric-metal composite. In this case a piezoelectric ceramic layer is first sandwiched between two dissimilar metal layers, and then the clamped composite is heated and cooled to room temperature. The difference in the thermal expansion coefficients of the two dissimilar metals causes the whole structure to warp, thus introducing pre-stress in the piezoelectric. One example of such pre-stressed transducers is "Thunder" which is used to harvest energy from shoes (Priya2007, Priya2007). This harvester is similar to the moonie harvester illustrated in Figure 2.5. In the case of automobile wheels, the pre-stress was provided by the pressure between the inner tube and the tire in order to benefit from its effects.

2.1.5 Methods for Improving Efficiency and Power Generation

Piezoelectric materials can be configured in various ways for effective power harvesting applications. These configurations can be changed through modification of piezoelectric materials, changing the poling and stress direction, layering the material to maximize the active volume, adding pre-stress to maximize the coupling and applied strain of the material, and tuning the resonant frequency of the device (Anton and Sodano2007, Anton and Sodano2007). The type of piezoelectric material selected for a power harvesting application can have a major influence on the harvester's functionality and performance. The most common type of piezoelectric material used in power harvesting applications is lead zirconate titanate, a piezoelectric ceramic known as PZT. Although PZT is widely used as a power harvesting material, its extremely brittle nature limits the strain that it can safely absorb without being damaged (Anton and Sodano2007, Anton and Sodano2007). Piezoceramics are susceptible to fatigue crack growth when subjected to high frequency cyclic loading (Anton and Sodano2007, Anton and Sodano2007). In order to eliminate this disadvantage of piezoceramic materials and improve upon their efficiency, more flexible piezoelectric materials such as PVDF that can be used in energy harvesting have been developed and are now available. Another effective way to improve the energy output of a power harvesting device is to stack a large number of thin piezoceramic wafers together, called the stack configuration, with the electric field applied along the length of the stack (Anton and Sodano2007, Anton and Sodano2007). Increasing the substrate and PZT thickness both gives higher charge outputs. However, increasing the substrate thickness

has a greater effect than increasing the PZT thickness (Anton and Sodano2007, Anton and Sodano2007). It has also been found that increasing the stiffness of the substrate increases the charge that can be generated (Anton and Sodano2007, Anton and Sodano2007). This was achieved in the current research by using the outer pressurized rubber as the substrate which is stiff by design. More stiffness was provided by application of heat glue which also helped control brittleness.

2.1.6 Relevant Equations and Calculations

Piezoelectric power is produced when a mechanical force at a particular frequency acts on a piezoelectric material. It is therefore common to look at the vibration of the element separately in the form of mechanical equations, and then relate the vibration to the electricity generated using electro-mechanical coupling

2.1.6.1 Mechanical Equations for Vehicle Vibrations

The purpose of a vehicle suspension system is to improve ride comfort, road handling as well as protect the road on which the vehicle is driven from extreme shock loads as the wheels pass (Florin et al.2013, Florin et al.2013). The main reason of modeling the mechanical system is therefore to understand the physical behavior of the tire as the vehicle moves and hence establish the forces transmitted to the harvester (Anil and Sreekanth2014, Anil and Sreekanth2014). With the assumption that the applied force is instantly and uniformly distributed throughout the device, this mechanical model can be simplified into a (quarter car) spring-mass damper system (Ledoux and J2011, Ledoux and J2011) as shown in Figure 2.6.

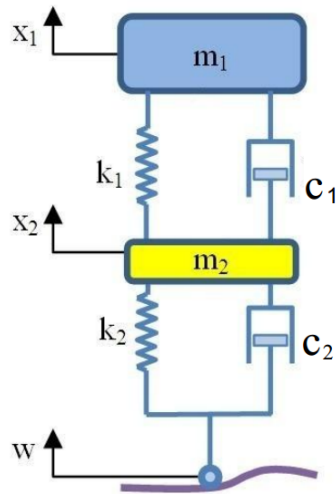


Figure 2.6: Quarter car mass damper system (Florin et al.2013, Florin et al.2013)

The quarter car system is always preferred due to its simplicity and versatility for almost any situation (Florin et al.2013, Florin et al.2013). From Figure 2.6 it follows that:

$$m_1\ddot{x}_1 + c_1(\dot{x}_1 - \dot{x}_2) + k_1(x_1 - x_2) = 0 \quad (2.3)$$

$$m_2\ddot{x}_2 + c_1(\dot{x}_2 - \dot{x}_1) + k_1(x_2 - x_1) + c_2(\dot{x}_2 - \dot{w}) + k_2(x_2 - w) = 0 \quad (2.4)$$

where m_1 is the sprung mass, m_2 is the unsprung mass, k_1 is the spring constant of the suspension system, k_2 is the vertical spring constant of the tire, c_1 is the viscous damping of the suspension system, c_2 is the viscous damping of the tire, x_1 is the vertical displacement of sprung mass, x_2 is the vertical displacement of unsprung mass, and w is ground support motion(system excitation).

Equations 2.3 and 2.4 are second-order differential equations of a passive suspension system. Solving this system of equations is tedious and so a Matlab Simulink software is used to simplify the work and eliminate errors (Florin et al.2013, Florin et al.2013).

This set of equations was solved by Simscape in order to give the forces experienced

at different points. Using Laplace transform (which employs the special parameter, s) with a couple of manipulations, it is possible to show that Equations 2.3 and 2.4 can be reduced to Equation 2.5 (Florin et al.2013, Florin et al.2013):

$$w(s)(c_2s + k_2) = m_1s^2x_1(s) + x_1(s)\frac{(m_1s^2 + c_1s + k_1)(m_2s^2 + c_2s + k_2)}{c_1s + k_1} \quad (2.5)$$

The same mass damper model can be developed for the harvester patch as shown in Figure 2.7, from where it follows that

$$F(t) = M_s\ddot{x} + C_s\dot{x} + K_sx \quad (2.6)$$

where $F(t)$ is the load on the piezoelectric patch, M_s is the mass of the patch, k_s is the effective spring constant of the harvester, c_s is the damping constant of the patch and x is the displacement at the harvester boundary (Anil and Sreekanth2014, Anil and Sreekanth2014).

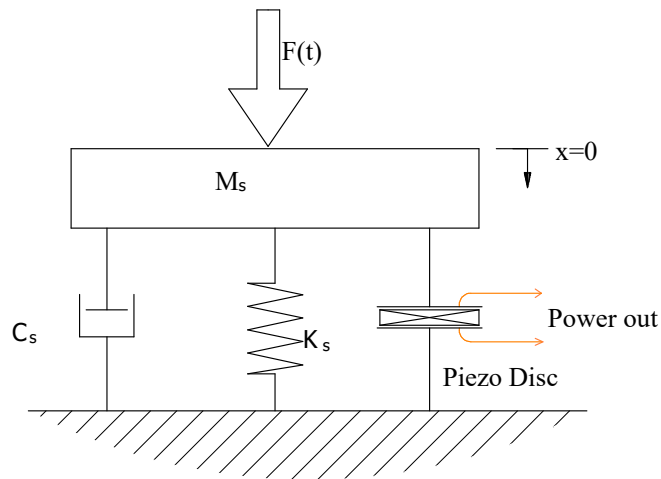


Figure 2.7: Tuned mass damper spring system (Motter et al.2012, Motter et al.2012)

The mechanical work done on the disc due to the compression can then be given by

(Kunchala and Sreekanth2014, Kunchala and Sreekanth2014):

$$W_{mech} = F(t) \times x_{piezo} \quad (2.7)$$

where W_{mech} is the mechanical work. The mechanical work can then be related to the electrical work which is the main focus of piezo-generation by using the relation (Kunchala and Sreekanth2014, Kunchala and Sreekanth2014):

$$W_{elec} = W_{mech} \times (k_{33})^2 \quad (2.8)$$

where W_{elec} is the electrical work and k_{33} is the electro-mechanical coupling constant of the piezoelectric material in use.

These equations are based on the assumption that the total strain in the piezoelectric material is the sum of mechanical strain induced by mechanical stress and controllable actuation strain caused by the applied electric voltage.

2.1.6.2 Electromechanical Equations

The electromechanical equations for a linear piezoelectric material can be written as (Pieter2013, Pieter2013):

$$\varepsilon_i = S_{ij}^D \sigma_j + g_{mi} D_m \quad (2.9)$$

$$E_i = g_{mi} \sigma_i + (\beta_{ij}^\sigma D)_k \quad (2.10)$$

where σ is the stress vector (N/m^2), ε is the strain vector (m/m), E is the vector of applied electric field (V/m), S is the matrix of compliance coefficients (m^2/N), D is the vector of electric displacement (C/m^2), g is the matrix of piezoelectric constants

(m^2/N), β is the impermittivity component (m/F).

Indices $i, j = 1, 2, 3$, Indices m and $k = 1, 2, 3$ refer to directions within the Cartesian coordinate system as illustrated in Figure 2.1. Superscripts D and σ represent measurements taken at constant electric displacement and constant stress respectively.

The equations above express the direct piezoelectric effect for generator application. Material properties that control the performance of piezoelectric energy harvesters are the dielectric constant, the piezoelectric strain coefficient, the electro- mechanical coupling coefficient, the Young modulus, the density, and the electrical and mechanical quality factors (Anuruddh et al.2014, Anuruddh et al.2014). The above mentioned favorable properties cannot be associated with one single material as illustrated in figure 2.1. However, lead-based materials such as PZT have been reported to have the best performance among all the known piezoelectric materials.

2.1.7 Electric Vehicles (EV)

The desire for cleaner energy powered transport means led to the development of the first four-wheeled electric car in 1897 (Trigg et al.2013, Trigg et al.2013). Challenges with sufficient power storage however quickly saw it dropped in preference for the more powerful internal combustion engine vehicle. Negative environmental impacts of the internal combustion engine have however seen the earlier abandoned EVs resurface. Under the Paris Agreement, European governments and the European Union (EU) are committed to a low-carbon transition, with a goal of net zero emissions by the second half of this 21st century (Gencsu et al.2017, Gencsu et al.2017). This further explains the renewed effort by the scientific community to equip the electric car with

either a powerful energy storage accumulator, or additional on-board energy harvesting alternatives to work with the batteries currently available.

At the end of 2012, total worldwide electric vehicle stock numbered over 180,000 (Trigg et al.2013, Trigg et al.2013). These electric vehicles derive some or all of their power from large, rechargeable batteries. The distance an EV can drive between recharges is known as its range.

Electric vehicles can be divided into three categories:

1. All-electric vehicles (EVs): The battery is the only power source in these vehicles as shown in Figure 2.8. This battery is charged through regenerative braking and plugging in the mains(Schroeder and Corkery2010, Schroeder and Corkery2010).
2. Plug-in hybrid electric vehicles (PHEVs): They can switch between running on electric battery which is charged by plugging in the mains or run on fossil fuels (Chandrika2010, Chandrika2010).
3. Hybrid electric vehicles (HEVs): Are powered by both a combustion engine and an electric motor that uses energy stored in a battery. The battery in HEVs is charged through regenerative braking using the same electric motor as a generator (Schroeder and Corkery2010, Schroeder and Corkery2010).

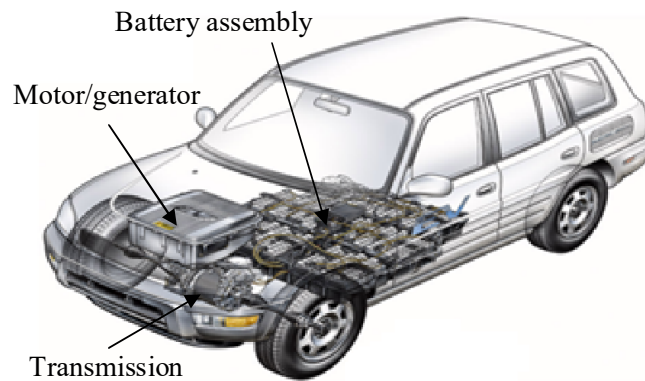


Figure 2.8: The general layout of an electric car (Anair and Amine2012, Anair and Amine2012)

Introduction of piezo-electric wheels will be beneficial to all three types of electric vehicles. This is because availability of an extra power source on board means it will be possible to use a slightly smaller and affordable battery without compromising on operational efficiency.

In 2009 the United States Advanced Battery Consortium (USABC) set up a threshold on the expectations that advanced batteries should meet in order for the battery electric vehicle to become a commercial success (Bakker2010, Bakker2010). The USABC specific power goals for future advanced batteries are shown in table 2.2.

The price of a these battery packs is however still a challenge to date (Bakker2010, Bakker2010). According to Bunsen et al.(Bunsen et al.2018, Bunsen et al.2018), as of May 2017, the average battery pack cost 274 USD/kWh and the average EV had a power consumption of 20-40 kWh/100 km. This data translates to a battery of USD 10,960 (excluding shipping costs) for just 200 km range in the lightest electric car in the market. Considering that a battery replacement is required after 5-10 years (Chandrika2010, Chandrika2010), and a new petrol car cost around the same

Table 2.2: USABC goals for advanced batteries for EVs 2009 (Bakker2010, Bakker2010)

Parameters(Units of fully burdened system)	Minimum Goals for long term commercialization	Long term Goal
Power Density (W/L)	460	600
Specific Power - Discharge, 80% DOD/30 sec(W/Kg)	300	400
Specific Power - Regen, 20% DOD/10 sec(W/Kg)	150	200
Energy Density - C/3, 20% Discharge Rate (Wh/L)	230	300
Specific Energy - C/3, 20% Discharge Rate (Wh/Kg)	150	20
Specific Power/Specific Energy Ratio	2:1	2:1
Total Pack Size(kWh)	40	40
Life (Years)	10	10
Cycle Life - 80% DOD (Cycles)	1000	1000
Power and Capacity Degradation (% of rated Spec)	20	20
Selling Price - 25,000 units @ 40 kWh (\$/kWh)	<150	100
Operating Environment (°C)	-40 to +50 20% performance loss (10% Desired)	-40 to 85
Normal Recharge Time (hrs)	6 (4 desired)	3 to 6
High Rate Charge %SOC @ 150 W/kg	20 -70 <30 minutes	40 -80 in 15 minutes
Continuous Discharge in 1 hour - No Failure (% of rated energy Capacity)	75	75

amount(for example a zero mileage Mazda Biante goes at 7800 USD on autoworld-japan.com), this price is quite high. This suggests that it is time the electric car stopped being limited to the the costly stored charge and instead exploration of other possibilities such as instantaneous generation of piezoelectricity which can help elongate the lifespan without requiring costly storage capacities, be done. Rates of electricity supplies from the grid have also historically been much more stable than either gasoline or diesel fuel costs (Beard et al.2015, Beard et al.2015). This stability coupled to the fact that primary energy consumption of a battery electric vehicle does not vary much

from ICE vehicle (Bakker2010, Bakker2010), justifies the need to optimize electric vehicles in particular and not ICE vehicles. General Motors estimates the annual energy use of the Chevy Volt will be 2,520 kWh, which is less than that required for a typical water heater or central air conditioning (Beard et al.2015, Beard et al.2015). However, just as gasoline vehicles vary in the miles they can travel on a gallon of gasoline, electric vehicles vary in how far they can go on a kilowatt-hour of electric power (Anair and Amine2012, Anair and Amine2012). A good illustration of this is the Smart Fortwo electric, the Mitsubishi iMiev and the Nissan Leaf which have primary energy consumptions of 1.48, 1.55 and 1.64 MJ/km, respectively (Bakker2010, Bakker2010).

2.1.8 Solar Powered Vehicles

Solar vehicles have very little difference from the electrical vehicles described above, apart from the fact that their power comes from solar. Their main limitation is low speed, high initial cost and also, inefficient rate of energy conversion (only 17%) (Wamborikar and Sinha2010, Wamborikar and Sinha2010). The problem with solar cell efficiency lies in the p-n junction structure which can only allow a maximum of 33.7% conversion of the solar irradiance into electric energy (Wamborikar and Sinha2010, Wamborikar and Sinha2010). The solar vehicles will therefore also benefit from piezoelectricity as the technology matures. At full maturity it has the potential to improve range of cars travelling on level terrains by upto 300% because under such conditions the car power consumption could go as low as 1 kWh/100 km at moderate speeds (Bunsen et al.2018, Bunsen et al.2018).

2.1.9 Vibration and Stress in Car Tires

The tire is a very complex structure consisting of several strengthening layers made of parallel fibers (Bogusz et al.2012, Bogusz et al.2012). Due to various causes such as road impact excitations, tires can vibrate in the following modes (demonstrated in Figure 2.9) (Kindt et al.2007, Kindt et al.2007) :

1. Whole tire vibrations which are caused by the road roughness and running deflection. These vibrations are important in the frequency band below 500 Hz (Kindt et al.2007, Kindt et al.2007) . The current research however did not consider this class of vibrations because their effect on a harvester positioned inside the tire is insignificant.
2. The tread block radial and tangential vibrations. This is important above 1000 Hz and was the main target in this research because any vibrations in the tread-block directly affects the harvester as mounted in the model.
3. Aerodynamic phenomena such as air pumping and tread groove resonances. This is important above 1000 Hz.

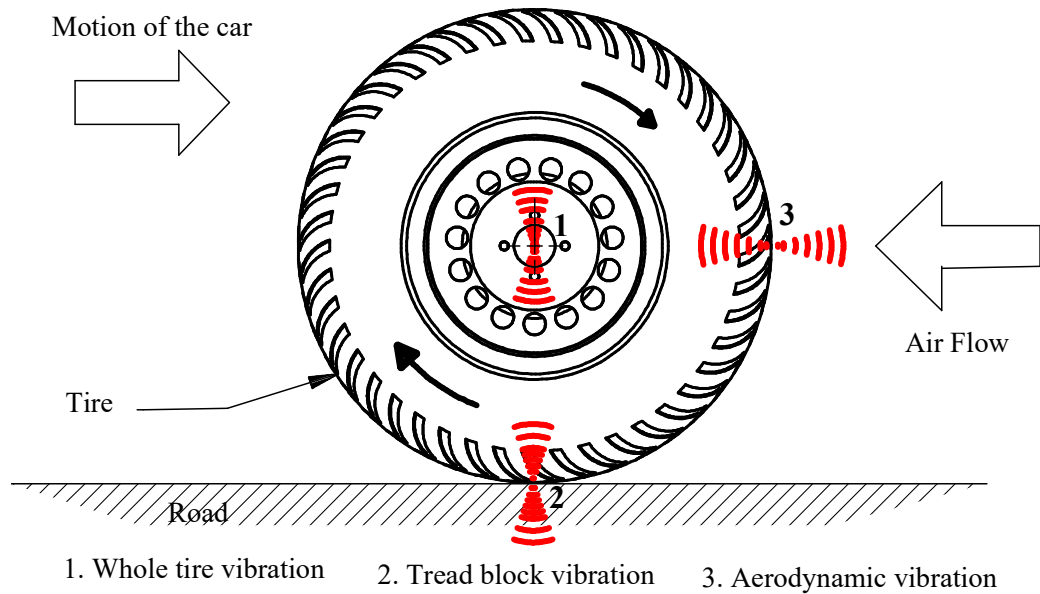


Figure 2.9: Main vibrations experienced in a tire

These vibrations are usually undesired and several measures are used to isolate the vibration from the occupants including using rubber wheels, suspension systems and cushions in seats. The only place with unmodified vibrations as a result remains to be the tire surface. Additionally as the vehicle moves, a new area of the tire continually deforms and relaxes in a cyclic pattern whose frequency is dependent upon the speed of the vehicle. All these different vibrations in a rolling tire are usually measured by means of a single point Laser Doppler Vibrometer (LDV) which allows contactless vibration velocity measurements (Kindt et al.2007, Kindt et al.2007).

In addition to measuring vibrations in terms of Velocity, it could also be measured in terms of displacement as well as acceleration interchangeably. The shape and period of the vibration remains the same regardless of whether one selects displacement, velocity or acceleration. The main difference between these units of measurement is that there is a phase difference between the amplitude and time curves of the three parameters. If

the phase of the wave is neglected, then the velocity level may be found by dividing the acceleration signal by a factor proportional to frequency, and the displacement is found by dividing the acceleration signal by a factor proportional to the square of frequency (Broch1984, Broch1984). In the current research displacement was selected.

The effects of changes in road conditions on vibrations experienced in vehicles has been investigated (Lakušić and Brčić2011, Lakušić and Brčić2011). The measurement of the vibrations of the car wheel holder was carried out continuously at a constant speed of 80 km/hr before the road was repaired and after repairs as shown in Figure 2.10. Before road repair, the tire holder experienced high amplitudes of up to 40 m/s², after the road repair this reduces to a maximum of around 10 m/s² which is 75% reduction in vibration. It was thus concluded that the nature of the road surface indeed does affect the kind of vibrations experienced in the tire. Hence the more need to explore the effect of road surface on power generation from the piezoelectric wheel.

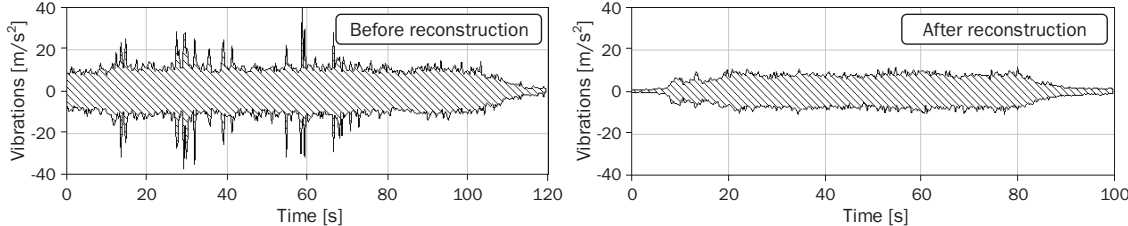


Figure 2.10: Time profile of car wheel holder vibrations (Lakušić and Brčić2011, Lakušić and Brčić2011)

Loads applied on the rotating wheel due to these vibrations are usually complex in nature and produce high resultant stresses (Machave et al.2015, Machave et al.2015). The reaction forces exerted by the road surface on the four tires balance the total weight of a car. This means the stress induced due to weight alone equals the force on the given wheel divided by the area of contact. The resultant deformation due to both the weight

and the pressure takes the form illustrated in Figure 2.11.

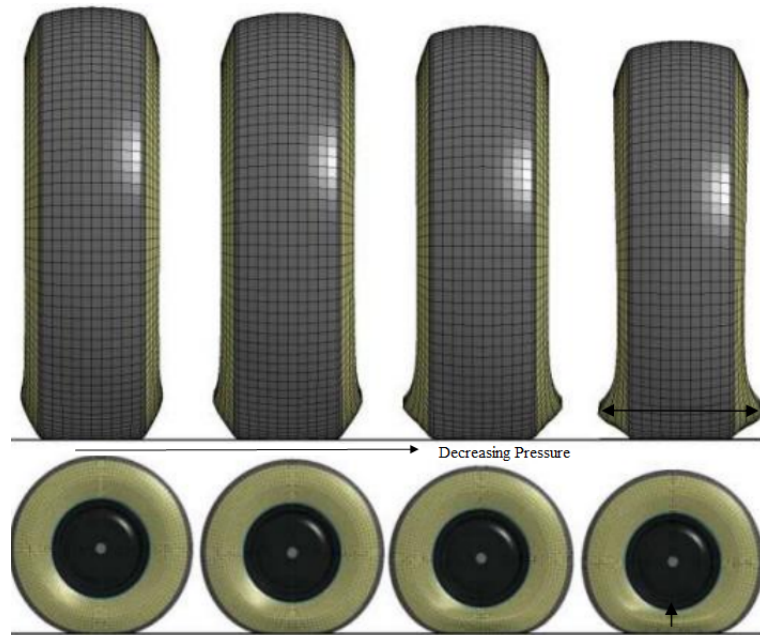


Figure 2.11: Change in wheel deformation with changing tire pressure (Lakušić and Brčić2011, Lakušić and Brčić2011)

This pictorial representation can be explained graphically using Figure 2.12.

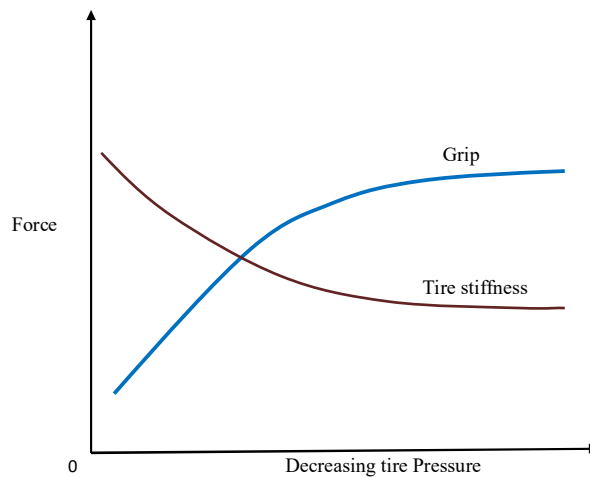


Figure 2.12: Variation of tire stiffness and grip with reducing tire pressure

As the tire pressure decreases, the size of the contact patch increases and hence the grip increases. The tire stiffness however reduces and eventually might not be enough to support the weight of the car.

The actual vibration frequency on the other hand however has to be measured due to complexities involved. In this research the vibrations were measured on the vehicle floor. This was done at the different speeds and on different road surfaces so as to accurately analyze the system behavior. The overall RMS value of vibration amplitude measured was used to give an indication of the severity of vibration.

2.1.10 Previous Works on Piezoelectricity Generation from Vehicles

A lot of research has been done on the possibility of generating power from normal day to day movements (Priya2007, Priya2007). Energy harvesting within the tire has been of greatest interest in the recent past for the purpose of powering sensors such as Tire Pressure Monitoring (TPMS) sensor, Vehicle Speed Sensor (VSS), Strain monitoring sensor etc. (Anil and Sreekanth2014, Anil and Sreekanth2014).

Anil and Sreekanth (Anil and Sreekanth2014, Anil and Sreekanth2014), used PZT wafers in shoes to convert mechanical walking energy into usable electrical energy. This system produced 1.3 mW at 3 V when walking. The same concept was applied in a bicycle as reported by Minazara et al. (Minazara et al.2008, Minazara et al.2008). Vibration accelerations and frequencies were measured and analysis done at various points on the bicycle before settling on the exact location to mount the harvester. Among the areas tested included; below the saddle, the frame, handle bars and later the spoke. The fork recorded the highest value of vibrations. Similarly in the case of a vehicle its expected that vibrations will be quite high on the wheel and probably on the chassis and suspension spring. However, considering that piezoelectric materials

respond to strains and not just vibrations alone, the tire surface which is in direct contact with the actuating road (as was used in the current research) should provide better strains and at higher frequencies.

Priya (Priya2007, Priya2007), performed an experiment on a cymbal with a 29 mm diameter, a 1 mm thickness under a force of 7.8 N and at a frequency of 100 Hz. At this frequency and force level, a power of 39 mW was generated from the cymbal, which was measured across a 400 k Ω resistor. The frequency produced from a tire at an average speed of 40km/hr (in the current research) was expected to be in this range, which means an application of 6000 similar cymbals in each car tires would likely give substantial power translating to 1 kW power from four such tires any time of the day or night.

Khameneifar and Arzanpour (Khameneifar and Arzanpour2008, Khameneifar and Arzanpour2008), carried out a research on energy harvesting from pneumatic tires using piezoelectric transducers. The PZT material that was fixed inside the tire was modeled as a cantilever beam in its first mode of vibration. The absence of direct compression of the element in this model led to very low power generation of a maximum of 2.95 mW for each stack using 30 k Ω load. This power was only sufficient for wireless sensors applications. In the current research, the cantilever model was avoided in favor of a new model involving elastic compression between outer surface and an introduced inner tube in order to improve performance.

Sadeqi et al. (Sadeqi et al.2015, Sadeqi et al.2015), improved the cantilever model in (Khameneifar and Arzanpour2008, Khameneifar and Arzanpour2008) by supporting

the piezo-electric element on the rim using four springs. This significantly increased the frequency bandwidth of the energy harvester allowing it to operate efficiently over a wide range of frequencies (48 - 62 rad/sec). The system however still did not perform as predicted due to absence of direct compression as was the case in the original cantilever model by Khameneifar and Arzanpour (Khameneifar and Arzanpour2008, Khameneifar and Arzanpour2008). This gave more reason to abandon the cantilever model in the current research.

Makki and Popiliev (Makki and Popiliev2011, Makki and Popiliev2011), carried out a research on piezoelectric power generation in automotive tires, to harvest power for use in operating pressure sensors or even run on-board devices. PZT and PVDF elements were bonded to various parts of the tire's inner liner. These elements then generated a maximum of 4.6 mW of power at a load resistance of 46 k Ω and a rotational wheel speed of 80 rpm roughly equal to 9 km/h. This bonding approach however still could not generate enough power for any use other than sensors. The reason for this being any additional increase of piezoelectric elements gave rise to challenges in holding them on the surface. In the current research the piezoelectric elements were placed between the inner and outer tube which allows for inclusion of several elements without bonding challenges.

Keck (Keck2007, Keck2007) proposed a new design of a piezoelectric generator to be used in a tire. In this new design, a metal-piezo bimorph structure was used to allow higher deflections in compressive stress direction of the piezo than it would be possible in tensile stress direction. The actual power generated was however only

15% of the predicted power due to mounting inefficiencies. Applying a pre-stress in this cymbal design could reduce the deviation between simulated results and that from the physical system by improving on physical coupling between the source of excitation and the piezoelectric element by upto 76% (Palosaari2017, Palosaari2017). This cymbal harvester was however not tested in the current research because it was not available in the market, instead the concept it employs of pre-stress was applied on the discs by means of an inner tube. The other difference was that whereas (Palosaari2017, Palosaari2017) designed their harvester for shoes, in this research the harvester was designed for car tires.

Valentin and Koyanagi (Valentin and Koyanagi2013, Valentin and Koyanagi2013), evaluated the energy harvestable from an airless tire equipped with piezoelectric bi-morphs on the lamellar spokes. In this research, 18 watts was generated from the spokes and data analysis showed that the longer the piezoelectric element along the spoke, the more the power generated due to increase in the harvesting material. This therefore suggests that the increase in the number of active piezoelectric elements is the key to higher power generation. The proposed research will take into consideration this finding by trying to maximize the number of elements fixed within a given volume.

Anil and Sreekanth (Anil and Sreekanth2014, Anil and Sreekanth2014), simulated piezoelectric power generation from tires using simulink software. In this research a constant force was assumed. Eventually it was concluded that, the normal forces available on the tire contact patch of the vehicles are sufficient to generate energy to

power the on board electronics and be able to recharge the batteries of Electric Vehicles if an efficient assembly/system is designed.

Manla et al. (Manla et al.2009, Manla et al.2009), proposed a new non-resonant piezo-electric transducer for powering pressure sensors in tires. The generator consisted of a tube with a piezoelectric beam mounted at each end. This tube allowed a small ball bearing to move freely, in response to forces acting on it and hence, impact on the piezoelectric beam. Even though this approach improved power production considerably, the system was too bulky and hence the more reason to try out the pre-stressed design.

Behera et al. (Behera et al.2015b, Behera et al.2015b), proposed a piezo-electric model consisting of frustum piezo-electric modules placed at the tube-tire interface. This design however was abandoned at the simulation stage due to challenges fabricating the prototypes. In our research, the above frustum model was be abandoned in favor of disc elements which are both safer to the tire as well as readily available.

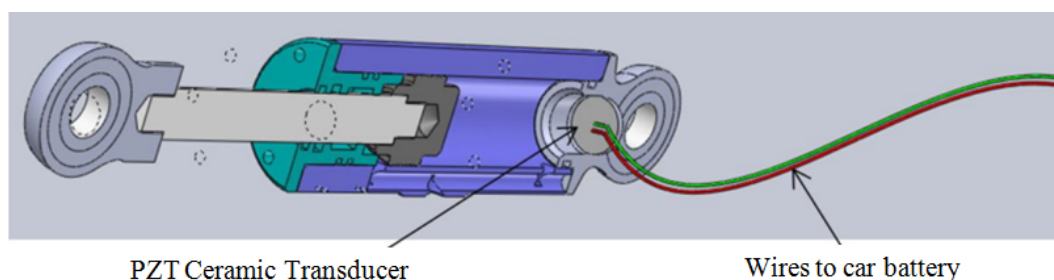


Figure 2.13: Piezoelectric shock absorber (Santoleri et al.2014, Santoleri et al.2014)

Santoleri et al. (Santoleri et al.2014, Santoleri et al.2014), developed an optimized piezoelectric shock absorber to serve as an additional energy source for electric and hybrid cars as shown in Figure 2.13. This design was estimated to have a lifespan of

5-10 years and would reduce the fuel consumption by 2-8% depending on the road condition. The actual power output was 25 watts in a lab setup. The current research therefore did not look at power harvesting from a shock absorbers and instead targeted the applicability of the same concept in car tires to avoid repetition. Though the two researches are quite different in terms of the targeted part of the car and the mode of operation (pure vibrations versus cyclic loading), it was desired that the lifespan matches the one estimated by Santoleri et al above.

2.2 Use of Simscape

Simscape is a programming environment for modeling, simulating and analyzing multi-domain systems developed by Mathworks company (Mathworks2007, Mathworks2007). This software makes it possible to rapidly model physical systems spanning mechanical, electrical, hydraulic and other physical domains while exploiting the capabilities of the original Simulink and MATLAB softwares. This is done by assembling the software-provided fundamental building blocks into a schematics based on the actual physical connections that exist in the components. Anil and Sreekanth (Anil and Sreekanth2014, Anil and Sreekanth2014) in their research on possible power generation from car tires, observed that Simulink a predecessor of Simscape was very highly suited for determining the mechanical forces experienced in any given tire. Behera et al. (Behera et al.2015b, Behera et al.2015b) on a quest to establish the best shape of a piezoelectric element for optimal power harvesting in car tires observed that Simscape was a very efficient way to predict the forces experienced at the tire-road interface dur-

ing actual driving. The above observations as well as simplicity is what motivated its selection as the modeling software for vehicle driving behavior.

In order to complete the simulation using Simcape, one has to specify the vehicle parameters as well as give information about the road surface being used. Simscape requires that the road surface be specified by means of an input signal which could be a step input, ramp input, combination of signals etc. In this study a sine wave input signal of amplitude 0.05 m was selected as recommended by Shirahatti et al. (Shirahatti et al.2008, Shirahatti et al.2008). This recommendation by Shirahatti follows their extensive involvement in industrial design fabrication and testing of racing car suspension systems, where they observed that this particular signal always gave the best output from simulink without much complexities.

Even though Simscape was adopted for the reasons listed above, it does have a few limitations, the main being the computational speed. With large power systems, the state-space solver used by the Simulink in Simscape can become really slow because of the software real-time constraint (less than 1000 buses) making it inefficient (Enockson2011, Enockson2011).

2.3 Use of COMSOL Multi-physics

COMSOL Multiphysics is a cross-platform finite element analysis, solver and multi-physics simulation software developed in 1986 by Svan te Littmarck and Farhad Saeidi in Sweden (Comsol1998, Comsol1998). It is composed of several modules classified into Electrical, Mechanical, Fluid, Chemical, Multipurpose, and Interfacing. One very attractive property of COMSOL is that it has an ability to couple any number of physics

phenomena together and input user-defined physics descriptions, with associated equations and expressions, directly in the graphical user interface. Together with the dedicated MEMs module which features piezoelectricity allow for unlimited creativity in a way that is a lot harder with traditional approaches. Badr et al.(Badr et al.2015, Badr et al.2015) in a desire to predict the electrical power harvestable from different mouse motion, found out that COMSOL was the most widely accepted software for piezoelectric simulation. This is because it is powerful and with an interactive interface. Farnsworth et al. (Farnsworth et al.2014, Farnsworth et al.2014) went on to specifically evaluate the capability of COMSOL'S piezoelectric module. At the end of the study, they concluded that for all the five experiments they did, optimal piezoelectric energy harvester designs were developed that matched the desired frequency response of 250 Hz in the real world. Madhuranath et al.(Madhuranath et al.2014, Madhuranath et al.2014) in their research on piezotires observed that as of 2014, COMSOL was the only software that could solve almost all problems in multi physics systems and create the real world of multi physics systems without varying their material properties. A quick inspection of COMSOL further reveals that there is a provision to customize the code to a specific requirement by linking the software to Matlab which makes it very powerful and yet highly adaptable. This software was therefore selected as the simulator of choice with piezo-electricity in this research for the same reasons mentioned above.

In order to use the software for Piezoelectric simulation, one must specify the following information in Figure 2.14

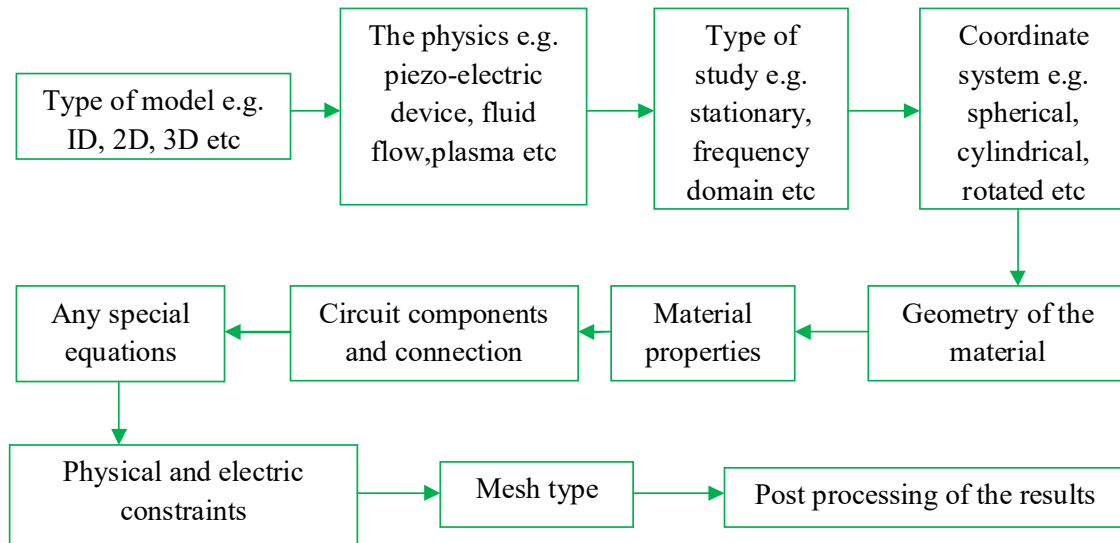


Figure 2.14: Information fed into COMSOL software

Eventually the results are given in the form of 3D diagrams, tables and different plots as specified by the user

2.4 Summary of Gaps

It is evident that though a pre-stress has been found to improve piezoelectric power generation (by up to 72%), this concept has not been tried out in car tires. This pre-stress has previously been used to address some of the challenges facing the implementation of the low profile piezoelectric energy harvesting system including: low power density, average reliability and cost effectiveness (Pieter2013, Pieter2013). This research therefore pursued this idea by exploring the performance of a new piezo-electric tire model featuring a pre-stress in its design, in an effort to develop further the application of piezo-electricity in automobiles.

It is also evident that non of the researchers reviewed in this research has successfully mounted a piezoelectric wheel on a vehicle and tested it. The current research therefore

also sought to successfully extract power from a running piezoelectric tire in actual operation as would be done once commercialized.

CHAPTER THREE

3.0 METHODOLOGY

3.1 Introduction

The primary aim of this research was to design and test a piezoelectric-lined tire whose PZT5A elements are assembled with a pre-stress instead of the widely used cantilever design. The variation in power production with changes in road condition was to be established in order to guide future application of pre-stressed elements in automobiles. The results further needed to be compared with those obtained for a PZT fitted suspension system which is at the time, the best piezoelectric energy harvester designed for a vehicle (Santoleri et al.2014, Santoleri et al.2014). To achieve these goals, a Nissan Wingroad DBA Y12 car that uses 185/70R14 tires was selected since it was available. This car was then modeled using Simscape 2017 in order to predict the kind of forces expected at the proposed harvester location. The harvester itself was then modeled using COMSOL multiphysics in order to decide on the best size of harvester to use. Eventually these elements were procured, fixed on a tire and tested.

3.2 Modeling of the Vehicle Using Simscape

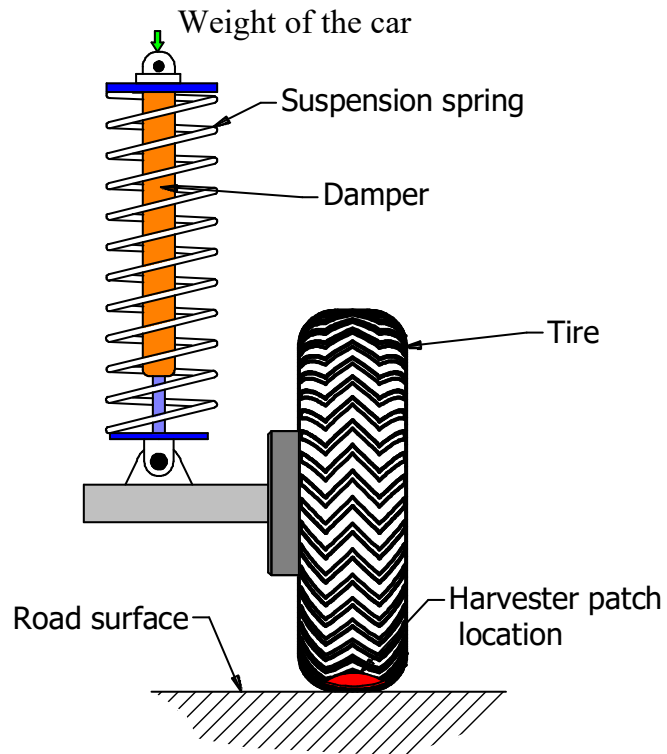


Figure 3.1: Physical model of the car

Using Figure 3.1 as the reference, the vehicle was modeled as a combination of springs, dampers and masses as shown in Figure 3.2. This model was selected with the assumption that the vehicle could be accurately simplified into lumped parameters represented by Mass, spring constant and damping coefficients as is the practice. The tire used was a new 185/70R14 tire with a pressure of 30 psi. The 185/70R14 tire was selected because it is the tires used by the test car selected and 30 psi is the recommended tire pressure.

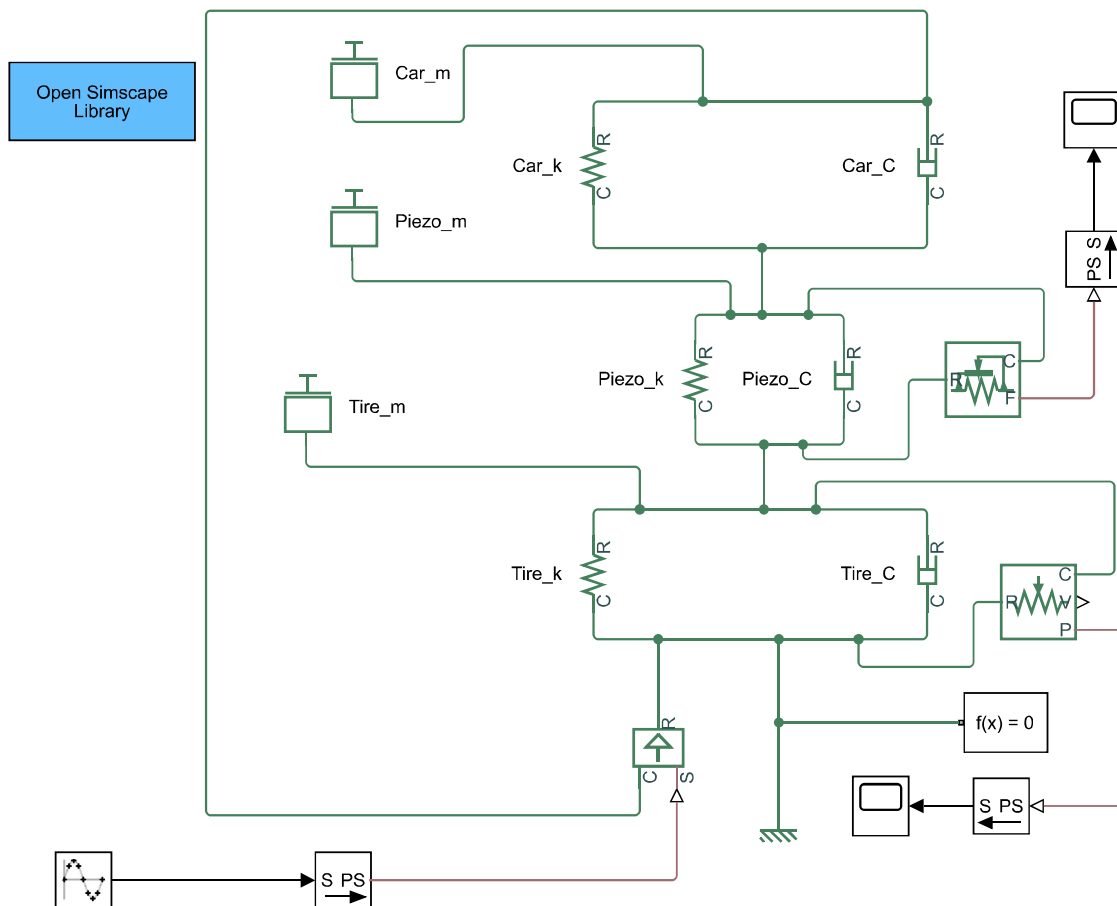


Figure 3.2: Model of car with piezoelectric tire in simscape

Where Car_m is the gross mass supported by one front tire, Car_k is the spring constant of the suspension spring, Car_C is the damping coefficient of the suspension system, $piezo_m$ is the weight of a single harvester plus the protection layer, $piezo_k$ is the spring constant of the harvester, $piezo_C$ is the damping coefficient of the harvester, $tire_m$ is the weight of the tire, $tire_k$ is the spring constant of the pressurized tire and $tire_C$ is the damping coefficient of the pressurized tire. Other symbols are explained in appendix VI.

The approximated values of these parameters from information provided by the respective manufacturers are shown in table 3.1. This was based on the part specification

of the car model selected.

Table 3.1: Parameters used in Simscape model

<i>Description</i>	<i>Symbol</i>	<i>Unit</i>	<i>Quantity</i>
<i>Mass Supported by one tire</i>	<i>Car_m</i>	<i>Kg</i>	3.25×10^2
<i>Spring stiffness of suspension</i>	<i>Car_k</i>	<i>N/m</i>	3.27×10^4
<i>Damping coefficient of suspension</i>	<i>Car_C</i>	<i>N/(m/s)</i>	2.31×10^2
<i>Mass of harvester</i>	<i>Piezo_m</i>	<i>Kg</i>	5.00×10^{-3}
<i>Spring stiffness of harvester</i>	<i>Piezo_k</i>	<i>N/m</i>	3.50×10^4
<i>Damping coefficient of harvester</i>	<i>Piezo_C</i>	<i>N/(m/s)</i>	1.33×10^{-2}
<i>Mass of tire</i>	<i>Tire_m</i>	<i>Kg</i>	1.63×10^1
<i>Spring stiffness of tire</i>	<i>Tire_k</i>	<i>N/m</i>	1.48×10^5
<i>Damping coefficient of tire</i>	<i>Tire_C</i>	<i>N/(m/s)</i>	3.86×10^7

In this study a sine wave input signal of amplitude 0.05 m was applied because it best represents excitation from most roads and has been previously used satisfactorily by researchers (Shirahatti et al.2008, Shirahatti et al.2008).

3.3 Modeling of Piezoelectric Element in COMSOL

The piezoelectric element was modeled in COMSOL 5.2 software as a 3D circular disc of radius 25 mm (most available disc diameter on the market) and thickness of 0.3 mm (arbitrary value before doing a parametric sweep over other thicknesses) as shown in Figure 3.3.

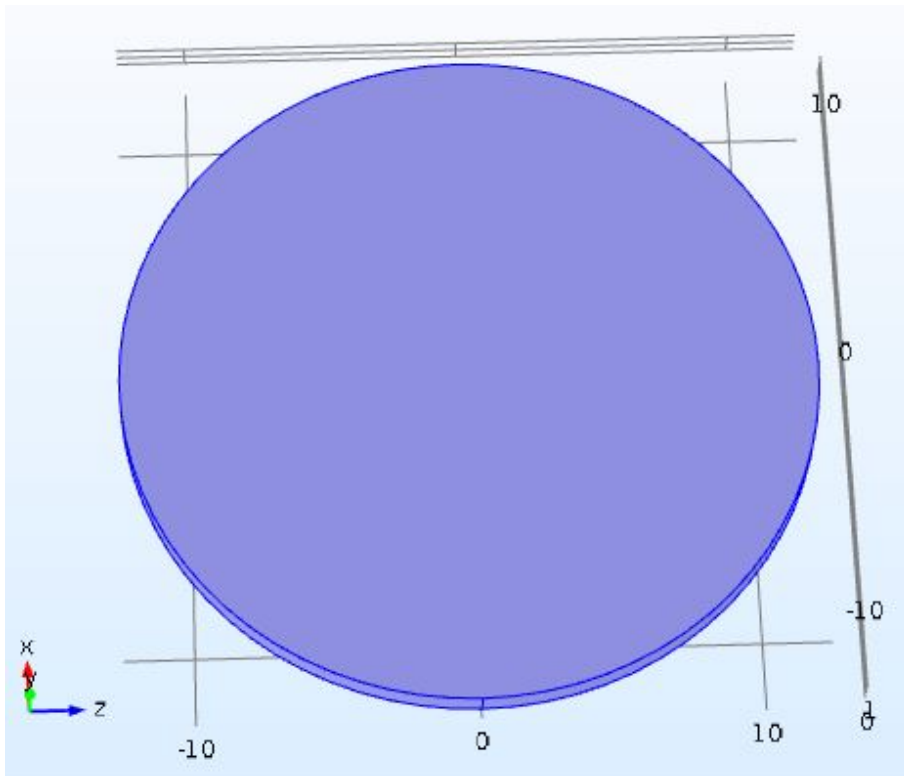


Figure 3.3: Piezoelectric disc model

To achieve this, piezoelectric module was selected in the COMSOL modeling wizard and stationary study selected from the available study options. A fixed constraint was then applied on one side of the disc in order to load the remaining side. Having established from Simscape that the force expected on each individual disc would be F_{load} Newtons, a varying boundary load starting from 60% F up to 140% F was applied on the opposite side. The selection of 60% F to 140% F was guided by the desire to load the element 40% above and 40% below the computed value in order to cater for road variations.

In order to evaluate electrical properties, one side of the disc was grounded. A swept tetrahedral mesh was then applied as shown in Figure 3.4. The tetrahedral mesh was selected because it best analyzes thin sections and sharp edges like the edges of the

discs used in this research (Behera et al.2015b, Behera et al.2015b).

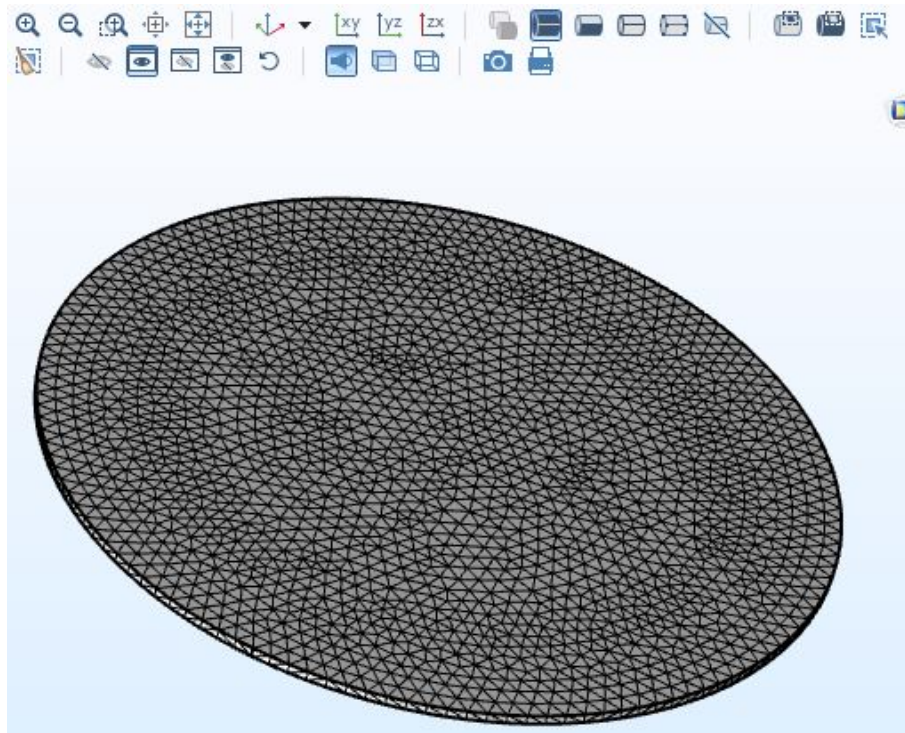


Figure 3.4: Meshed piezoelectric disc

This was followed by a parametric sweep on disc thickness and applied load. The parametric sweep was done in order to evaluate the effect of varying the disc thickness and applied force on voltage and consequently the power output. The power output per unit volume for each of the thicknesses was then computed and plotted. The plotted graphs from this simulation are what determined the optimum element size to use in the experimental tests (impact test and road test). This was done by reading off the element thickness that gave out the highest power per unit volume. In addition to power output, this simulation gave stress and voltage distribution plots.

To establish the power given out by a given disc, a resistor of 47 k Ω was connected to the two faces of the disc to represent the load and the simulation repeated. This simulation as well as the one done in section 3.2 only required the simulation to be

run once. This is because due to the nature of the simulations, the output was always definite.

3.4 Development of the Experimental Model and Testing

3.4.1 Discs Used

Based on the simulation explained in the previous sections, two types of piezoelectric discs were selected because maximum power output per unit volume was found to occur at two different locations on the graph.

1. Disc 1 Was 25 mm in diameter, 0.3 mm thick backed with a 0.2 mm thick brass plate as shown in Figure 3.5 a.
2. Disc 2 Was 25 mm in diameter, 2 mm thick with no backing plate as shown in Figure 3.5 b.

The piezoelectric material selected for both discs as earlier mentioned in the literature review was PZT 5A.

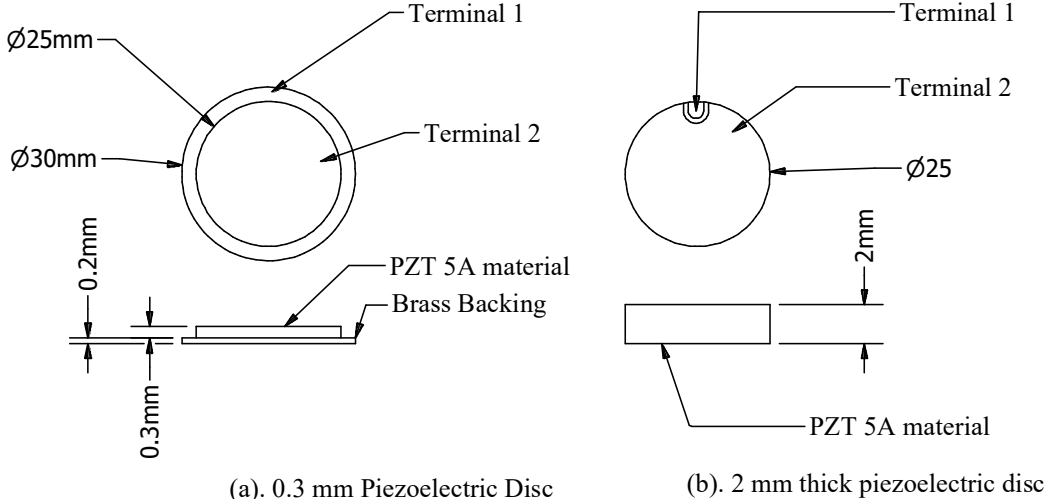


Figure 3.5: Dimensions of selected discs

3.4.2 Wiring of The Discs

The different piezoelectric elements (as established from the earlier mentioned simulation) were soldered into arrays of 6 (based on space limitation) parallel connected discs as shown in Figure 3.6 and 3.7. The six members in each array were connected to each other via short flexible connecting wires in such away that each disc was provided with two alternative paths through which the output is obtained. This ensured that in case any of the connection fails, the power production from the patch is not adversely affected. Two individual arrays were in turn connected in series with each other via similar flexible connecting wires to form a cluster of 12 as illustrated in Figure 3.7.

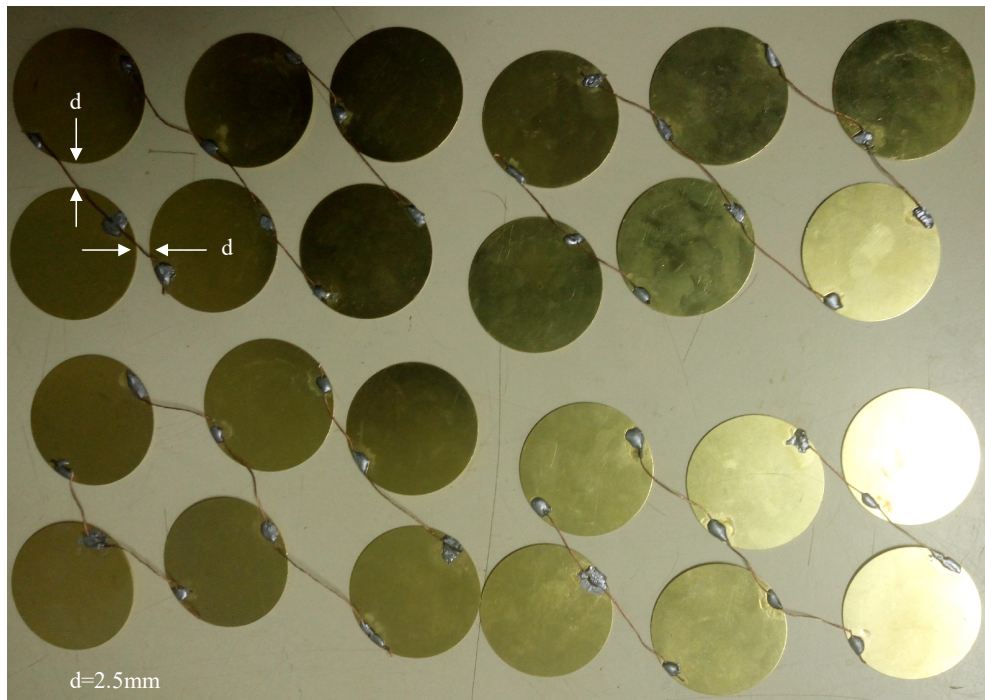


Figure 3.6: Wiring of the piezoelectric elements; Rear View.

3.4.3 Assembly of the Patch-tire Units

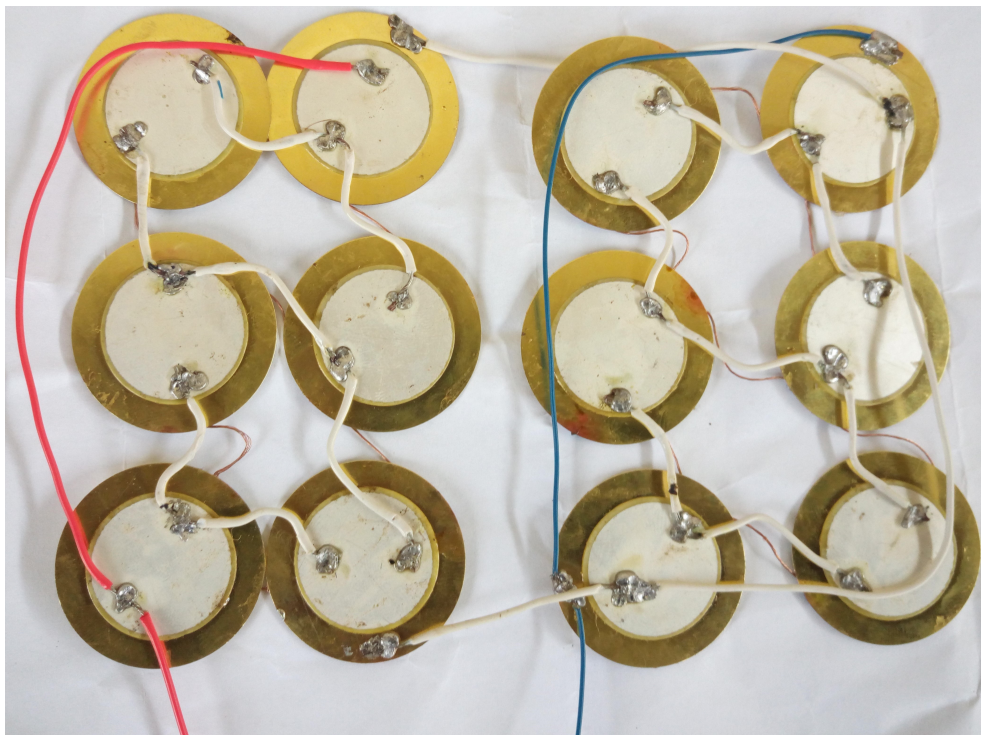


Figure 3.7: Assembly of the piezoelectric elements; Front View.

Flexible wires between elements were chosen as opposed to soldering the discs directly to each other for two reasons:

1. To reduce the effect of the disc array on the deformation pattern of the tire
2. To minimize chances of joint failure since the tire is expected to experience severe bending and impact forces

After developing the element assembly above, each cluster of 12 was provided with its separate rectifier, then encased with heat glue (Ethylene-vinyl acetate). The purpose of this heat glue blanket on the elements include:

1. It protects the elements from each other's sharp edges.

2. Protect the tires surface from the disc's sharp edges which under high pressure can easily transform into shear cutters
3. Reduce chances of short circuiting when in operation by keeping the elements at a fixed distance from each other
4. Develop a patch that can be easily moved from one tire to another or retrieved in case it is damaged
5. Provide each element with an extra layer of damping to protect it from excessive impact forces expected in the course of operation

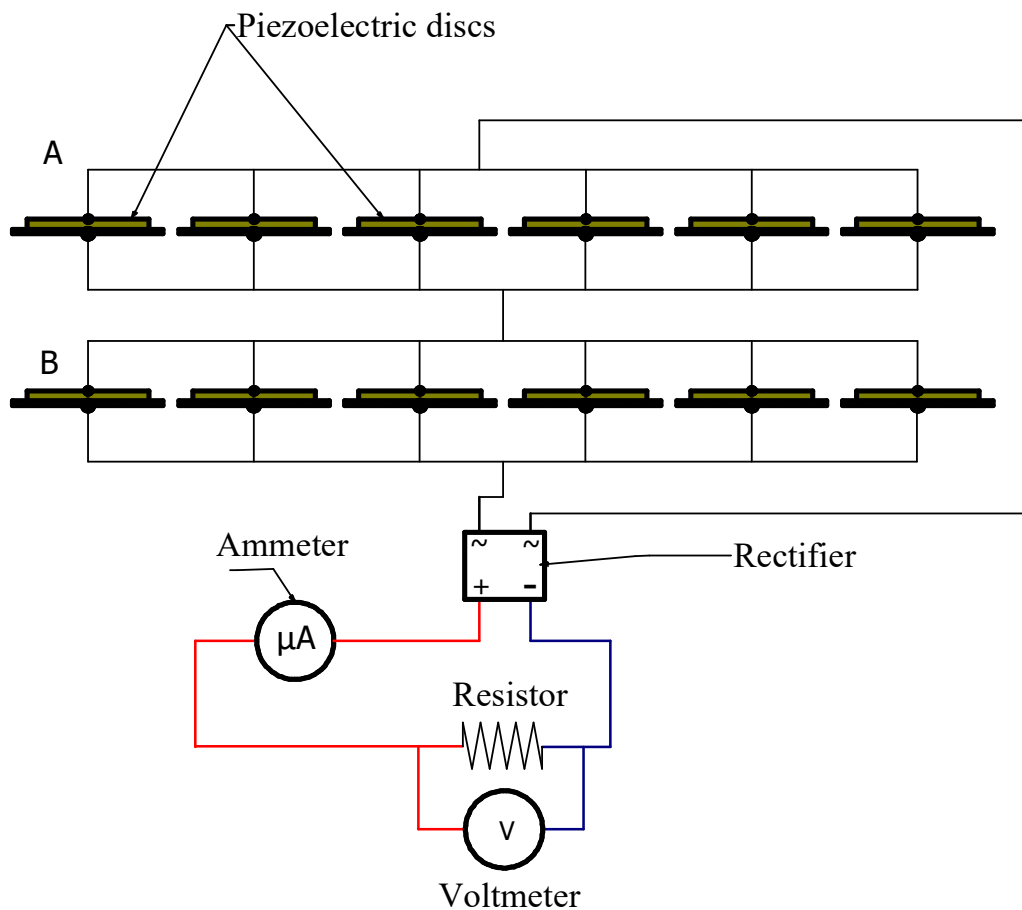


Figure 3.8: Power harvesting circuit diagram

Figure 3.8 shows the circuit diagram for including the measuring instruments, where

the piezo discs are the harvesters used and A & B are the two arrays connected in series to each other. Two tires were then assembled. For the first tire, contact glue was applied between the tire and the patch. For tire 2, the patch was placed between the tire and an introduced inner tube without any additional adhesive. This was done in order to provide a comparison between the performance of the pre-stressed element and the regularly installed elements. The tire was then pressurized to hold the patch in place. Figure 3.9 shows the glued patch in the tire.



Figure 3.9: Gluing of the piezoelectric patch in the car tire

3.4.4 Terminals Through the Rim

In order to extract electric power from a pressurized tire, two connections with the following properties were required.

1. Insulated from the tire rim as well as from each other to prevent short circuiting
2. Airtight to prevent leakage from the tire
3. Rigid to withstand the expected vibrations in a moving car tire
4. Physically safe to the tire and the introduced inner tube

This was achieved by drilling two holes in the rim and introducing two nozzles labeled N2 and N3 as shown in Figure 3.10



Figure 3.10: Introduced electric terminal-nozzles for power harvesting

Inside these nozzles, connecting cables were screwed (from inside the tire) as shown in Figure 3.11 which were then connected to the elements placed in the tire for all subsequent testing.

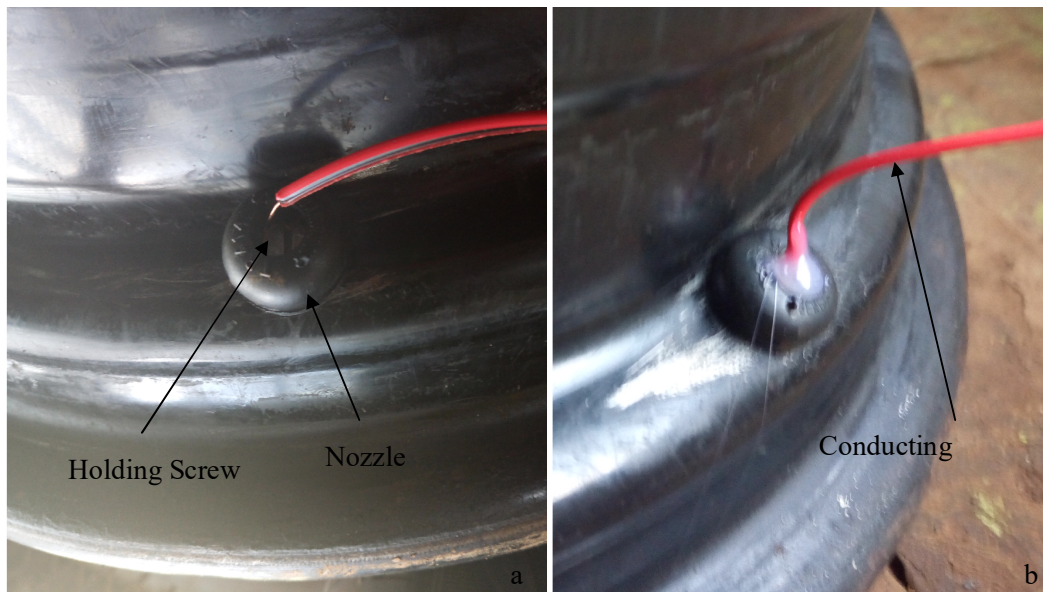


Figure 3.11: Connection of cables in the nozzles

Figure 3.12 is a section drawing through the nozzle showing the connection used inside

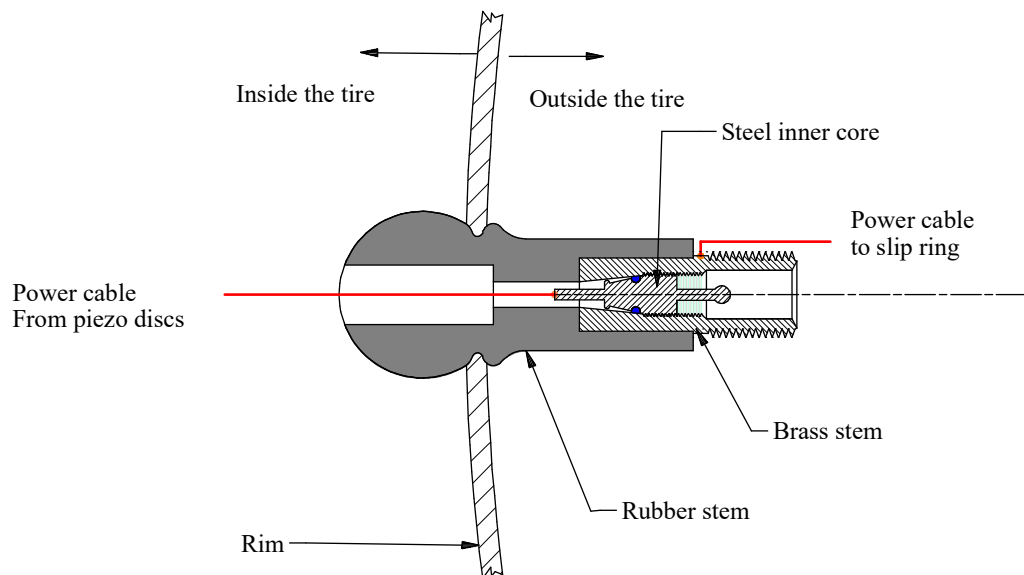


Figure 3.12: Section drawing of the nozzle as modified in the current research

To deliver the power at the terminals into the vehicle, a slip ring was fabricated for coupling with a stationary brush on the car body. This was fabricated from a 2 mm

thick mild steel plate using a nibbling machine and mounted as illustrated in Figure 3.13. Copper is preferable but was left out due to cost implications in relation to the available research funds.

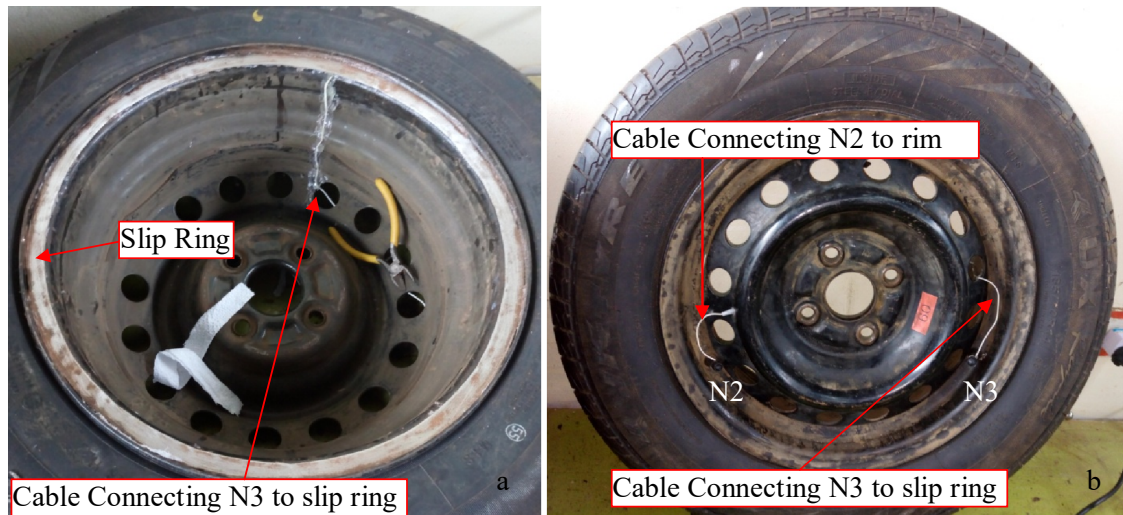


Figure 3.13: Slip ring mounted on the tire

3.4.5 Power Delivery into the Inner Vehicle Compartment

For the power to be tapped effectively from the patch in the tire, the negative terminal from the harvesting circuit was connected to the vehicle body through the rim as earlier indicated. The positive terminal on the other hand was connected to the slip ring. This made it necessary to fabricate a spring loaded harvesting brush which is electrically isolated from the vehicle frame. The working drawings for this probe are indicated in appendix III,IV and V and the fabricated probe was as shown in Figure 3.14.

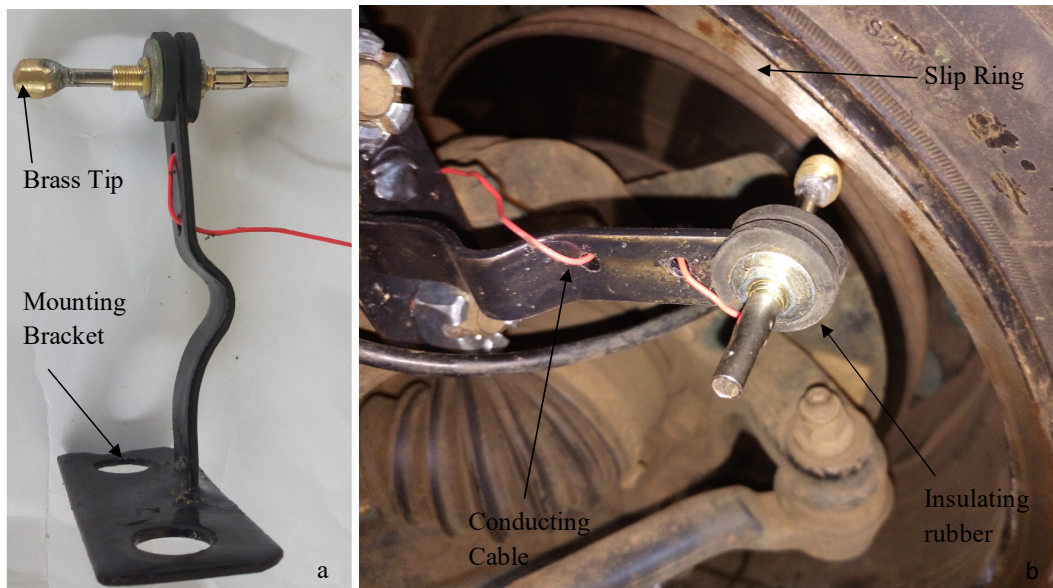


Figure 3.14: Power harvesting probe

The entire circuit diagram was as shown in Figure 3.8.

3.4.6 Stationary Tests

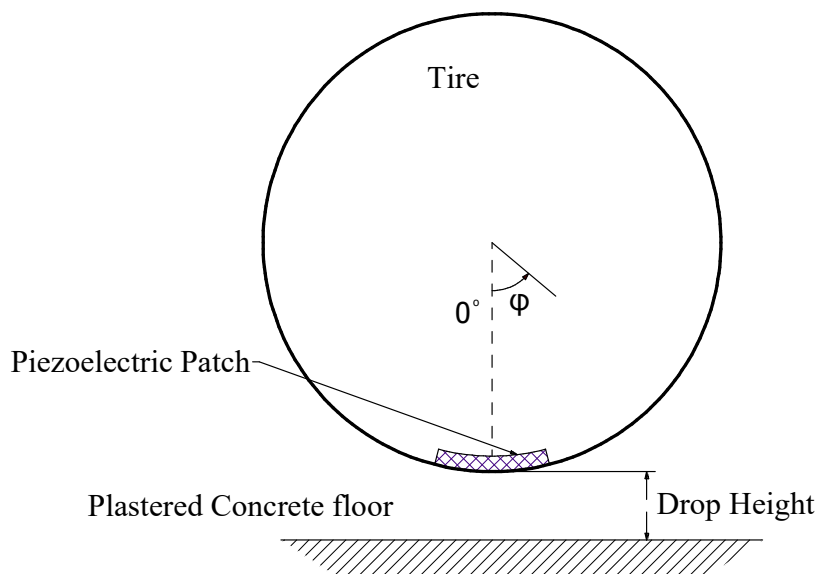


Figure 3.15: Initial angular position of the patch in the tire

Before mounting the assembled tires to a vehicle for a drive test, the tires were taken through a series of tests to establish their behavior beforehand. This was done by dropping the tire from pre-determined heights (2 cm, 4 cm, 6 cm, 8 cm, 10 cm and 12

cm) and measuring the peak output voltage and current. Figure 3.15 shows the angular position of the harvester at the beginning of the test. In order to determine the actual impact forces, following relation was used:

$$F_{impact} = \frac{m.g.h}{d} \quad (3.1)$$

Where F_{impact} is the impact force (N), m is the mass being dropped (Kg), g is the gravitational acceleration constant (m/s^2), h is the height of drop (m) and d is the tire compression after impact (m).



Figure 3.16: Tire deflection measuring probe

This equation however requires that the tire deflection after impact is measured once inflated to the operation pressure (30 psi). This was done using a self made telescopic probe with the capability to instantaneously change length by the deflection on impact.

This probe is shown in Figure 3.16. The stationary tests for the specified range of drop heights were done in three different ways:

1. With the tire constantly at 30 psi and patch constantly at 0°
2. With the tire constantly at 30 psi for varying patch positions
3. With the patch constantly at 0° position but varying tire pressures

During these tests, the peak output electrical properties (current and voltage) were recorded using two AVD-830D universal multi-meters with a load of 47 kΩ. To measure the peak out values a digital video camera was used to capture the displayed current and voltage simultaneously then later on recorded in an excel sheet for processing.

This data was used to compute the power by means of equation 3.2

$$Power = Voltage \times Current \quad (3.2)$$

3.4.7 Road Tests

The piezoelectric tires were fixed on a DBA-Y12 Nissan Wingroad and the vehicle taken for a drive on different terrains and at different speeds. During this drive, five parameters were recorded

1. Road inclination in degrees using a digital inclinometer level box
2. Voltage across a 47 kΩ resistor using a universal multimeter
3. Current in the above circuit using a universal multimeter
4. Vehicle vibrations due to road surface unevenness using a TES 3101 vibration

meter operating in data log mode

5. Vehicle speed using a GPS speedometer installed on an android platform

The digital inclinometer (Model 1-LR03(AAA)1.5V) as well as the accelerometer for the vibration meter (model TES 3101) were both mounted on the vehicle floor and the data recorded continuously during the drive. Figure 3.17 shows the actual equipment appearance.

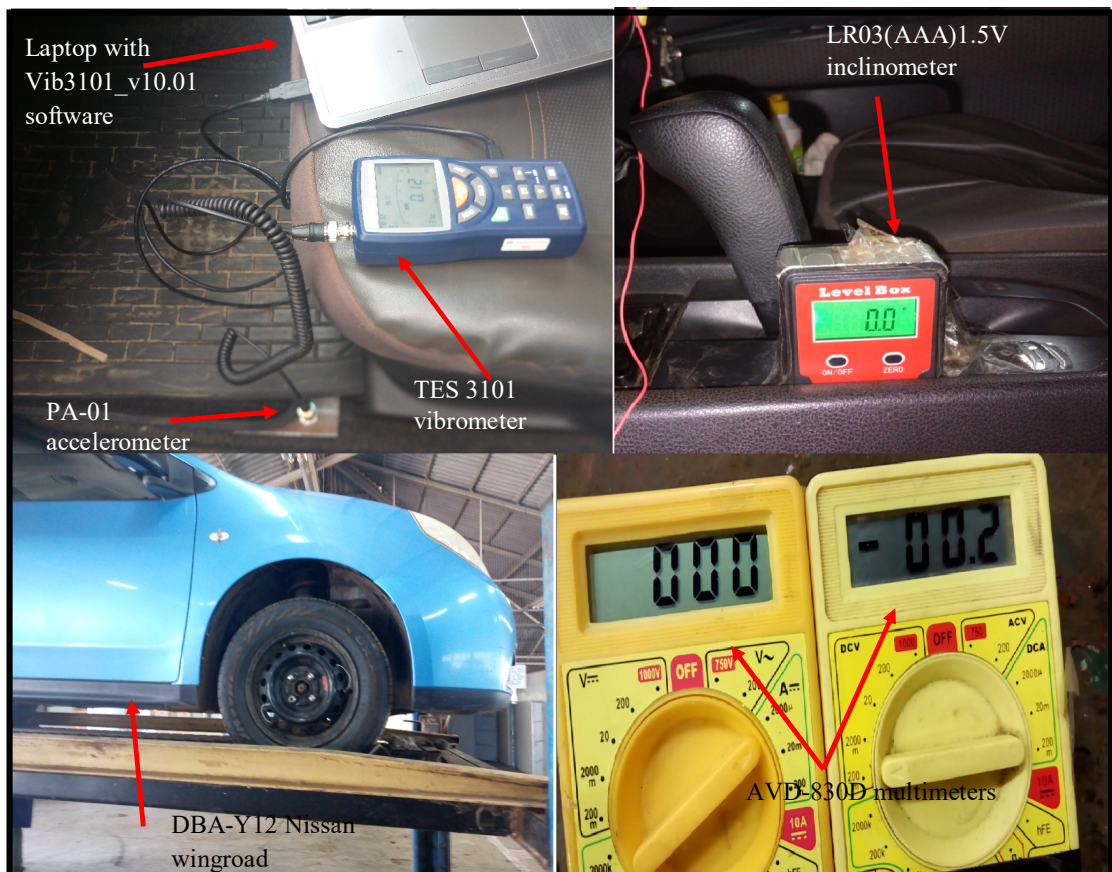


Figure 3.17: Equipment used during the experimental tests

Since the vibration recorded was already damped (It is impractical to mount the vibration meter on the tire surface), it means the only change in amplitude and frequency was of interest and not the absolute value of amplitude.

CHAPTER FOUR

4.0 RESULTS AND DISCUSSION

4.1 Introduction

This chapter presents the results obtained from simulation as well as experimental testing of the developed piezoelectric wheels. The finite element analysis (FEA) simulation results will be discussed in relation to how they influenced piezoelectric element selection for the physical testing as well as their performance. Results from experimental stationary testing of the selected elements in the laboratory will then be presented, and finally the results from road tests will be presented and discussed particularly how they compare with previous similar tests done by other researchers.

After the Simscape simulation with piezoelectric discs assumed to be at the 0° position, the plot shown in Figure 4.1 was generated.

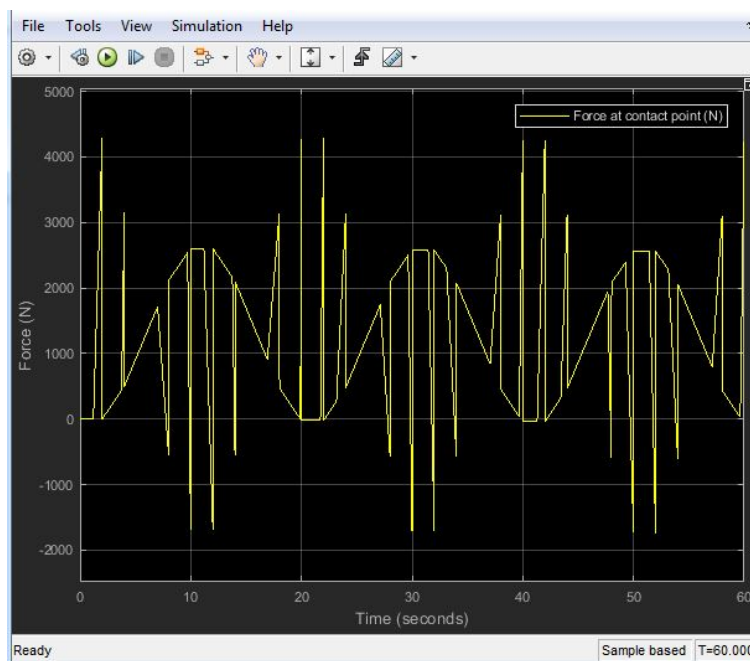


Figure 4.1: Screen shot of simulation showing force variation at the point of contact

From the simulation results, the force at the contact patch traces the input sine wave signal but along the way has sharp rises and sharp drops as shown in Figure 4.1. This is because starting from rest, the acceleration due to the sine wave encounters spring and damper next to the ground, giving the graph the first spike which is the highest because of the inertia force. Next, the sine acceleration encounters the second spring and damper on its way which gives the graph the second spike. However the first spike having set the entire system on an upward displacement, this second spike is slightly smaller than the first one. The effect of this occurrence is that the whole system (tire assembly and the car itself) now accelerates upwards faster than the signal. At this point, the second (main) damper pulls the system back to the signal resulting in the first down-shoot in force due to tension. The first damper then has to finish the pulling of the entire system back to the signal giving the second down-shoot (which is bigger). The sine wave at this point pushes the system to reach the peak and starts to decelerate. Again the damper next to the ground pulls the entire system to follow the signal which gives the third down-shoot, then the second damper pulls it which accelerates the system downwards faster than the signal. This downward acceleration is again stopped in two stages just like the upward acceleration and the process goes on and on.

From Figure 4.1, it is deduced that a maximum force of 4.3×10^3 N is expected at the contact area of the system. To get this value, the Simscape software used applies equations 2.4 all the way to 3.1 but with a sine input in order to solve for the force, eliminating the need to repeat the same kind of computation manually. By direct mea-

surement, the contact area of the above 185/70r14 tire was found to be $0.024m^2$ (at 30psi and the car weight of 325 Kg). From physics,

$$Contact\ point\ Pressure = \frac{Force}{Area} \tag{4.1}$$

Using equation 4.1 above, the pressure in the tire carcass at the contact point is found to be 179.2 kPa. This is done with the assumption that every reaction(from the road) is accompanied with an equal and opposite reaction. Selecting a disc diameter of 25 mm which is the most common in the market, the force on each disc is found to be 50.26 N. A range of forces 20 N above and 20N below this value (30 N-70 N) was used for the next study for reasons earlier explained in the methodology section 3.3.

The adopted range of values from Simscape was applied in COMSOL as explained in the methodology section3.3. A 3D solid stress distribution plot was generated from this operation as shown in Figure 4.2.

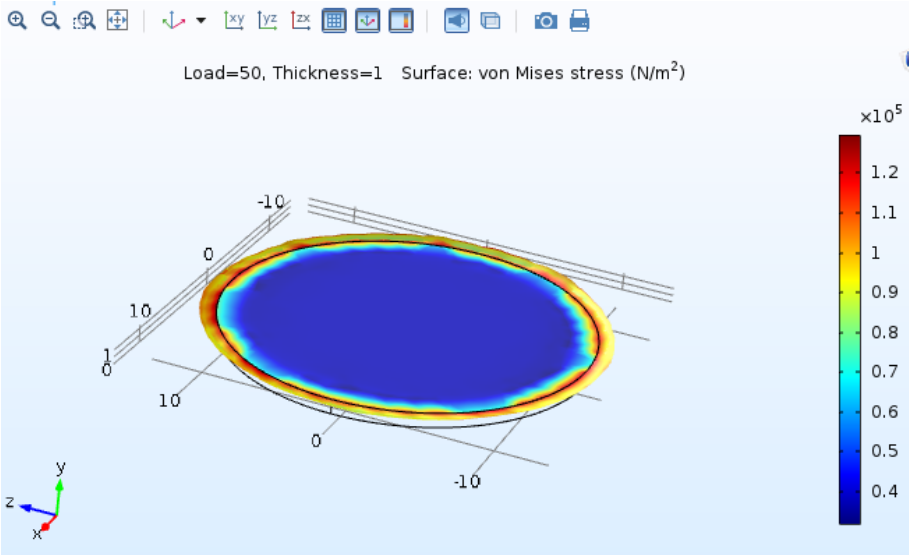


Figure 4.2: Stress distribution in the piezo electric disc after loading

Figure 4.2 revealed that maximum stress when a disc is loaded uniformly, occurs close

to the edges. This observed stress distribution could be due to the fact that when a solid disc is axially loaded uniformly, then the only direction the material within can escape is towards the edge. It then follows that the material at the edges will experience the greatest deformation since it experiences the least restriction to its deformation. Since strain is directly proportional to stress (Timoshenko1959, Timoshenko1959), it then follows that this region will experience some of the highest Von Mises stresses in the disc.

The observed simulated distribution can also be explained in terms of expected hoop and radial stresses. Maximum hoop stress (tensile in nature) when a solid disc is compressed, is expected to occur at the edge of the disc. This is because the edge stretches the most since all the material within the disc works to stretch the outer most layer. Similarly maximum radial stress (compressive in nature) is expected to occur towards the edge. This again is because all the material within the solid disc has to push against the material towards the edge when the disc is loaded axially. At the edge itself the radial stress is however zero since there is no more material ahead to be pressed against. Therefore, since the axial stress remains constant throughout the cross section, it then follows that maximum effective stress (Von Mises stress) must occur towards the edge because that is where all the extremes occur

This observation suggests that if a PZT element working under compression was to fail while in use by crushing, then the failure is very likely to start around the edge. Consequently when soldering terminals on these discs, the edges of the disc ought to be avoided in order to give the element a better lifespan.

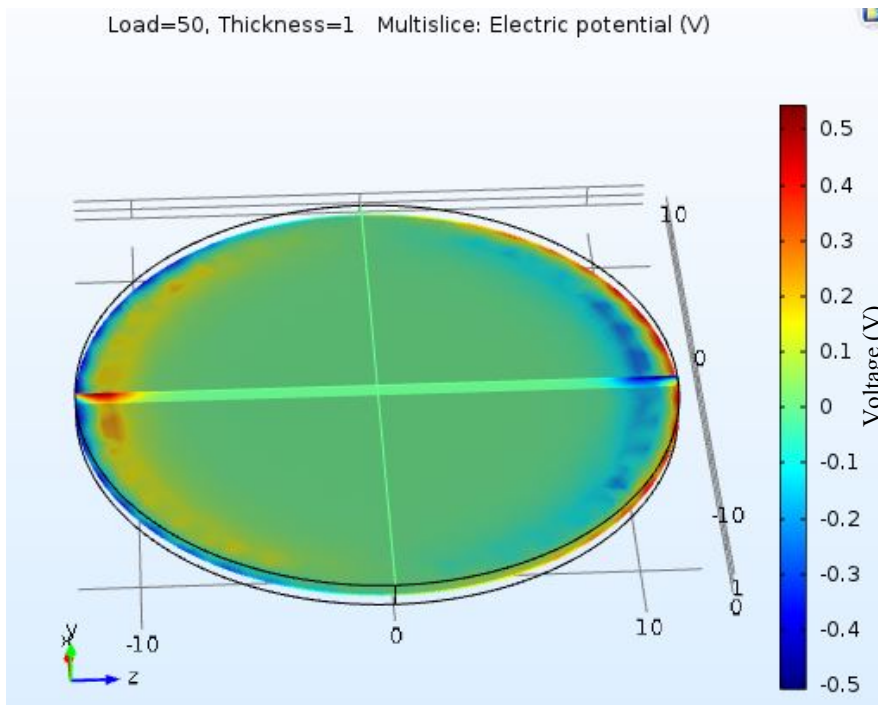


Figure 4.3: Electromotive force distribution plot

From the same simulation a voltage distribution plot for the element was generated as shown in Figure 4.3. As expected, the highest potential difference occurred at the edges of the disc where compressive stress was maximum. Makki et al. (Makki and Popiliev2011, Makki and Popiliev2011) carried out a similar study to establish the best disc design for maximum power generation. They found out that for any disc of fixed thickness and diameter, the output is higher when the disc has a frustum shape thus increasing the length of the edge that produces the highest power intensity. It is therefore more beneficial to use several small diameter discs in a tire as opposed to a large disc. The smaller discs increase the ratio of edges in the assembly to the overall volume. As a result the regions experiencing maximum pressure in the assembly increase leading to generation of higher emf. This observation was taken into consideration in this research, and as a result 12 small diameter plates used (diameter 25mm) in each

patch.

A series of disc thickness was evaluated to establish the effect on produced power, as shown in Figure 4.4.

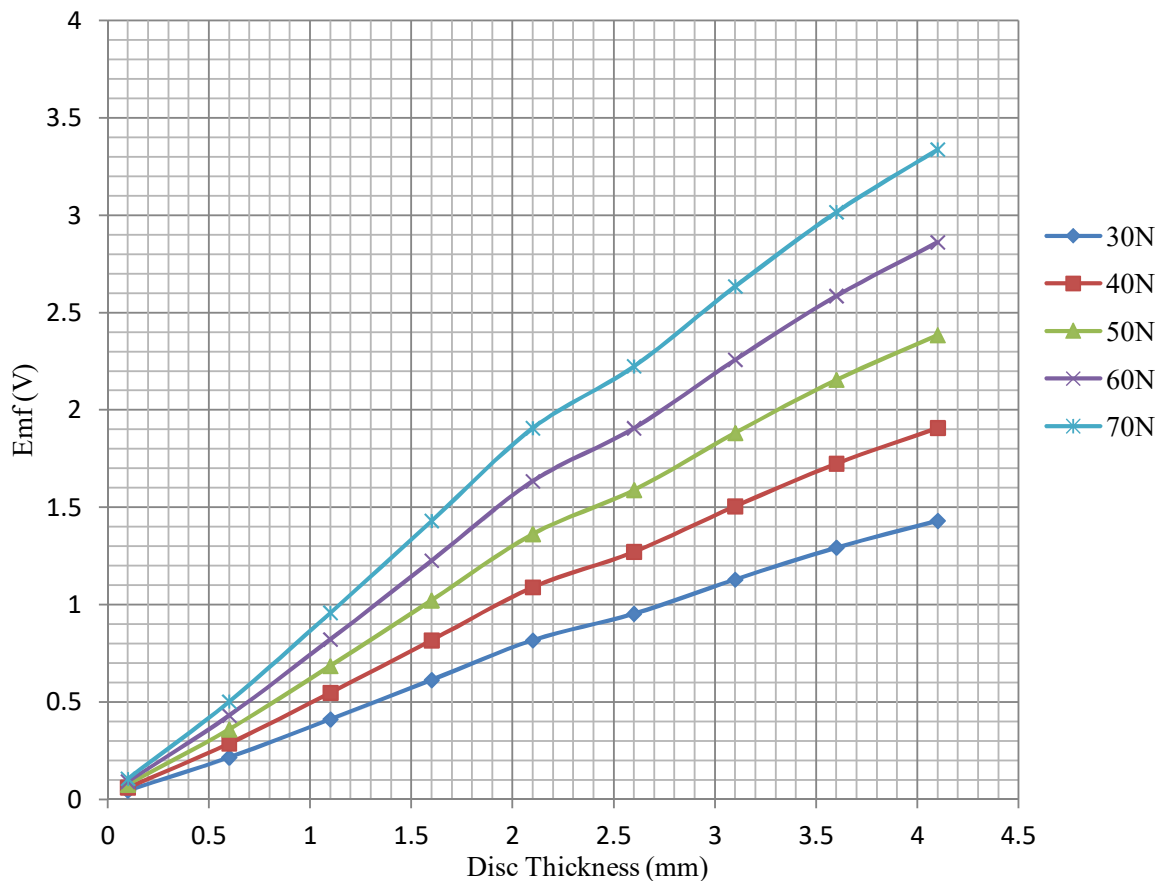


Figure 4.4: Variation of Voltage generated with element thickness for different forces

From Figure 4.4 it was observed that as the applied force increased, so did gross power production irrespective of the element size. This phenomenon was also reported by Mohamad et al (Mohamad et al.2015, Mohamad et al.2015) who observed that, as strain increases in any piezoelectric material, the resultant local charge separation increases and consequently, the power output also increases. Figure 4.4 also showed that the forces expected in the rotating tire are below levels likely to damage the piezoelectric elements (the exact forces were not available from the manufacturers/literature)

such that the electrical output vanishes completely. This data from the COMSOL simulation was processed further to see variation in voltage generated per unit volume as shown in Figure 4.5.

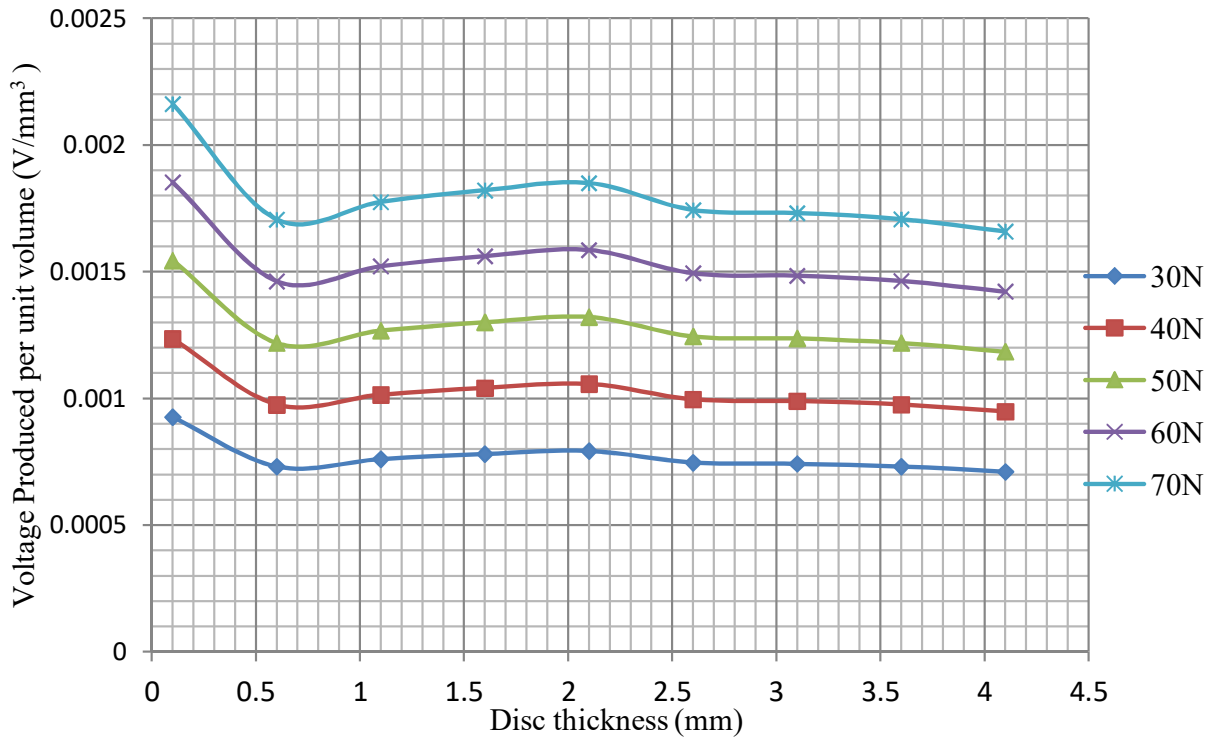


Figure 4.5: Variation of voltage generated per unit volume with element thickness for different forces

From Figure 4.5, it was observed that the most efficient piezoelectric disc elements are those of thickness 0.1-0.4 mm followed by those of 2 mm thickness (by visual inspection). Currently no other research has been presented on this property of PZT materials. The observation could however be attributed to the increased effectiveness of the poling process for thin materials making them better generators per unit volume than thicker ones. It could partially also be due to the higher ratio of high stress regions to the volume ratio as earlier discussed

In the 0.1 - 0.4 mm thickness range, the most readily available elements are the 0.3 mm

size due to their better physical stability compared to thinner ones. For this reason the 0.3 mm thick and 2 mm thick piezoelectric discs were selected for use in the current research.

4.2 Stationary tests for 0.3 mm Thick Disc

The 0.3 mm thick disc was found to give out 0.6 m Watts from simulation. This subsection presents the preliminary tests done on the the pre-stressed tire in the lab with the same disc size embedded in it to establish its characteristics before mounting on the vehicle.

4.2.1 Drop Test of the Tire with an Inner Tube and Elements Between Inner Tube and Tire Carcass

The pre-stressed tire assembly with the patch placed between the inner tube and tire carcass was taken through a drop test as outlined in the methodology section 3.4.6 . This was done so that the quality of the tire can be verified prior to mounting on a moving vehicle.

Table 4.1: Impact force developed for the 16.25 kg tire at 30 psi pressure

$Mass(kg)$	$h \times 10^{-2}(m)$	$d \times 10^{-2}(m)$	$F_{impact}(N)$
16.25	2	0.45	708.5
16.25	4	0.70	910.9
16.25	6	0.90	1062.8
16.25	8	1.05	1214.6
16.25	10	1.20	1328.4
16.25	12	1.35	1417.0

In order to relate the mentioned heights of fall with the resultant impact force, equation 3.1 was used. The computed impact forces were as shown in Table 4.1

These values were henceforth adopted for all computations for the tire having 30 psi

pressure. For the same tire when operated at a different pressure, a table similar to table 4.1 was prepared. The electrical output flowing from the tire during the test was connected to a resistor of 47 kΩ through a KBP206 full bridge rectifier.

4.2.1.1 Power generation by elements at the 0° position

This tire was then taken through the complete drop test (2 cm to 12 cm at intervals of 2 cm) with the patch positioned directly at the contact point which is considered the zero degrees position. The results were as shown in table4.2.

Table 4.2: Drop test for tire with inner tube with patch at 0° position

<i>Drop(cm)</i>	<i>F_{impact}(N)</i>	<i>Voltage(V)</i>	<i>Current(mA)</i>	<i>Power(mW)</i>
0	0.0	0.00	0.00	0.00
2	708.5	2.64	0.61	1.61
4	910.9	3.20	0.83	2.66
6	1062.8	4.44	0.92	4.08
8	1214.6	3.97	1.47	5.84
10	1328.4	3.83	1.55	5.94
12	1417.0	3.85	1.55	5.97

This data was plotted as shown in the graph in Figure 4.6 and the equation of the best fitting trend line extracted using Microsoft excel.

From this plot, the power output from the piezoelectric patch increases steadily with increasing impact force up to 1200 N after which the output remains more or less constant at 6 mW. This translates to 0.5 mW per disc. From simulation the disc had given out a peak of 0.6 mW with the same electrical load which means there is still room for improvement particularly with the rectifier used. Maximum power output occurring at 8 cm drop height (which corresponds to 1200 N) however doesn't mean maximum power output when the tire is mounted on a car will occur when the car drives through

an 8 cm pothole. Rather it means maximum power output will be witnessed when the tire experiences the corresponding force of 1200N.

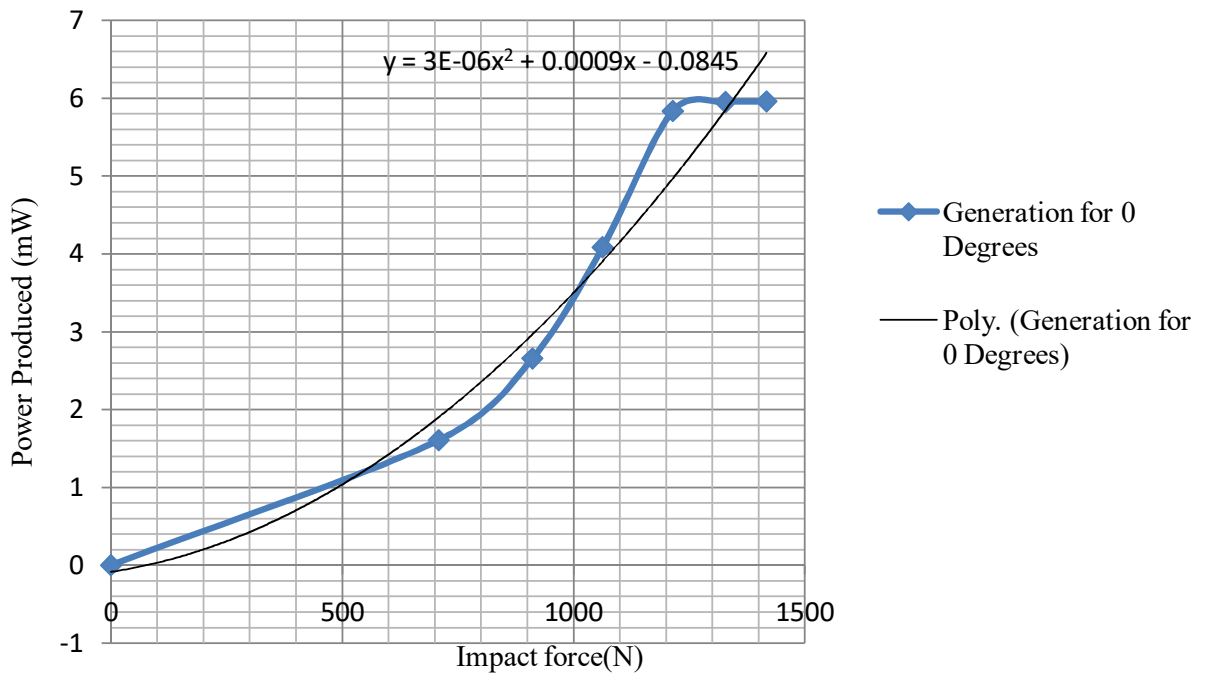


Figure 4.6: Variation of power output with impact force for patch positioned at $\psi = 0^\circ$

This means even on a perfectly flat road since the tire is going through cyclic loads as a result of the weight of the vehicle, maximum power will be produced provided that the car moves at a speed above 45 km/hr as will be seen in the next section. From the test drive results (in the next section as well), potholes and irregularities in the road however enables the piezoelectric elements in the tire to generate the maximum output even at speeds much lower.

The results as seen in Figure 4.6 suggest that with the adopted piezoelectric discs specifications, the patch only needs a force of 1200 N in order to give out its maximum power production. Any additional force above 1200 N should be accompanied with introduction of an additional layer of harvesters if more power is to be produced.

This observation could be due to the fact that any given piezoelectric material of a given size has a maximum and definite number of dipoles that can be created when the load applied is limitless (Piyush2016, Piyush2016). Therefore when the applied force goes beyond the value required to create the available dipoles, the extra force is wasted because the output can not go beyond the maximum possible for that harvester size. As the force applied increases further, internal short circuiting starts taking place which is accompanied with a drop in output and at times, total damage of the harvester (Garimella et al.2015, Garimella et al.2015). From the same graph in Figure 4.6, the power production can be approximated by a polynomial trend-line of degree 2, which is represented as shown in equation 4.2

$$P_{0^{\circ}} = \frac{3q^2}{10^6} + \frac{9q}{10^4} - 0.0845 \quad (4.2)$$

Where P_o is the power output of the patch in mW and q is the force at the contact patch.

This output is however for the entire patch composed of 12 discs. To get the output per disc, equation 4.2 is divided by 12 to give equation 4.3.

$$p_{0^{\circ}} = \frac{2.5q^2}{10^7} + \frac{7.5q}{10^5} - \frac{7}{10^3} \quad (4.3)$$

As seen in Figure 4.6, this equation is true for $1 \leq q \leq 1200N$. It is good to point out that since q includes the weight of the tire under consideration, it can never have a value of zero.

4.2.1.2 Power generation by elements at points away from 0° position

In order to approximate the total output for a given tire, the contribution from elements located at other positions other than the contact point was evaluated and added. The test done to get the the data in table 4.2 was done for angular position $\psi = 10^\circ, 20^\circ$ degrees all the way to $\psi = 180^\circ$ in steps of 10° and results plotted as shown in Figure 4.7

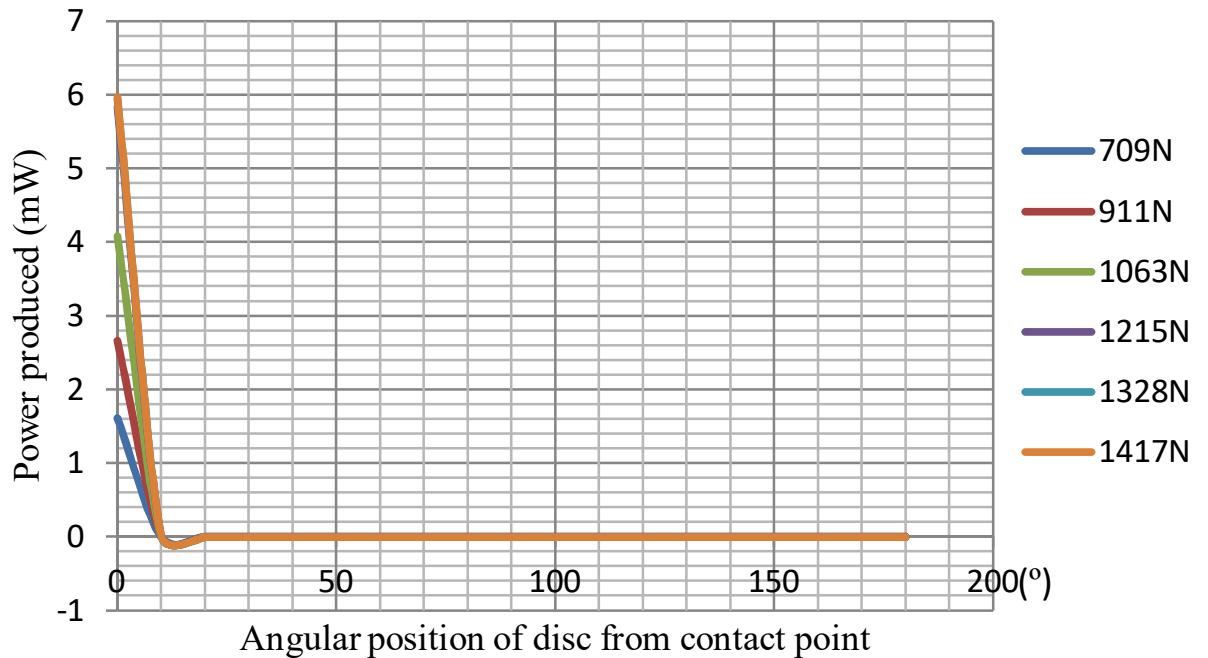


Figure 4.7: Power production at various angular positions from contact point

From Figure 4.7, the maximum generation of piezoelectric power occurs between $\psi = 0^\circ$ and $\psi = 10^\circ$. This is because the intensity of change in tire deformation as well as tire-surface vibrations is highest at this (contact) point. This region therefore requires the greatest attention when sizing a piezoelectric tire for a given application. The same area also experiences the highest variation in generated power with changing impact force. Based on this observation the power generations needs to be evaluated

independently for the $\psi=0^\circ$ position, $\psi=10^\circ$ position $\psi=20^\circ$ position and $\psi=20^\circ-180^\circ$ region before coming up with a generalized formula.

Since $\psi=0^\circ$ has already been done as represented in Figure 4.6, $\psi=10^\circ$ becomes the next point of interest.

4.2.1.3 Power generation by elements at 10° position

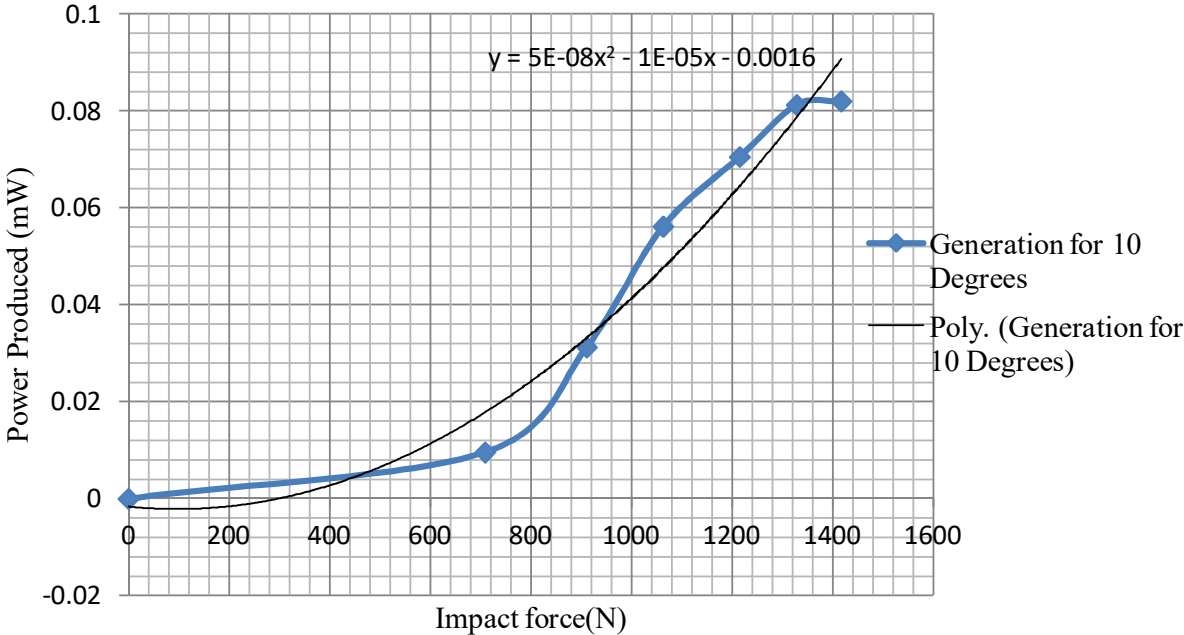


Figure 4.8: Variation of power output with changing impact force for patch positioned at $\psi = 10^\circ$

Similar to $\psi=0^\circ$, a plot of power against impact force when the patch is positioned at the $\psi=10^\circ$ position is as shown in Figure 4.8. The selection of the 10° position in this case is based on the deductions from section 4.2.1.2.

Similar to the patch at $\psi=0^\circ$ position, the power output from the piezoelectric patch at $\psi=10^\circ$ increases steadily with increasing impact force. This time round the increase however continues all the way to 1400N as opposed to the 1200N witnessed earlier. This could be attributed to the cushioning effect within the tire between the zero de-

grees position (where the force originates) and the new location of the patch which reduces effective magnitude of disturbance reaching the new position. The power output also levels out at a very low value of 0.08 mW which is 1.33 percent of the output witnessed when the same element is at $\psi=0^\circ$ position. This power production can be approximated by a polynomial trend-line of degree 2 (it is the closest to the plot made), which is given by:

$$P_{10^\circ} = \frac{5q^2}{10^8} - \frac{q}{10^5} - 0.0016 \quad (4.4)$$

Where P_{10} is the power output of the patch in *mW* and q is the force at the contact patch.

This output is however for the entire patch composed of 12 discs. To get the output per disc, equation 4.4 is divided by 12. This action gives equation 4.5

$$p_{10^\circ} = \frac{4.17q^2}{10^9} - \frac{8.33q}{10^7} - \frac{1.33}{10^4} \quad (4.5)$$

Where p_{10} is the power output per disc. This equation holds true for $1 \leq q \leq 1400N$.

4.2.1.4 Power generation by elements at 20°-180° position

For easier analysis of the peak power for angles between $\psi=20^\circ$ and $\psi=180^\circ$, a scatter diagram is plotted as shown in Figure 4.9, and a trend line that best captures the scatter plotted as shown. This approach is selected since these values as seen from Figure 4.7, are very close to each other in relation to the outputs observed for the positions $\psi=0^\circ-10^\circ$. From Microsoft excel, the trend line on the figure is described by equation

4.6:

$$P_{20^{\circ}-180^{\circ}} = -\frac{4\psi^4}{10^6} + \frac{4\psi^3}{10^5} - \frac{\psi^2}{10^4} + \frac{\psi}{10^6} - \frac{2}{10^5} \quad (4.6)$$

Where ψ is angular position of the patch measured from the contact point in *Radians* and q is the force at the contact patch.

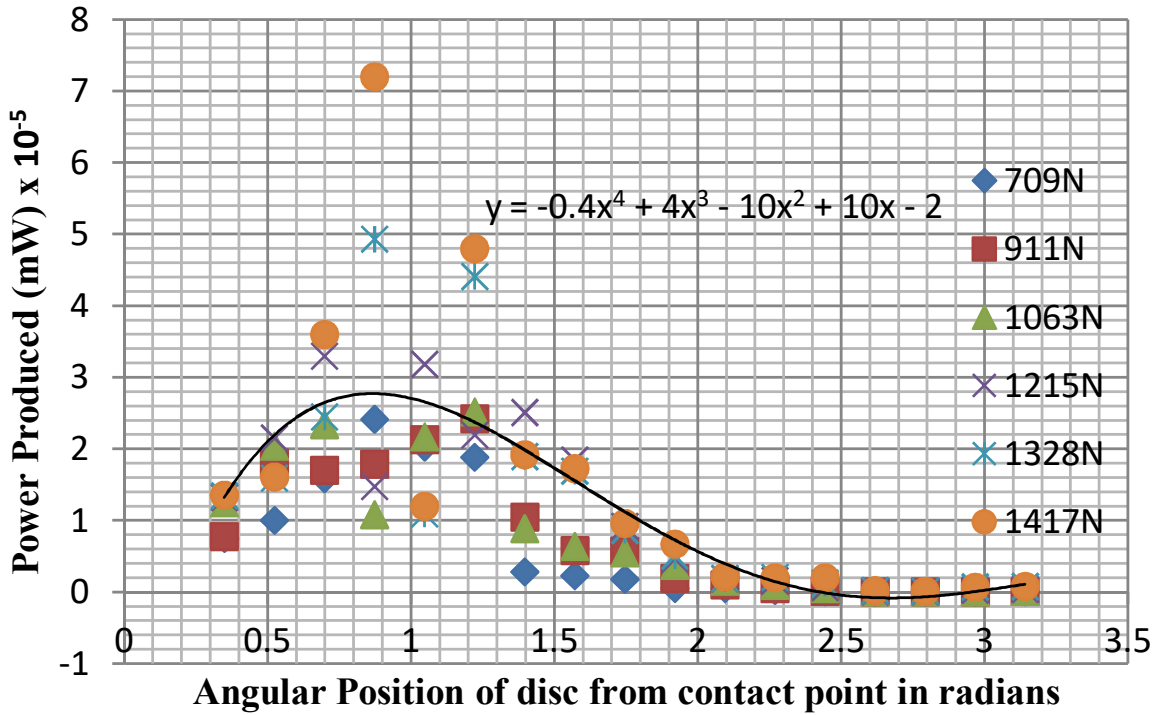


Figure 4.9: Variation of Power output with angular position for patch positioned at 20°-180°

For the 20°-180° interval it is observed that the maximum power is now produced at around 45° whereas for the full 0°-180° interval maximum power is generated at the 0° point. This could be because at the 0° location the element is directly at the source of the disturbance and at 45° location the tire experiences a slight bending effect due to the interaction between the weight of the upper half of the tire and the reaction acting on the lower part of the tire as a result of the impact with the ground. It follows that

peak power produced per element will be given by:

$$P_{10^\circ-180^\circ} = -\frac{3.33\psi^4}{10^7} + \frac{3.33\psi^3}{10^6} - \frac{8.33\psi^2}{10^6} + \frac{8.33\psi}{10^6} - \frac{1.66}{10^6} \quad (4.7)$$

4.2.1.5 Total produced power

Based on a visual inspection of the results as presented in Figure 4.7 and observations made during the experiment, the following assumptions can be adopted with sufficient accuracy:

1. For the span $\psi = 0^\circ-10^\circ$, the effect of angular changes is approximately linear and hence the power produced by an element mid way can be taken to be the average of the value calculated for that element separately by equation 4.3 and 4.5
2. For the span $\psi = 10^\circ-20^\circ$, the effect of angular changes is also linear and hence can be taken care of by interpolating the values computed separately by equation 4.5 and 4.7
3. For the span $\psi = 20^\circ-180^\circ$, the effect of changing contact force as the vehicle moves is negligible on the power production observed in elements positioned in this region due to the cushioning effect of the harvesters by the pressurized tire, hence only the effect of varying angular position(which appears to have effect on the power production) needs to be analyzed. Therefore equation 4.7 will be sufficient for this region.

Total power production p_{tot} becomes

$$p_{Tot} = 2 \left(\frac{n_{0^\circ} p_{0^\circ}}{2} + \frac{1}{2} \left(\sum_{i=0^\circ}^{10^\circ} p_{0^\circ} + \sum_{i=0^\circ}^{10^\circ} p_{10^\circ} \right) + n_{10^\circ} p_{10^\circ} + \frac{1}{2} \left(\sum_{i=10^\circ}^{20^\circ} p_{10^\circ} + \sum_{i=10^\circ}^{20^\circ} p_{20^\circ} \right) + \sum_{i=20^\circ}^{180^\circ} p_{20^\circ-180^\circ} \right) \quad (4.8)$$

Substituting equations 4.3,4.5 and 4.7 in 4.8 gives

$$p_{Tot} = 2 \left(\frac{n_{0^\circ}}{2} \left(\frac{2.5q^2}{10^7} + \frac{7.5q}{10^5} - \frac{7}{10^3} \right) + \frac{n_{0^\circ-10^\circ}}{2} \left(\frac{2.5q^2}{10^7} + \frac{7.5q}{10^5} - \frac{7}{10^3} + \frac{4.17q^2}{10^9} - \frac{8.33q}{10^7} - \frac{1.33}{10^4} \right) + n_{10^\circ} \left(\frac{4.17q^2}{10^9} - \frac{8.33q}{10^7} - \frac{1.33}{10^4} \right) + \frac{n_{10^\circ-20^\circ}}{2} \left(\frac{4.17q^2}{10^9} - \frac{8.33q}{10^7} - \frac{1.33}{10^4} - \frac{3.33\psi_{20^\circ}^4}{10^7} + \frac{3.33\psi_{20^\circ}^3}{10^6} - \frac{8.33\psi_{20^\circ}^2}{10^6} + \frac{8.33\psi_{20^\circ}}{10^6} - \frac{1.66}{10^6} \right) + \sum_{i=20^\circ}^{180^\circ} \left(-\frac{3.33\psi^4}{10^7} + \frac{3.33\psi^3}{10^6} - \frac{8.33\psi^2}{10^6} + \frac{8.33\psi}{10^6} - \frac{1.66}{10^6} \right) \right) \quad (4.9)$$

Truncating the small terms in equation 4.9 followed by simplification gives:

$$p_{Tot} = \left(n_{0^\circ} \left(\frac{2.5q^2}{10^7} + \frac{7.5q}{10^5} - \frac{7}{10^3} \right) + n_{0^\circ-10^\circ} \left(\frac{2.54q^2}{10^7} + \frac{7.42q}{10^5} - \frac{7.13}{10^3} \right) + 2n_{10^\circ} \left(\frac{4.17q^2}{10^9} - \frac{8.33q}{10^7} - \frac{1.33}{10^4} + 2 \sum_{i=20^\circ}^{180^\circ} \left(-\frac{3.33\psi^4}{10^7} + \frac{3.33\psi^3}{10^6} - \frac{8.33\psi^2}{10^6} + \frac{8.33\psi}{10^6} - \frac{1.66}{10^6} \right) \right) \right) \quad (4.10)$$

Where n_{0° is the number of PZT discs at the zero position, $n_{0^\circ-10^\circ}$ is the number of PZT discs between 0° and 10° position and $n_{10^\circ-20^\circ}$ is the number of PZT discs between 10° and 20° position. Taking an example of the 185/70r14 tire used whose specs are:

Diameter = 614.6 mm

Width =185 mm

The inner diameter of the tire, can be computed by subtracting twice the tire thickness from the outside diameter which gives 594.6 mm. Since each element has a supporting

disc of diameter 35 mm and requires an additional spacing of 2.5 mm, the maximum number of discs that can be fitted on the face of the tire becomes

$$\frac{\textit{Tire Width}}{\textit{Disc Space}} = \frac{185\textit{mm}}{37.5\textit{mm/piece}} = 4.93 \textit{ pieces} \quad (4.11)$$

Four pieces per row is however picked since it would be unsafe to force a fifth element along the face of a pressurized tire. This is because edge of the fifth element would be digging into the side of the tire potentially cutting it open. Similarly the maximum number of rows that can be placed along the perimeter of the tire becomes:

$$\frac{\textit{Tire Circumference}}{\textit{Space taken by one disc}} = \frac{\pi \times 594.6\textit{mm}}{38.5\textit{mm/piece}} \approx 48 \textit{ rows} \quad (4.12)$$

In this case 1mm is added to the previous 37.5mm to account for any possible increase or decrease in the diameter during operation. It then follows that:

$$n_{0^\circ} = 1 \textit{ row} \times 4 \textit{ pieces/row} = 4 \textit{ pieces} \quad (4.13)$$

Since 1° corresponds to a distance of $1868 \text{ mm} \div 360^\circ = 5.189 \text{ mm/degree}$ on the circumference, the segment that remains after placement of the four discs above will be given by:

$$\textit{Remaining angular space} = 10^\circ - \frac{18.75 \textit{ mm} \times 360^\circ}{\pi \times 594.6 \textit{ mm}} = 6.386^\circ \quad (4.14)$$

correspond to 33.14 mm along the circumference which can only accommodate one row(of 4 discs) and spreads to the 10° point though a bigger portion falls in the 0° - 10°

region. The following values can therefore be reasonably adopted

$$n_{0^\circ-10^\circ} = 3 \text{ pieces} \quad (4.15)$$

$$n_{10^\circ} = 1 \text{ piece} \quad (4.16)$$

It can similarly be shown that:

$$n_{10^\circ-20^\circ} = 4 \text{ pieces} \quad (4.17)$$

$\psi_{20^\circ} = 0.349 \text{ radians}$ (4.18) With this information, equation 4.10 can be rewritten to:

$$p_{Tot} = \left(4 \left(\frac{2.5q^2}{10^7} + \frac{7.5q}{10^5} - \frac{7}{10^3} \right) + 3 \left(\frac{2.54q^2}{10^7} + \frac{7.42q}{10^5} - \frac{7.13}{10^3} \right) + 2 \left(\frac{4.17q^2}{10^9} - \frac{8.33q}{10^7} - \frac{1.33}{10^4} + 4 \left(\frac{4.17q^2}{10^9} - \frac{8.33q}{10^7} - \frac{1.35}{10^4} \right) + 2 \int_{\pi/9}^{\pi} \left(-\frac{3.33\psi^4}{10^7} + \frac{3.33\psi^3}{10^6} - \frac{8.33\psi^2}{10^6} + \frac{8.33\psi}{10^6} - \frac{1.66}{10^6} \right) \right) \quad (4.19)$$

After evaluation this equation simplifies to

$$p_{Tot} = \frac{1.787q^2}{10^6} + \frac{5.276q}{10^4} - \frac{5.025}{10^2} \quad (4.20)$$

Where $q \leq 1200N$. Any load above 1200 N should be accompanied with introduction of an additional layer for best performance.

It follows that the number of layers of harvesters required in the tire for maximum power output will be given by:

$$\text{Number of Layers} = \frac{\text{Car's Gross Weight}}{4 \times 1200} \quad (4.21)$$

Where the 4 in the denominator is meant to reduce the weight to that required in a quarter car model.

Therefore the power generation for a 185/70R14 piezoelectric tire with one layer filled with the maximum number of (0.3mm thick, 25mm diameter) PZT 5A elements per layer (192), will have its output given by equation 4.20. For any other type of tire, the power output is given by equation 4.10. It then follows that if we take the example of the Nissan Wingroad car used (weighing 1300 kg), the number of layers that need to be installed for maximum power generation comes to 2.65 and the total power that can be produced in one complete cycle will be given by 4.22.

$$P_{Tot} = \left(\frac{1.787 \times 3188^2}{10^6} + \frac{5.276 \times 3188}{10^4} - \frac{5.025}{10^2} \right) = 19.8 \text{ Watts} \quad (4.22)$$

The power produced at any given instance is however equivalent to the power produced by elements between 0° and 10° position (discs in the contact patch). This is given by 4.23

$$\frac{20^\circ}{360^\circ} \times 19.8 \text{ watts} = 1.1 \text{ watts} \quad (4.23)$$

This is power output is quite low (0.0792%) for direct powering of the vehicle since the same car requires 20-25 kW to maintain moderate highway speed. However keeping in mind that Kenya is estimated to have more than 2.84 million registered vehicles (Ceic2019, Ceic2019), if each of these cars was to get 0.0396% (half of 0.0792% to

account for differences in power rating of different vehicle) of its power requirement from piezo-electricity, the overall fuel saving would be equivalent to driving 117,414 pollution free vehicles in the country. With other opportunities of improvement still available, this particular source of electricity has great potential as one of the future source of power in hybrid and electric vehicles.

4.2.2 Variation of Power Generation with Changing Tire Pressure for 0.3 mm Discs

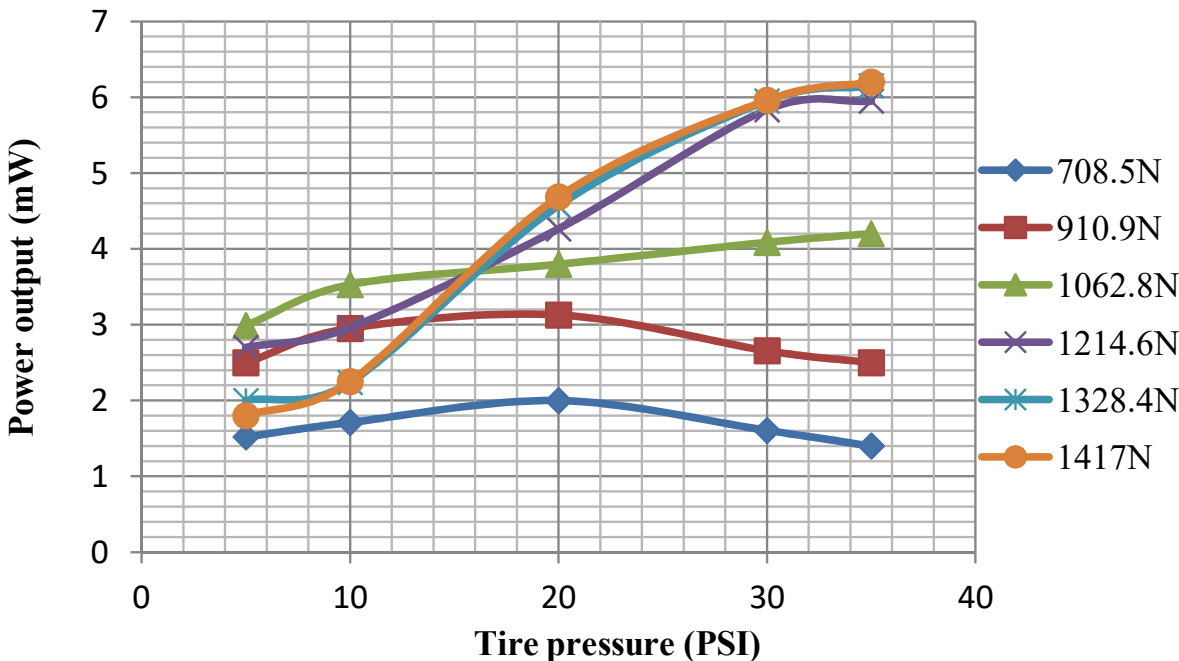


Figure 4.10: Effect of increasing pressure on a piezoelectric tires with inner tube and 0.3mm discs

From the graph shown in Figure 4.10, increasing tire pressures in a piezoelectric tire having an inner tube, produces continuously increasing power irrespective of the load size up to 20 psi. This is mainly because as the pressure increases from 0 to 20 psi, the patch is held against the tire carcass more firmly making transmission as well as distribution of the applied force to the elements more effective hence better power genera-

tion. This deduction agrees with the observation made by Farnsworth et al. (Farnsworth et al. 2014, Farnsworth et al. 2014) where they observed that, in order to optimize the efficiency of power generation, it is important that the energy harvesting system should maximize the coupling between the kinetic energy source and the transduction mechanism. Li et al. (Li et al. 2014a, Li et al. 2014a) in their paper also noted that aside from the resonance matching between the energy harvester and the primary input frequency of the host, strain distribution within the piezoelectric material is also an important aspect in achieving maximum efficiency when harvesting piezoelectricity. From the graph shown in Figure 4.11, any further increase in pressure from 20 psi was accompanied by an increase in the output only if the force at the contact point is above 1062 N, otherwise the output power decreased. This could be because at 20 psi, the best physical coupling possible for the elements in the 185/70R14 tire has already been achieved. Further increase in pressure therefore demands that bigger forces are applied to counter the additional pressure applied in the tire before gaining additional power output. As a result the rate of increase in power output with increasing tire pressure starts going down if the force is above 1062 N, otherwise the power output starts decreasing with increase in pressure. Garimella et al. (Garimella et al. 2015, Garimella et al. 2015) on an almost similar research to that in section 4.2.2, investigated the effect of pressure loading on PZT. They observed that when the pressure exceeded 50 kbar, the output current and hence the power dramatically decreased. They concluded that this could have resulted from internal short circuiting of the generator due to massive generation of electrical charges. Figure 4.10 suggests that though some form of short

circuiting might be taking place at pressures beyond 20 psi, the occurrence affects very small isolated portions of the harvester in a gradual manner as the pressure increases. This allows forces that are big enough (above 1062 N) to continue generating higher power output with increasing pressure up to 35 psi while forces that are below this value start experiencing a decline in output with increasing tire pressure from 20 psi as shown in Figure 4.11.

It can therefore be concluded that if the design of a 185/70r14 piezoelectric tire allocates each layer of piezoelectric discs between 1062 N and 1200 N of the force expected at the tire-road interface, then the best operation range of the tire is between 20 psi and 35 psi. The optimum pressure is however 30 psi.

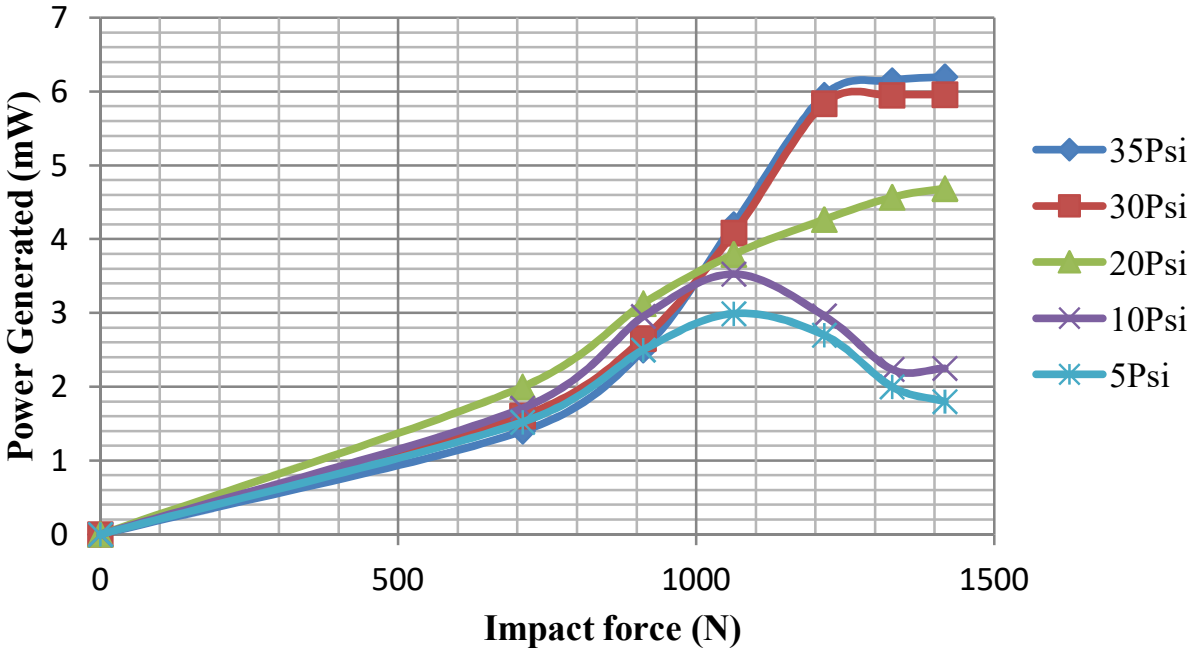


Figure 4.11: Effect of increasing impact force on a (0.3mm disc)piezoelectric tires with inner tube

4.2.3 Drop Test of the Tubeless Tire with Piezoelectric Elements

The tests done in section 4.2.1 were repeated for the tubeless tire. The weight of the tire this time round was 16kg

The results were summarized graphically in Figure 4.12.

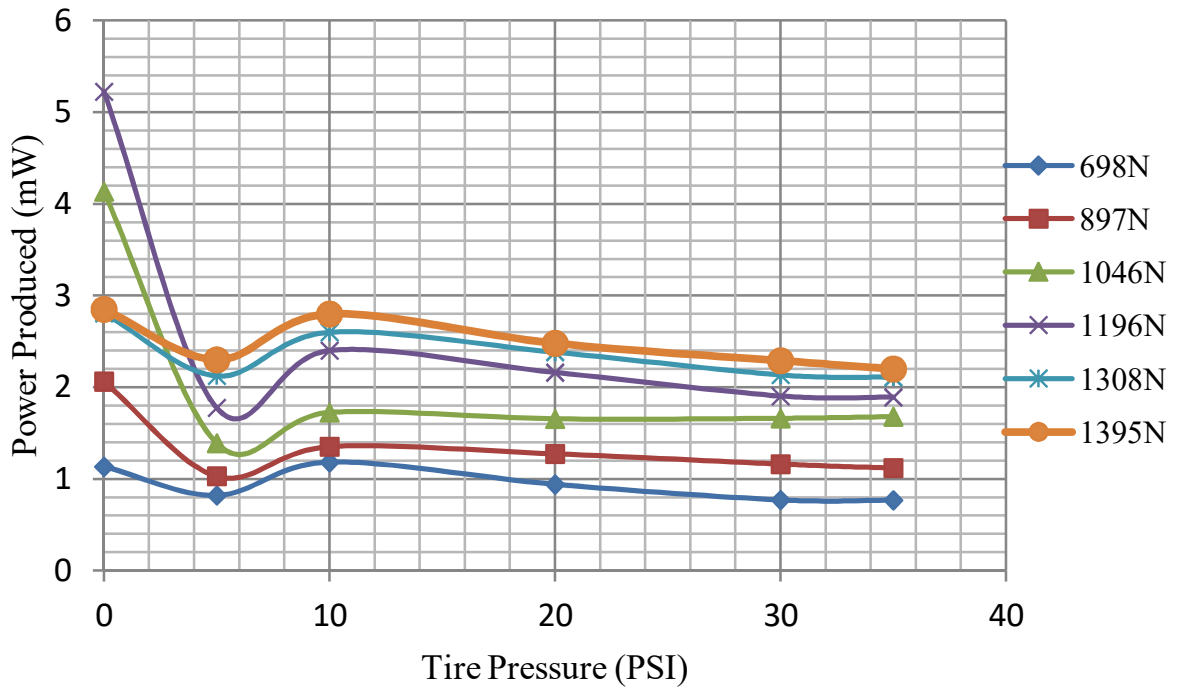


Figure 4.12: Power production in a pressurized tubeless tire with changing drop height

The patch as seen in Figure 4.12, appeared to give out highest amounts of power when the tire pressure is zero. Though it was expected that the output would increase with pressure, the observation can be attributed to the increased ease of deforming the patch considering the glued patch could easily follow the outer tire deformation without the need for supporting pressure. However at the same 0 psi tire pressure, forces above 1196 N appear to give out less power as compared to lesser forces. This could be due to increase in non-uniformity of force distribution in the patch with the increasing impact forces. The power output then drops for pressures from 0 psi to 5 psi. The

main reason for this is the increasing spring constant of the tire with the initial increase in the air inside which absorbs most of the impact. Between 5 psi and 10 psi the output increases as the rigidity of the host increases improving force transmission. After 10 psi the output however appears to continuously reduce. This could be due to the reduced deformation of the tire meaning less deformation of the patch since the holding contact glue imparts less pressure on the patch compared to an inner tube. All in all, the tire with an inner tube performs several times better than the one with contact glue when impact force is applied.

4.3 Stationary Tests for 2 mm Thick Disc

The earlier mentioned drop test was repeated with a patch composed of six pieces of 2mm thick piezoelectric discs. The performance was as tabulated in Table 4.3

Table 4.3: Drop test for 2 mm thick elements

<i>Height (cm)</i>	<i>V (mV); 30psi</i>	<i>V (mV); 20psi</i>	<i>V (mV); 10psi</i>	<i>V (mV); 5psi</i>
2	0.4	0.3	0.1	0.1
4	0.5	0.4	0.2	0.1
6	0.7	0.6	0.3	0.1
8	0.9	0.7	0.3	0.1
10	0.8	0.6	0.4	0.2
12	0.6	0.5	0.2	0.2

The results from the 2mm thick element were quite unexpected for two reasons.

1. The electric current generated was so low that it couldn't be measured after going through the full bridge rectifier
2. The power output was less than that of the 0.3 mm thick piezoelectric elements for the same force

The poor performance in comparison to the 0.3 mm discs can however be partly explained by the research findings by Huidong et al. (Li et al.2014a, Li et al.2014a). They found out that a thin and flat form factor allows a piezoelectric element to readily react to the motion of the host structure (Li et al.2014a, Li et al.2014a). Thus, the piezoelectric materials used in most of the piezoelectric energy harvester designs and configurations explored to date, possess a thin-layer geometric shape. These findings encourage the idea of using several 0.3 mm disks as opposed to one thick piezoelectric element.

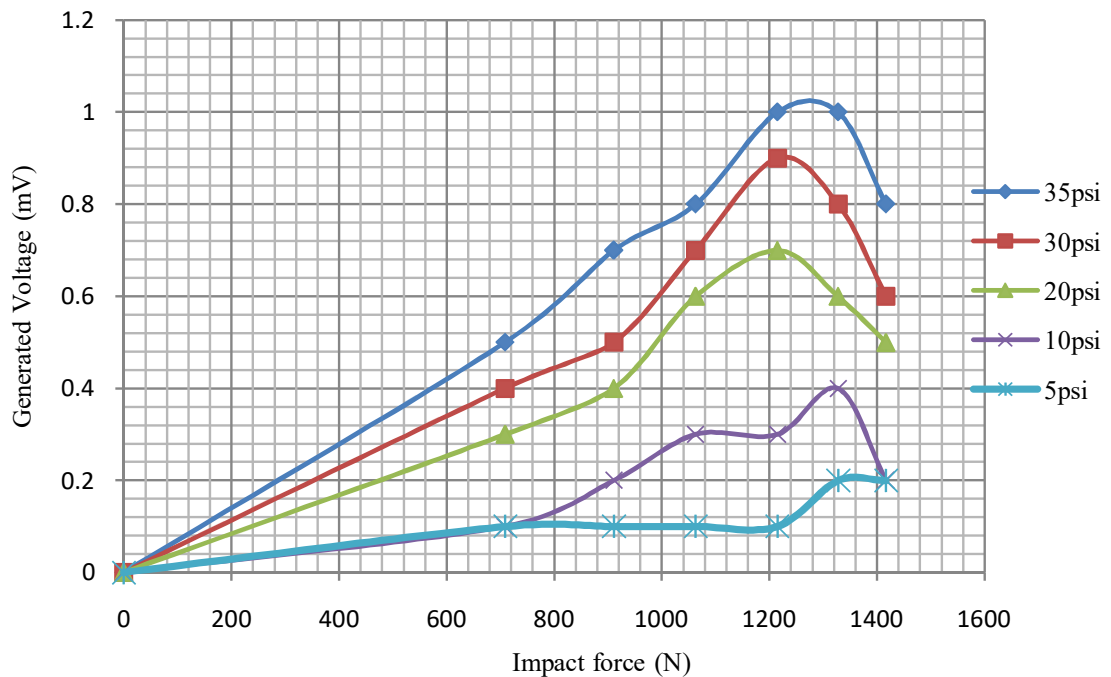


Figure 4.13: Effect of increasing impact force on a 2 mm thick piezoelectric element pre-stressed between the inner tube and tire carcass

To better interpret as well as compare these results with the previous ones, the drop height in Table 4.3 was converted to impact force (as previously done) and plotted as shown in Figure 4.13 and 4.14. From Figure 4.13 it can be observed that for all the different tire pressures, an increase in impact force of up to 1200 N led to an increase

in the generated voltage. The element's power production however started to decline with any further increase in impact force beyond 1200 N unlike in the case of a 0.3 mm thick element whose power output increased or remained constant after reaching 1200 N provided the tire pressure was above 20 psi as shown in Figure 4.11 . Considering that thicker piezoelectric discs are expected to have a greater damping constant this could be the reason behind the decline. The output therefore rises with increase in impact force, but beyond 1200 N, it becomes increasingly difficult for the thick disc to absorb the impact energy and instead transmits the energy to the supporting inner tube behind leading to low outputs.

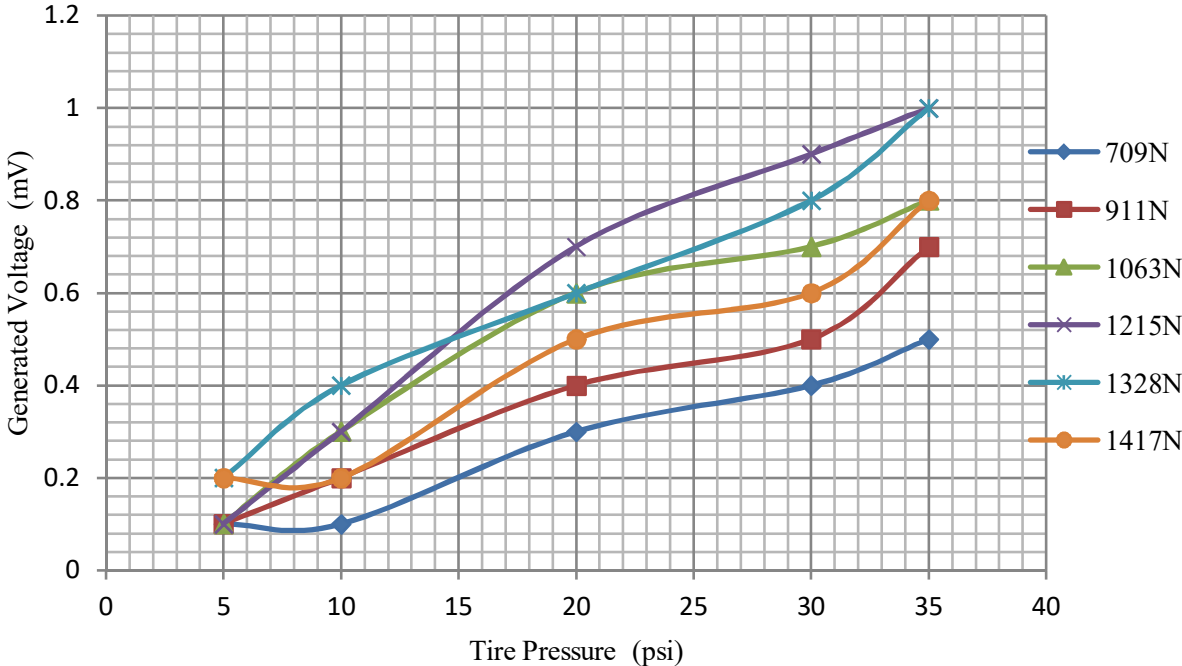


Figure 4.14: Effect of tire pressure on a 2 mm thick piezoelectric element pre-stressed between the inner tube and tire carcass

As can be seen in Figure 4.14 it was observed that for the 2 mm thick element in a tire with an inner tube, increase in tire pressure continuously improved the emf voltage generated. This could be attributed the increasing efficiency in the coupling between

the surface on which the tire is dropped and the element in the tire with the increasing pressure. Since the element is thicker, it also means the generated electrons require a relatively high electric potential to send them across the semiconductor PZT material (Anton and Sodano2007, Anton and Sodano2007).

4.4 Power Generation on a Rough Road

The tire assembled with an inner tube was fixed on a car and the vehicle taken for testing on a rough road. It is good to note that this particular test was re-done seven times because the tire kept on failing after a few hundreds of meters drive.



Figure 4.15: Condition of the rough road used in the research

The initial tire failure was in the form of widespread shearing of the connecting wire in the tire leading to open circuits and hence zero output at the terminals after a short drive. A couple of trials revealed that the shearing of cables was being caused by the brass piezoelectric disc edges pressing against the cables when the tire is pressurized and moving on the road.

The immediate attempt at solving this was to cover the discs with machined and filleted

nylon discs. Although this approach reduced the shearing as well as protected the discs from excess bending, it greatly reduced the output and had to be abandoned. Eventually the remedy adopted was to hold the cables away from the discs when applying the initial layer of heat glue(Ethylene-vinyl acetate) forming a protective layer between the disc and the cables surrounding the patch. Figure 4.15 shows the condition of the rough road used. In the end the tire still failed when taken through potholes, but for other rough road conditions the results were as shown in Figure 4.16

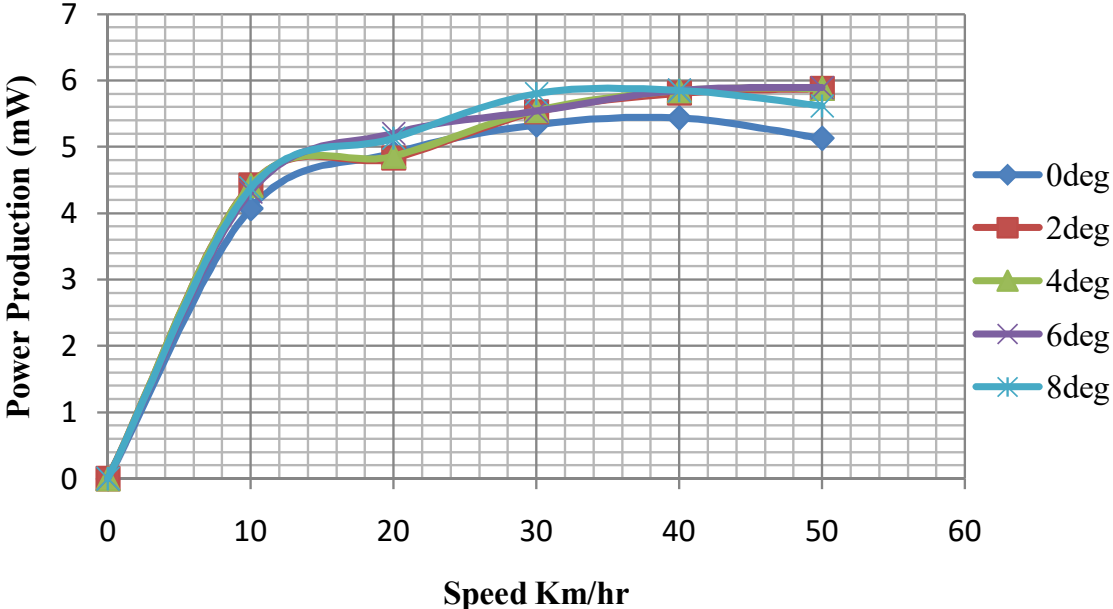


Figure 4.16: Variation of power generated with changing Vehicle speed for different rough road inclinations

From this graph, it was established that the results from the drop experiment were a very close approximation of what is generated when the tire is fixed on a vehicle at speeds above 20 km/hr. This is because the the maximum power generated per layer of piezoelectric discs in the tire doesn't change irrespective of whether the tire is in the lab or on a vehicle. Therefore since the weight of the car is sufficient to provide the maximum force required to enable the layer give out the maximum power it is

capable of, maximum power per element is given out (0.5 mW). This maximum output is however not given out until the vehicle reaches a speed of around 30 km/hr because piezoelectric materials being frequency dependent, the force needs to be applied at certain minimum speeds for best performance (Li et al.2014b, Li et al.2014b). This speed was however expected to vary from road surface to road surface because the irregularities on the road also result in minor impacts on the tire surface, which result in additional power generation.

It was also realized that change in road gradient or inclination affects the power output by less than 2% and in a rather random manner. This effect is the same whether the vehicle is going uphill or downhill. This could be due to the fact that changes in the terrain have little effect on both the weight of the car as well as the impacts on the tire surface. The effect of road gradient on power output of a piezoelectric wheel can therefore be safely assumed to be negligible.

Changes in speed generally had a major effect on the power output of the piezoelectric wheel for all rough road gradients. The peak power generation was achieved between 35 and 40 kilometers per hour for whichever gradient as seen in Figure 4.16. Speeds above 50km/hr on rough road were not tested for safety reasons.

To make a quick comparison between a pre-stressed tire and a tubeless tire, a graph of power output from the tubeless tire was also plotted as shown in Figure 4.17.

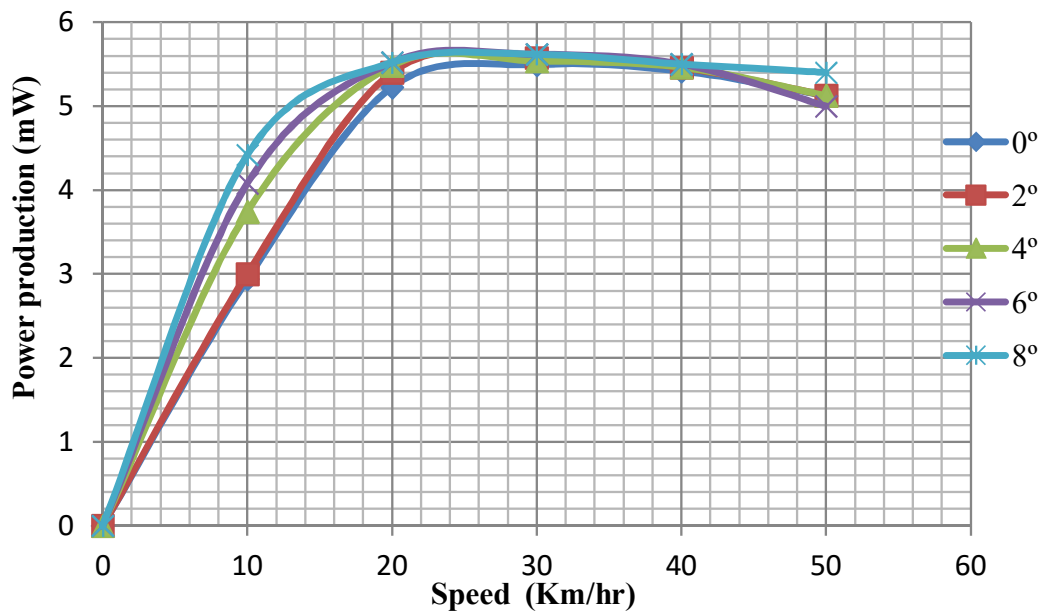


Figure 4.17: Variation of power generated with changing speed for tubeless tire

From these graphs, the tubeless tire achieves its peak output at around 25km/hr(Figure 4.17) unlike the tire with an inner tube which achieves the peak output at 35-40 km/hr under the same conditions (Figure 4.16). Its also observed that the peak output for the tubed tire is 5.26 % higher (6 mW against 5.7 mW) than that of the tubeless tire. It is therefore inferred that a piezoelectric tire in which the elements are pressurized between an inner tube and the tire carcass has slower response to acceleration as compare to a tire in which the harvesters are fixed on the inner lining by glue alone. This tire with an inner tube however had better power output at average car speeds (30-80) than the tire without. The main reason for the low response to speed by the tire with an inner tube could be because the inner tube exerts slightly more pressure on the element than the conta glue. The tire therefore has to be excited slightly more in order for the discs to vibrate with the same intensity as the disc held with conta glue. The power output is however better probably because with the firmer support from the inner tube, force

can be absorbed by the disc more uniformly resulting in higher power outputs.

4.5 Power Generation on a Tarmacked Road



Figure 4.18: A photograph of the tarmac road used in the research

The study done for the rough road in section 4.4 was repeated for tarmacked road, in this case the Thika superhighway shown in Figure 4.18. The results were as plotted in graph in Figure 4.19.

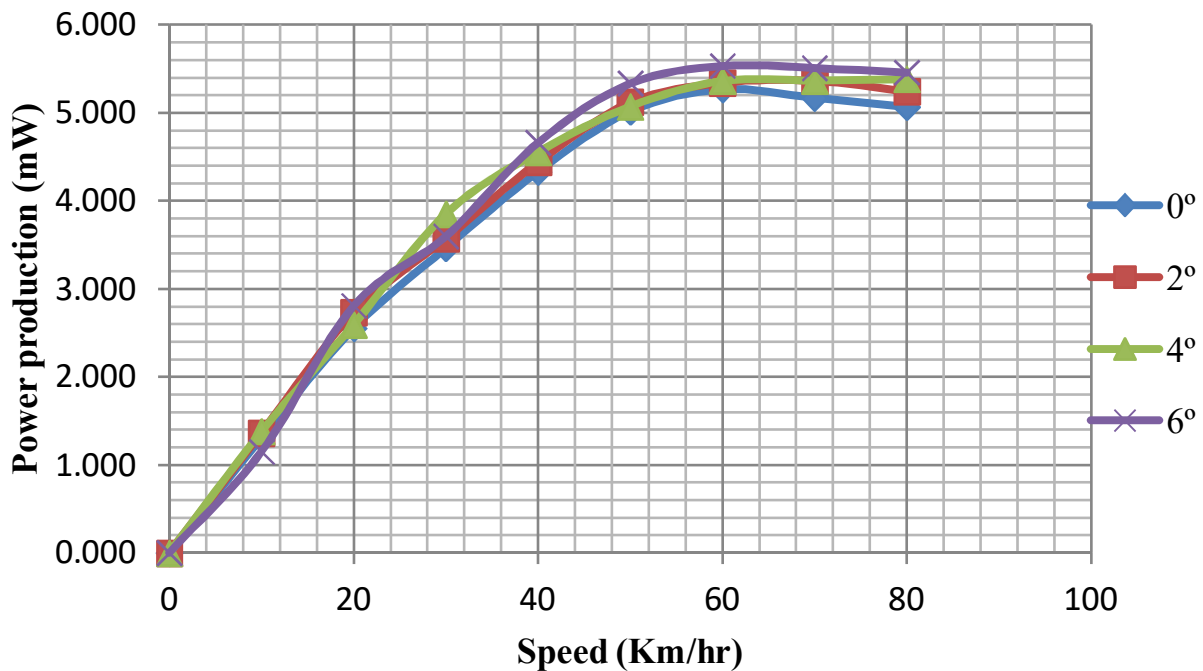


Figure 4.19: Variation of power generated with speed for different tarmac road inclinations

In this case it was possible to test for speeds of up to 80 km/hr. The steepest road incline was however only 6 degrees.

From the graphs in Figure 4.19, it was observed that, similar to the case of rough roads, the road steepness has very little effect on the power produced in comparison to the vehicle speed. The possible explanation for this is again the same with that given for rough roads. The peak power produced was however achieved at relatively higher speeds (55-60 km/hr). The reason for this could be because there are fewer irregularities on the road surface, there are few resultant impacts on the tire surface which translates to lesser excitation of the piezoelectric discs. The wheel therefore has to rotate at higher rotation speeds in order to create the same excitation witnessed on a rough road. Thus, using a piezoelectric wheel in off-road environments has the disadvantage of reducing the element lifespan due to the excessive impacts when one hits potholes, but on the

positive side requires lesser speed to produce the same amount of power.

4.6 Variation of Power Generated with Vehicle Vibrations

To understand the general effect of vibrations and hence the road surface on power production from a pre-stressed tire, a TES 3101 vibration meter was used to log real time vibrations as the vehicle was being driven. There were however three major challenges in doing this

1. Identifying the most suitable measuring point to take the vibrations
2. Choosing one parameter from: amplitude, velocity or acceleration to measure since the meter could only do one
3. Deciding how to handle the mixed number of unsteady frequencies coming from the vehicle

Eventually the sensor was fixed on the floor opposite the driver's seat and root mean square(rms) amplitude measurement selected since it best describes the condition of the road surface. The results were as plotted in Figure 4.20

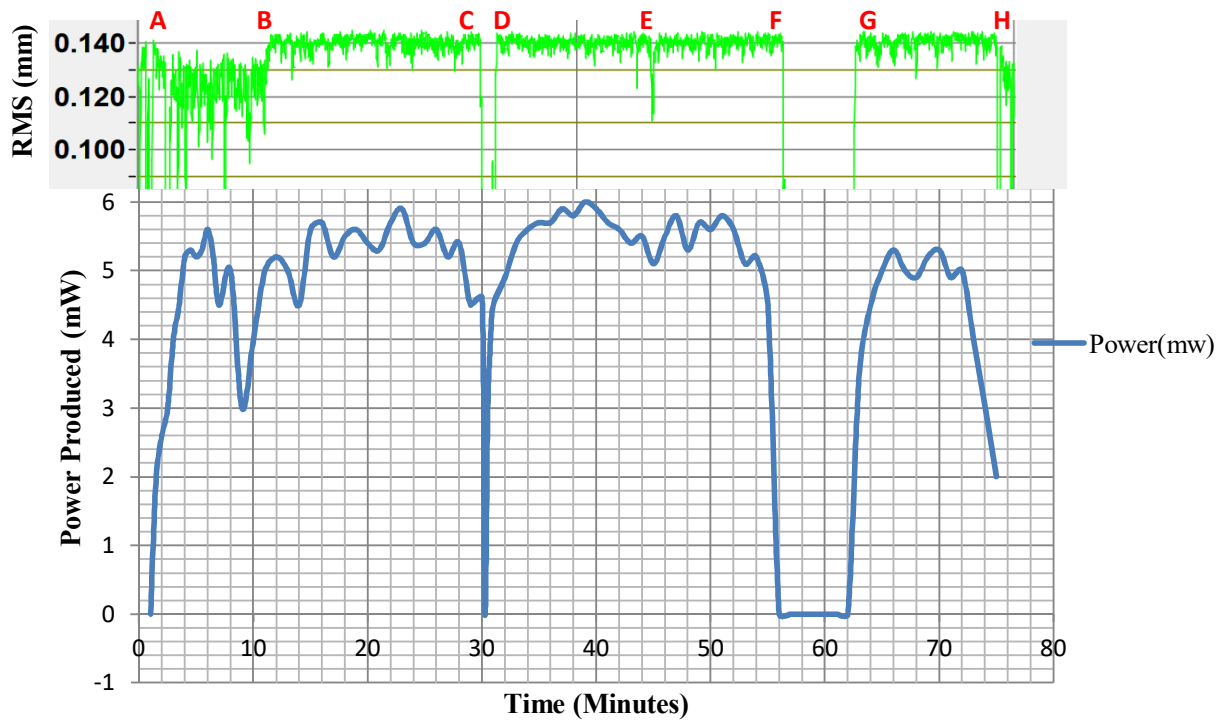


Figure 4.20: Variation in power output with changing vibrations

In the graph in Figure 4.20, section AB represents a driving period from Juja town to Kenyatta road and back to Juja-Gatundu road a distance of 6.2 Km. In this region the amplitude was low because of the smooth tarmacked road surface. The vibrations frequently would go to almost zero at some instances because of the frequent deceleration to avoid "matatus" picking passengers on the road. Section BC represents a drive on Juja-Gatundu rough road towards Gatundu direction. The amplitude of vibration in the AB region was on average 17 percent higher than on the tarmacked road. Section CD represents a short stop to allow a heavy commercial lorry to turn. Section DE is a continuation of the trip. At E a U-turn was made to go back to the college. At F, a short break was taken to check a mechanical problem with the car. H is the time of arrival back in the college.

From the graph in Figure 4.20, it was observed that the output of a piezoelectric disc once mounted in a car tire is directly affected by the frequency of vibrations. When the frequency is high(indicated by a dense plot on the RMS scale) the output too was high, but whenever the frequency reduced, even if the amplitude of rotation was relatively constant, the output quickly declined. This observation agrees with what was observed by Li et al. (Li et al.2014b, Li et al.2014b), who found out that increase in the frequency of the source always increases power output of a piezoelectric harvester as long as the harvester's natural frequency has not been exceeded.

4.7 Comparison with Previous Researches on Cars

From the various tests done in this research, the maximum power harvested from a pre-stressed tire was 6 mW for every patch of 12 discs. This translates to 0.5 mW per disc. Makki and Popiliev(Makki and Popiliev2011, Makki and Popiliev2011), did a similar research without pre-stress but the same resistance load and generated 4.6 mW of power. It was therefore expected that more power than that observed would be generated considering the advantages of pre-stress. The actual output was however only 30% higher.

Santoleri et al. (Santoleri et al.2014, Santoleri et al.2014) in their shock-mounted piezoelectric harvester, were able to generate 25 watts. This harvester still remains the best ever made probably because only one rectifier was required, eliminating any possible sources of inefficiencies in their circuit.

CHAPTER FIVE

5.0 CONCLUSIONS AND RECOMMENDATIONS

5.1 Conclusions

Based on the outcome of this research, the following conclusions are made:

- (a) For piezoelectric discs of diameter 25 mm loaded by a force of 30 N to 70 N, the most efficient thickness is 0.1 mm - 0.3 mm followed by 2 mm
- (b) When a piezoelectric disc with one face fixed is loaded compressively with a uniformly distributed load on the opposite face, the maximum Von Mises stress occurs towards the edge (from the simulation done).
- (c) The power output of one layer of pre-stressed PZT 5A discs positioned in a 185/70R14 car tire is given by equation

$$p_{Tot} = \frac{1.787q^2}{10^6} + \frac{5.276q}{10^4} - \frac{5.025}{10^2} \quad (5.1)$$

Where $q \leq 1200N$. Any load above 1200 N should be accompanied with introduction of an additional layer for best performance.

- (d) With the circuit and PZT 5A discs used in this reseach, a 1300 Kg Nissan Wingroad can be able to produce 1.1 Watts from all four wheels provided each wheel is fitted with the maximum number of discs which is .
- (e) The PZT 5A ceramics performance improves by 30% when mounted in a car tire with a pre-stress as compared to mounting it using conta glue alone.

- (f) The vehicle fitted with piezoelectric discs as done in this research, starts producing maximum power between 20 Km/hr and 35 Km/hr on rough roads and between 45 Km/hr and 55 Km/hr on tarmacked roads.

All the four objectives of the research as outlined in section 1.3.2 were met.

5.2 Recommendations

From this research work, the following recommendations are made:

- (a) With availability of smaller and more efficient rectifiers in the market, every piezoelectric disc should be given its separate rectifier to avoid voltage cancellation in order to improve the output further.
- (b) Since the output started declining after two-three days of testing, discs with steel backing plates which protect the harvester in a better way should be tested
- (c) For simplicity the available disc piezo ceramics were adopted in the research. It is recommended that Spherical elements should be tested to find out their performance since they would be more friendly to the tire in the long run considering they don't have any sharp edges.
- (d) Cymbal generators though currently not on the market, have been known to give out upto 20 times more power than a disc generators of the same size and should be tested in this configuration at the earliest opportunity
- (e) The piezoelectric technology has a lot of potential and should be studied more aggressively to develop better PZT materials, better signal conditioning circuits as well as better configurations for power harvesting in cars

References

- Ahman, M., Rogier, J., and Elisa, D. (2009). Hybrid electric vehicles: An overview of current technology and its application in developing and transitional countries. Technical report, United Nations Environmental program, Nairobi.
- Al-Momani, M. and Omar, M. (2007). *International Journal of Mechanical and Materials Engineering*.
- Anair, D. and Amine, M. (2012). Electric vehicles' global warming emissions and fuel-cost savings across the united states. Technical report, US department of Energy, Cambridge.
- Anil, K. and Sreekanth, N. (2014). Piezoelectric power generation in tires. *International Journal of Electrical, Electronics and Computer Systems*, 2:11–16.
- Anton, S. and Sodano, H. (2007). A review of power harvesting using piezoelectric materials (2003-2006). *Smart Materials and Structures*, 16:R1.
- Anuruddh, K., Anshul, S., Rajeev, K., Rahul, V., and Vishal, C. (2014). Finite element analysis of vibration energy harvesting using lead-free piezoelectric materials: A comparative study. *Journal of Asian Ceramic Societies*, 2:138–143.
- Badr, B., Delaney, K., and Dechev, N. (2015). Design piezoelectric energy harvesting using comsol for mice telemetry device. In *2015 COMSOL Conference in Boston*, pages 1–8. COMSOL.
- Baier, P. and Schulz, A. (1978). Engine knock sensor using piezoelectric rod oscillator. US4305013A.
- Bakker, D. (2010). Battery electric vehicles: Performance, CO₂ emissions, lifecycle costs and advanced battery technology development. Technical report, Copernicus institute University of Utrecht.
- Bauer, G. (2015). *Photovoltaic solar energy conversion*. Springer, Berlin.
- Beard, G., Pat, C., and Keith, W. (2015). Plug-in electric vehicle handbook for consumers. Technical report, US department of Energy, Newyork.
- Behera, M., Mishra, A., Purushottam, P., and Rout, S. (2015a). Design and simulation of model for energy harvesting from vehicle tires using piezoelectric modules.

- International Journal of Scientific and Engineering Research*, 6:1106–1111.
- Behera, M., Mishra, A., Purushottam, P., and Rout, S. (2015b). Design and simulation of model for energy harvesting from vehicle tires using piezoelectric modules. *International Journal of Scientific and Engineering Research*, 6(10):1106–1111.
- Ben-Chaim, M., Shmerling, E., and Kuperman, A. (2013). Analytic modeling of vehicle fuel consumption. *Energies*, 6:117–127.
- Bogusz, P., Gotowicki, P., Małachowski, J., and Baranowski, P. (2012). Assessment of mechanical properties of off-road vehicle tire: Coupons testing and finite element model development. Technical report, Poland Military University of Technology, Kaliskiego.
- Broch, T. (1984). Measurement of Vibration. 2850 Nærum Denmark.
- Bunsen, T., Cazzola, P., Gerner, M., Paoli, L., and Tetter, J. (2018). Towards cross-modal electrification. Technical report, International Energy Agency, France.
- Ceic (2017 (accessed March 3, 2019)). *Kenya Road Transport: No of Motor Vehicles: Registered*.
- Chandrika, N. (2010). Electric vehicles. *Postnote*, pages 1–4.
- Chen, X., Yang, T., Wang, W., and Yao, X. (2012). Vibration energy harvesting with a clamped piezoelectric circular diaphragm. *Ceramics International*, 38:271–274.
- Chiara, F., Kyoungcho, A., and Hesham, R. (2016). Power-based electric vehicle energy consumption model: Model development and validation. *Applied Energy*, 168:257–268.
- Colbert, J. (1965). Piezoelectric ultrasonic transducer. US3376438A.
- Comsol (1998). Comsol multiphysics users guide. Technical report, COMSOL.
- Dakua, I. and Afzulpurkar, N. (2013). Piezoelectric energy generation and harvesting at the nano-scale: Materials and devices. *Journal of Nanomaterials and Nanotechnology*, 3:21–37.
- Dhingra, P., Jhilmam, B., Anjushree, P., and Sukanya, M. (2012). Energy harvesting using piezoelectric materials. *International Journal of Computer Applications*, pages 38–42.
- Dongwon, K. and Gabriel, R.-M. (2009). A rectifier-free piezoelectric energy harvester

- circuit. *2009 IEEE International Symposium on Circuits and Systems*, pages 1085–1088.
- Duan, H., Wang, W., Tong, Q., and Quek, S. (2010). Applications of piezoelectric materials in structural health monitoring and repair: Selected research examples. *Materials*, 3.
- Ebrahimi, F. and Ogawa, T. (2013). Piezoelectric materials and devices- practice and applications. Turkçe Mugla Sitki Koçman University, Department of Metallurgical and Materials Engineering.
- EnerGuide (2018). 2018 fuel consumption guide. Technical report, Natural Resources Canada.
- Enocksosn, S. (2011). Modeling in mathworks simscape by building a model of an automatic gearbox. Technical report, UPPSALA Universitet.
- EPRI (2019). Consumer guide to electrical vehicles. Technical report, Electrical Power Research Institute.
- Fakhri, A., Al-sallami, W., and Al-Esawi, N. (3015). The current world energy situation and suggested future energy scenarios to meet the energy challenges by 2050 in the uk. 4:212–218.
- Farnsworth, M., Tiwari, A., and Dorey, R. (2014). Modelling, simulation and optimisation of a piezoelectric energy harvester. In *3rd International Conference on Through-life Engineering Services*, pages 142–147. Cranfield University.
- Fathauer, H. (1974). Ultrasonic sensor. US3881353A.
- Florin, A., Ioan-Cozmin, M., and Liliana, P. (2013). Passive suspension modeling using matlab, quarter car model, input signal step type. *New Technologies and Products in Machine Manufacturing Technologies*, 7:258–263.
- Garimella, G., Sastry, V., and Mohiuddin, M. (2015). An approach to generate electricity from vibrations. *Procedia Earth and Planetary Science*, 11:445–446.
- Gencsu, I., McLynn, M., Runkel, R., Worrall, L., and Trilling, M. (2017). Phase-out 2020: Monitoring europe’s fossil fuel subsidies. Technical report, Climate Action Network (CAN) Europe, Delphi.
- Jürgen, N. and Thilo, B. (2006). Application of piezoelectric materials in transporta-

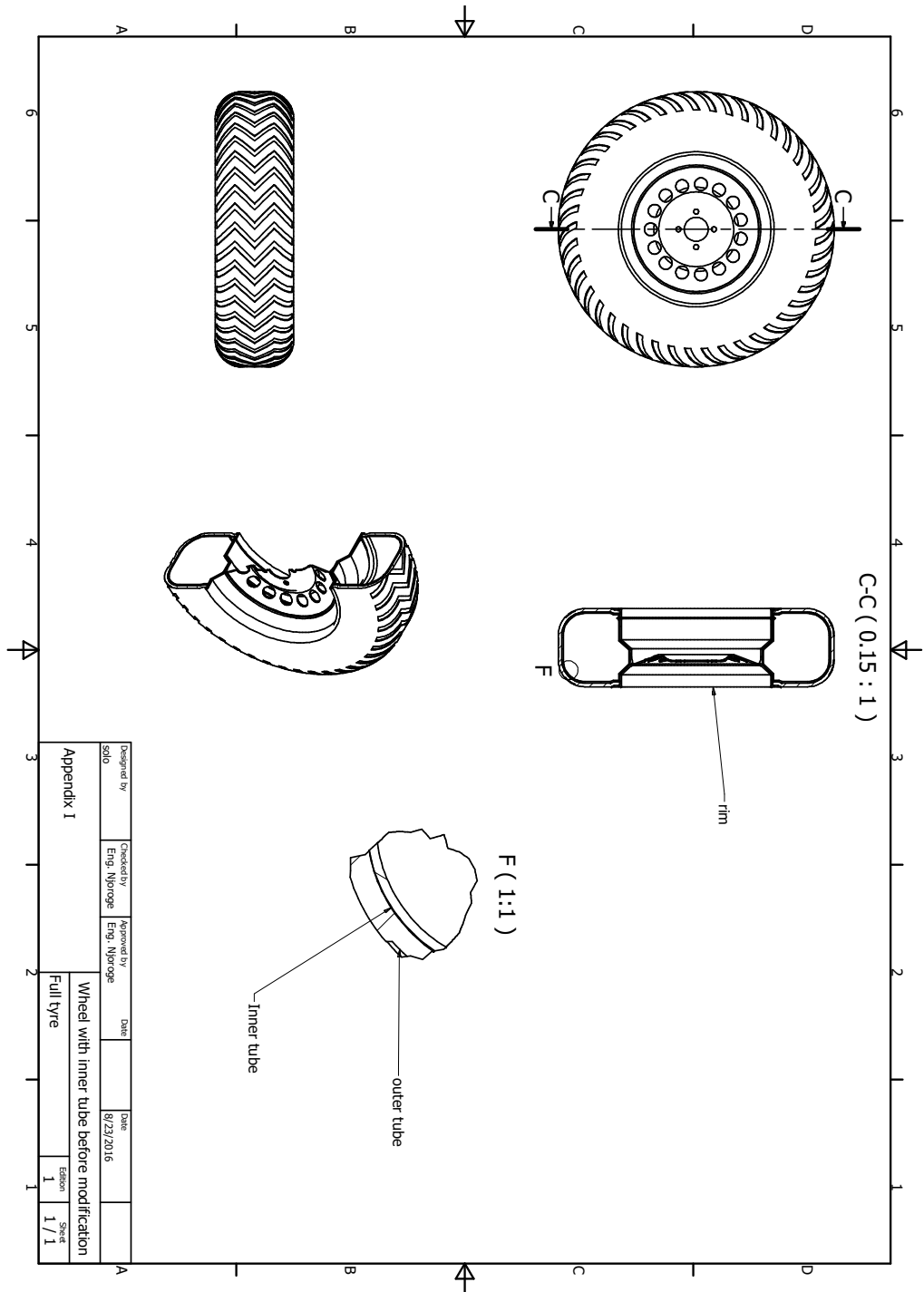
- tion industry. *Global Symposium on Innovative Solutions for the Advancement of the Transport Industry*, 3:4–6.
- Keck, M. (2007). A new approach of a piezoelectric vibration-based power generator to supply next generation tire sensor systems. In *2007 IEEE Sensors*, pages 1299–1302.
- Khameneifar, F. and Arzanpour, S. (2008). Energy harvesting from pneumatic tires using piezoelectric transducers. volume 2, pages 428–435.
- Kindt, P., De’Coninck, F., Sas, P., and Desmet, W. (2007). Analysis of tire / road noise caused by road impact excitations. Technical report, Katholieke Universiteit Leuven.
- Kong, L., Li, H., Boey, F., and Zhang, T. (2014). *Waste Mechanical Energy Harvesting (II): Nanopiezoelectric Effect*, volume 24. pringer, Berlin, Heidelberg, 1 edition.
- Konka, H. and Kun, L. (2010). Characterization of composite piezoelectric materials for smart joint applications. Technical report, Louisiana State University.
- Kunchala, A. and Sreekanth, N. (2014). Piezoelectric power generation in tires. *Indonesian Journal of Electrical Engineering and Computer Science*, 2:11–16.
- Lakušić, S. and Brčić, D. (2011). Analysis of vehicle vibration – new approach to rating pavement condition of urban roads. *Journal of Promet – Traffic and Transportation*, 23:485–494.
- Lallart, M. and Guyomar, D. (2008). An optimized self-powered switching circuit for non-linear energy harvesting with low voltage output. *Smart Materials and Structures*, 17.
- Lebeau, K., Lebeau, P., Macharis, C., and Mierlo, V. (2013). How expensive are electric vehicles? a total cost of ownership analysis. *World Electric Vehicle Journal*, 6:996–1007.
- Ledoux, A. and J, C. (2011). Theory of piezoelectric materials and their applications in civil engineering. Technical report, Massachussets Institute of Technology.
- Leinonen, M., Jaakko, P., Maciej, S., Jari, J., and Heli, J. (2011). Energy harvesting from vibration and walking with piezoelectric materials. Technical report, University of Oulu, Oulu.

- Li, H., Chuan, T., and Daniel, Z. (2014a). Energy harvesting from low frequency applications using piezoelectric materials. *Applied Physics Reviews*, 1(4):041301.
- Li, H., Chuan, T., and Deng, D. (2014b). Energy harvesting from low frequency applications using piezoelectric materials. *Journal of Applied Physics Reviews*, 1:1–20.
- Machave, G., Sambhaji, P., and Kathar, R. (2015). Study of influence of pressure and load on wheel rim by radial fatigue test. *International Journal of Engineering Sciences and Research Technology*, 4:298–303.
- Madhuranath, T., Girija, K., Praharsa, R., and Rao, K. (2014). Design and simulation of piezotyres using comsol multiphysics 4.3b software tool. *European Journal of Applied Engineering and Scientific Research*, 2:1–7.
- Makki, N. and Popiliev, R. (2011). Piezoelectric power generation in automotive tires. In *Proceedings in Smart Materials, Structures and NDT In Aerospace Conference*, volume 4 of *QC*, pages 1–10. Canadian Institute for NDE.
- Manla, G., White, N., and Tudor, J. (2009). Harvesting energy from vehicle wheels. In *Solid-State Sensors, Actuators and Microsystems Conference, 2009. TRANSDUCERS*, pages 1389–1392. IEEE.
- Mathworks (2007). Simscape user’s guide. Technical report, The MathWorks, Inc.
- Minazara, E., Vasic, D., and Costa, F. (2008). Piezoelectric generator harvesting bike vibrations energy to supply portable devices. Technical report, Pres Universud.
- Mohamad, S., Thalass, M., Noordin, A., Hassan, M., Ibrahim, Z., and Yahya, M. (2015). A potential study of piezoelectric energy harvesting in car vibration. *Journal of Engineering and Applied Sciences*, 10:8642–8647.
- Motter, D., Felipe, D., and Samuel, S. (2006). Vibration energy harvesting using piezoelectric transducer and non- controlled rectifiers circuits. Technical report, Western Parana State University, Iguacu.
- Motter, D., Jairo, L., Aguiar, F., and Silva, S. (2012). Vibration energy harvesting using piezoelectric transducer and non-controlled rectifiers circuits. *Journal of the Brazilian Society of Mechanical Sciences and Engineering*, 34:378–385.
- Nuffer, J. and Bein, T. (2006). Application of piezoelectric materials in transportation

- industry. pages 238–242.
- Outlook, W. E. (2013). World energy outlook 2018. Technical report, International Energy Agency, Paris.
- Palosaari, J. (2017). Energy harvesting from walking using piezoelectric cymbal and diaphragm type structures. Technical report, University of Oulu.
- Pieter, D. (2013). Power harvesting using piezoelectric materials: Applications in helicopter rotors. Technical report, University of Twente.
- Piyush, P. (2016). Use of vibration energy for charging electric car. *International Journal of Mechanical Engineering and Technology*, 7:59–65.
- Priya, S. (2007). Advances in energy harvesting using low profile piezoelectric transducers. *Electroceram*, pages 165–182.
- Raj, S., Srinath, S., Jamal, A., and Ranjith, A. (2015). An application of piezo electric effect in an automotive vehicle. *International Journal of Modern Trends in Engineering and Science*, 02:16–18.
- Sadeqi, S., Arzanpour, S., and Hajikolaie, K. (2015). Broadening the frequency bandwidth of a tire-embedded piezoelectric-based energy harvesting system using coupled linear resonating structure. *IEEE/ASME Transactions on Mechatronics*, 20(5):2085–2094.
- Santoleri, C., Poska, M., Schwarz, E., and Bunker, M. (2014). The piezoelectric shock absorber. Technical report, Green Delphi mega-trend, Delphi.
- Schroeder, D. and Corkery, P. (2010). Clean cities hybrid and plug-in electric vehicles all-electric vehicles. Technical report, US Department of Energy, Newyork.
- Shah, R., Nayak, A., and Pant, B. (2015). Design and simulation of piezoelectric mems cantilever. In *COMSOL Conference, Pune, India*.
- Shirahatti, A., Prasad, P., Panzade, P., and Kulkarni, M. (2008). Optimal design of passenger car suspension for ride and road holding. *Journal of Brazilian Society of mechanical sciences and Engineering*, 30:66–76.
- Timoshenko, S. (1959). Theory of Plates and Shells. Stanford University.
- Townley, A. (2010). Vibrational energy harvesting using {MEMs} piezoelectric generators. Technical report, University of Pennsylvania.

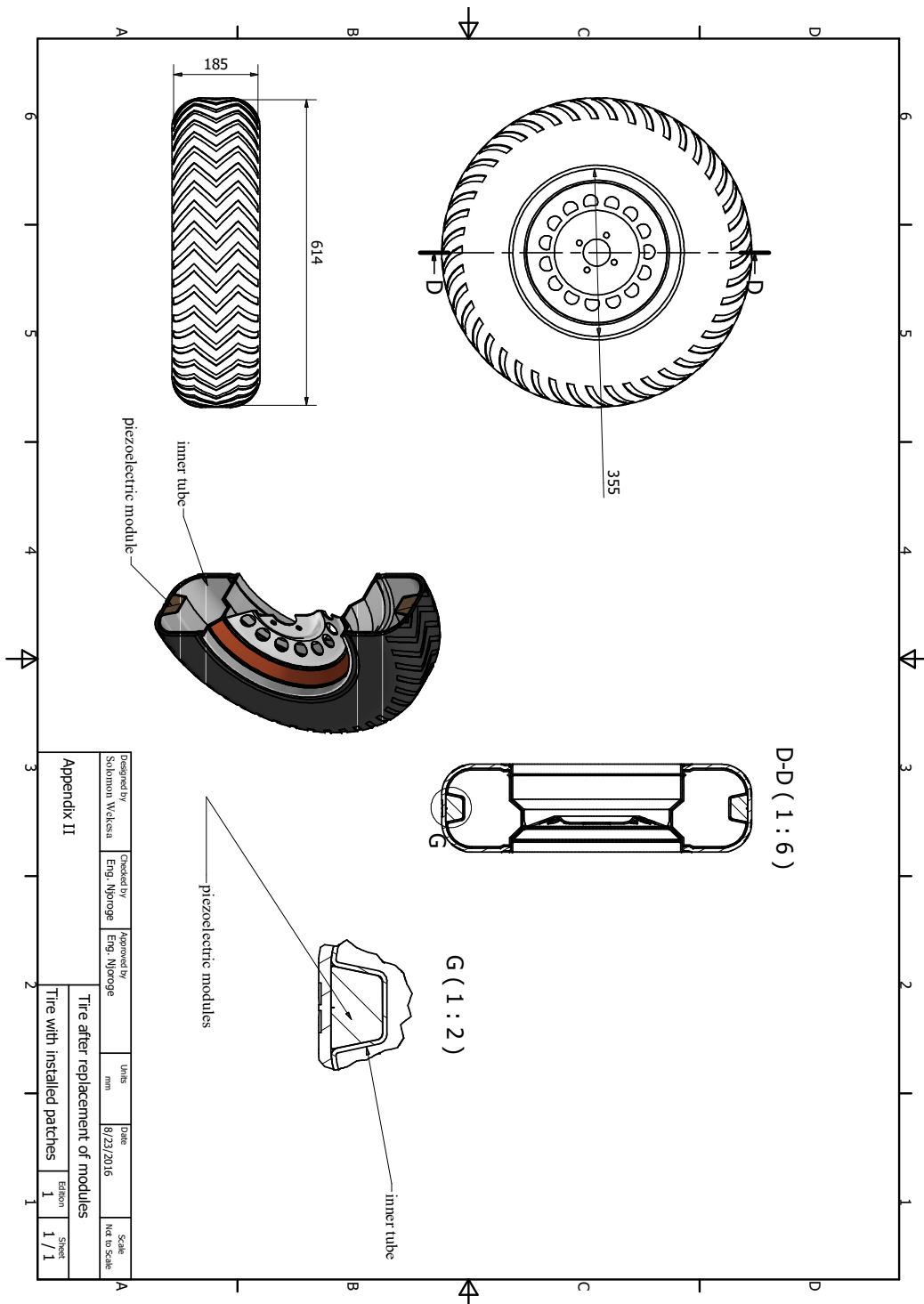
- Trigg, T., Paul, T., and Lew, F. (2013). Understanding the electric vehicle landscape to 2020. Technical report, Global EV Outlook, Paris.
- Uchino, K. (2017a). *The Development of Piezoelectric Materials and the New Perspective*.
- Uchino, K. (2017b). The development of piezoelectric materials and the new perspective. Technical report, Pennsylvania State University, United States.
- Valentin, C. and Koyanagi, K. (2013). Evaluation of the energy harvestable from an airless tire equipped with piezoelectric bimorphs on the lamellar spokes. *Journal of Telecommunications and Information Technology*, 4:79–84.
- Walter, C. (1920). Piezo-electric resonator. US1450246A.
- Wamborikar, T. and Sinha, A. (2010). Solar powered vehicle. volume II. World Congress on Engineering and Computer science.

Appendix I: Normal car tire before modification



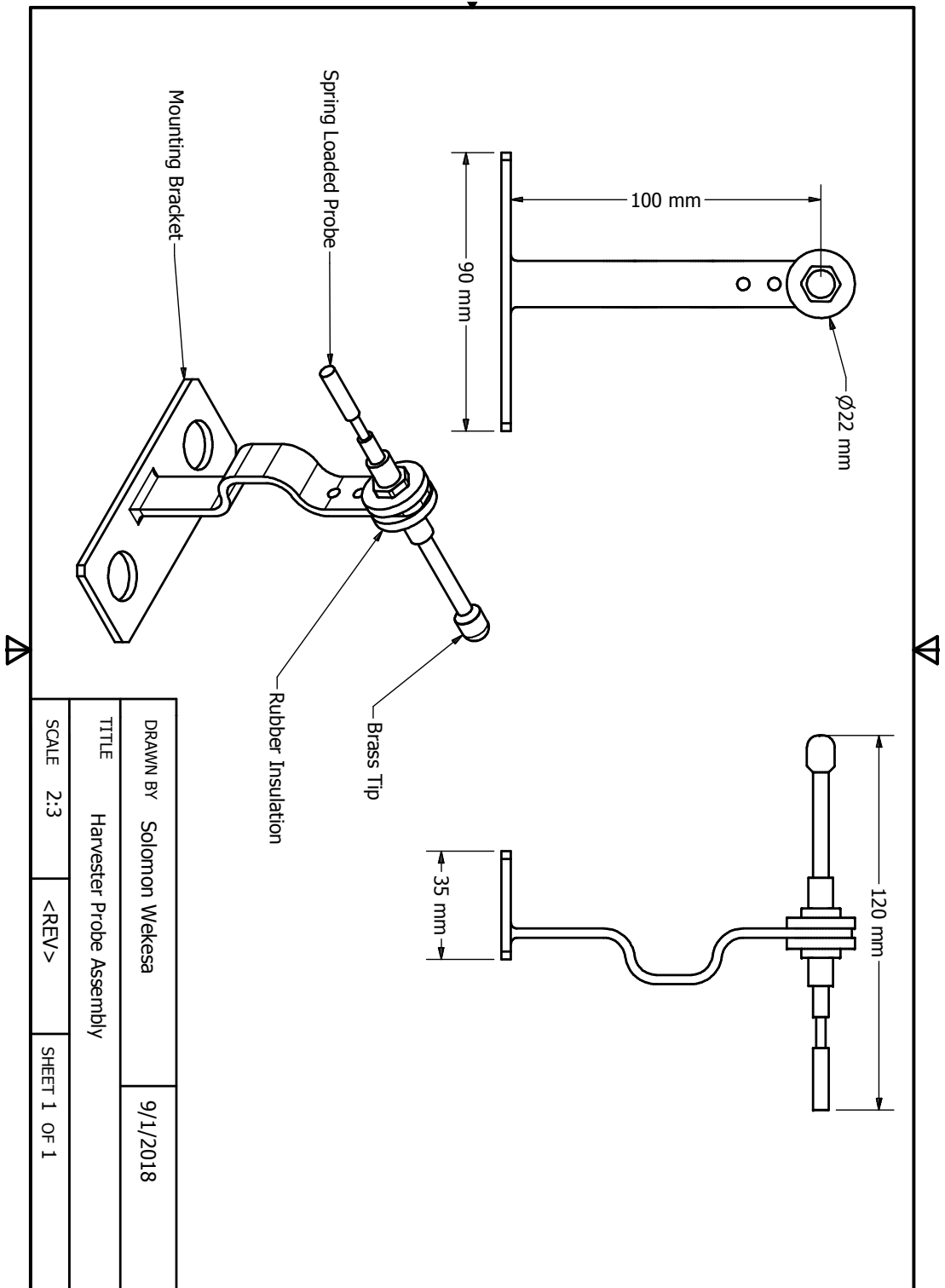
Designed by SOLU	Checked by Eng. M/George	Approved by Eng. M/George	Date 8/23/2016
Appendix I		Wheel with inner tube before modification	
Full type	Edition 1	Sheet 1 / 1	

Appendix II: Car tire after modification



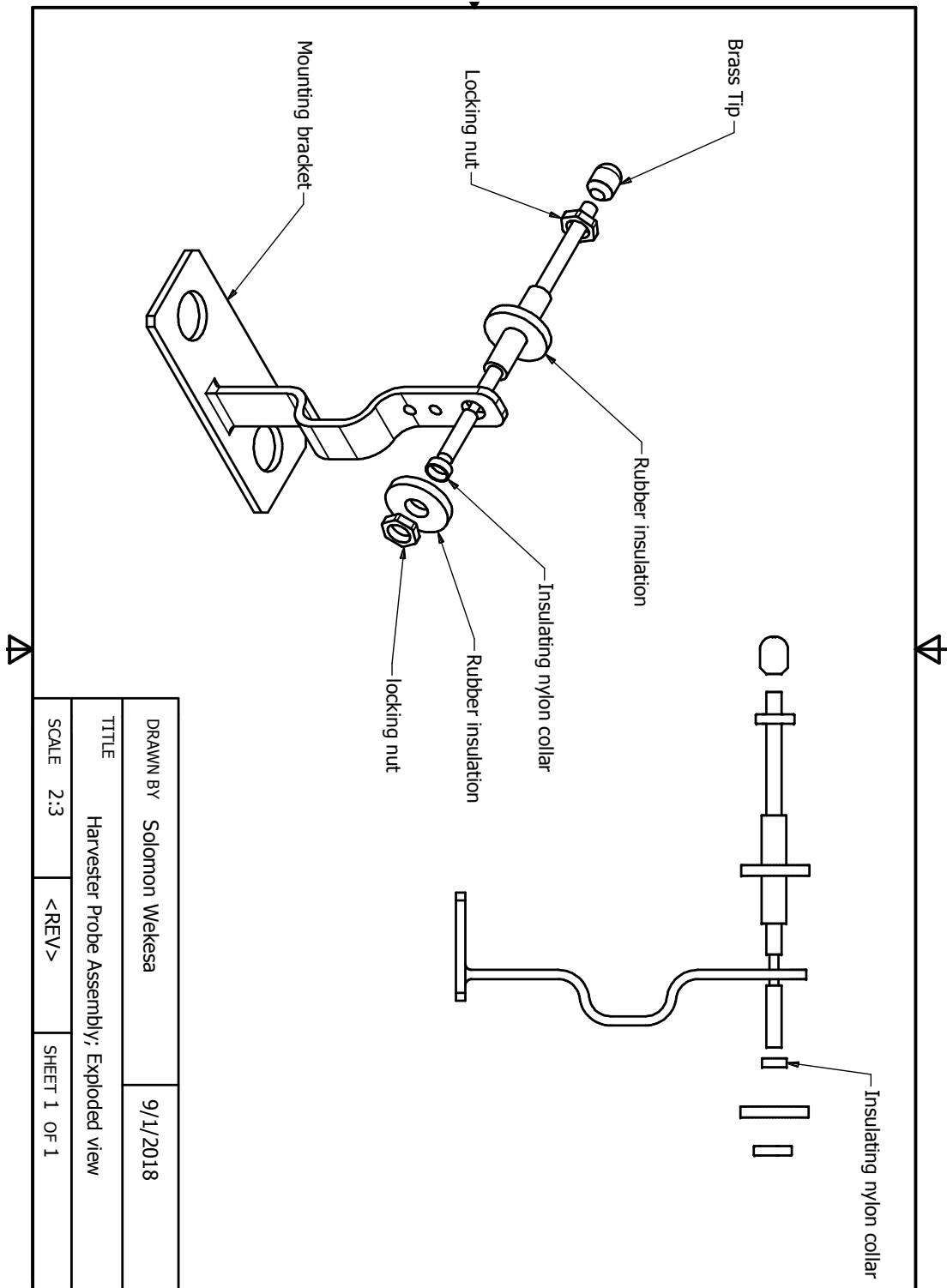
Designed by Solomon Wellesli	Checked by Eng. Mjoroge	Approved by Eng. Mjoroge	Units mm	Date 8/23/2016	Scale Not to scale
Appendix II			Tire after replacement of modules		
Tire with installed patches			Edition 1	Sheet 1 / 1	

Appendix III: Harvesting Probe



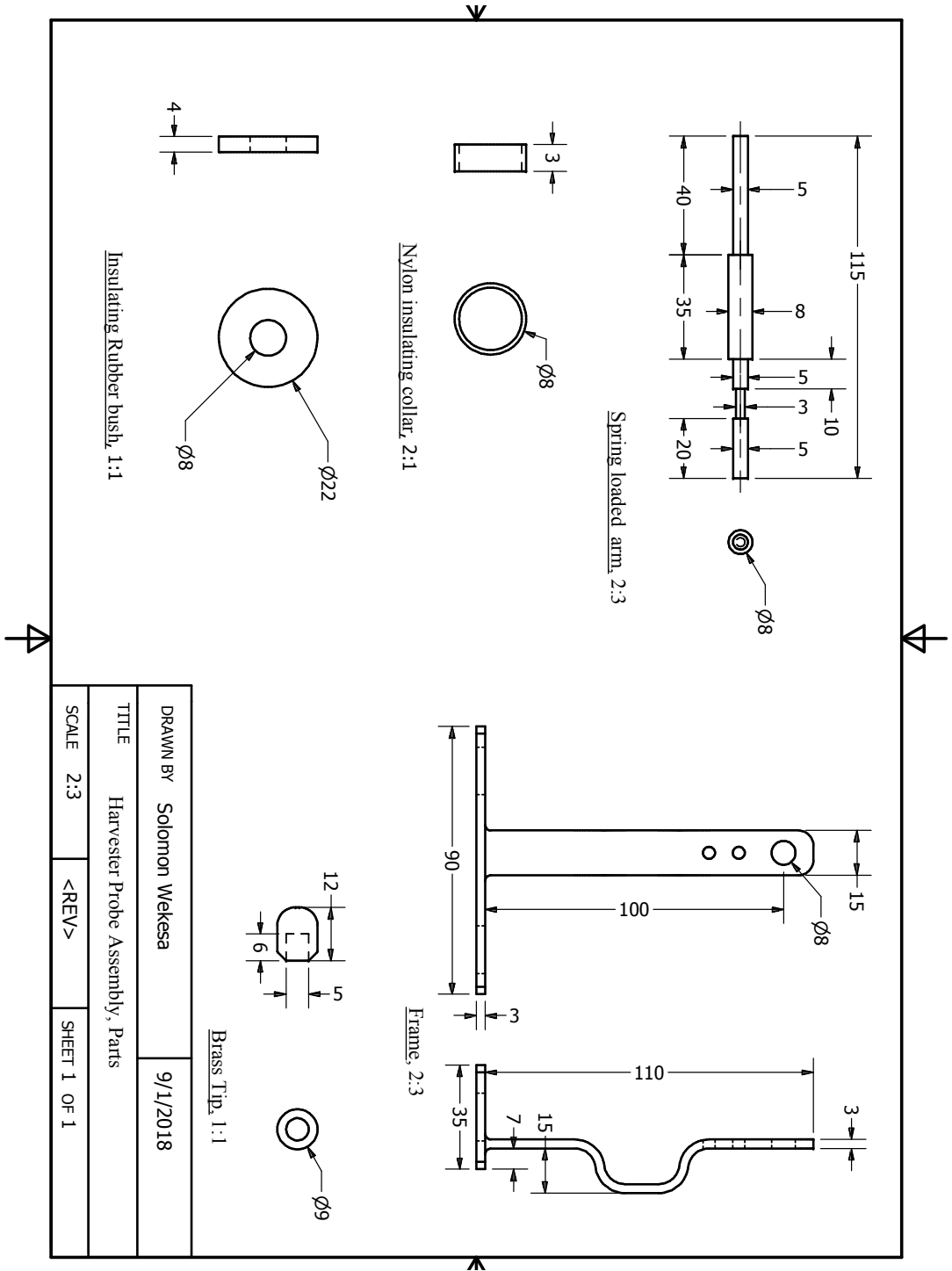
DRAWN BY	Solomon Wekesa	9/1/2018
TITLE	Harvester Probe Assembly	
SCALE	2:3	<REV>
		SHEET 1 OF 1

Appendix IV: Harvesting Probe: Exploded view


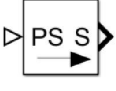



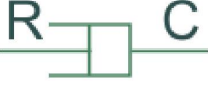

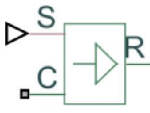
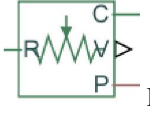
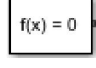




DRAWN BY	Solomon Wekesa	9/1/2018
TITLE	Harvester Probe Assembly; Exploded view	
SCALE	2:3	<REV>
		SHEET 1 OF 1

Appendix V: Harvesting Probe components



Appendix VI: Simscape symbols

1.  Scope for displaying graphical output
2.  PS-Simulink converter. Converts the input physical signal to a unitless simulink output signal
3.  Simulink-PS Converter. Converts the unitless simulink input signal to a physical signal
4.  An ideal translational Mass
5.  An ideal linear spring. R and C are the force application points
6.  A linear Translational damper. R and C are the force application points
7.  Ideal force sensor. F is the force output. R and C are the force application points
8.  Ideal Translational Velocity Source. Port S is the physical signal port. R and C are the velocity application points
9.  Ideal Translational motion sensor. V is the output for velocity and P the output for position. R and C are the force application points
10.  Solver Configuration. Defines the solver setting to use for simulation
11.  Sine wave source
12.  Mechanical translational reference